Nonlinear collective effects in photon-photon and photon-plasma interactions

Mattias Marklund* and Padma K. Shukla*

Department of Physics, Umeå University, SE-901 87 Umeå, Sweden

Strong-field effects in laboratory and astrophysical plasmas and high intensity laser and cavity systems are considered, related to quantum electrodynamical (QED) photon-photon scattering. Current state-of-the-art laser facilities are close to reaching energy scales at which laboratory astrophysics will become possible. In such high energy density laboratory astrophysical systems, quantum electrodynamics will play a crucial role in the dynamics of plasmas and indeed the vacuum itself. Developments such as the free-electron laser may also give a means for exploring remote violent events such as supernovae in a laboratory environment. At the same time, superconducting cavities have steadily increased their quality factors, and quantum nondemolition measurements are capable of retrieving information from systems consisting of a few photons. Thus, not only will QED effects such as elastic photon-photon scattering be important in laboratory experiments, it may also be directly measurable in cavity experiments. Here implications of collective interactions between photons and photon-plasma systems are described. An overview of strong field vacuum effects is given, as formulated through the Heisenberg-Euler Lagrangian. Based on the dispersion relation for a single test photon traveling in a slowly varying background electromagnetic field, a set of equations describing the nonlinear propagation of an electromagnetic pulse on a radiation plasma is derived. The stability of the governing equations is discussed, and it is shown using numerical methods that electromagnetic pulses may collapse and split into pulse trains, as well as be trapped in a relativistic electron hole. Effects, such as the generation of novel electromagnetic modes, introduced by QED in pair plasmas is described. Applications to laser-plasma systems and astrophysical environments are also discussed.

PACS number(s): 12.20.Ds, 52.35.Mw, 95.30.Cq

CONTENTS

---

*Also at Institut für Theoretische Physik IV, Ruhr-Universität Bochum, D-44780 Bochum, Germany; Centre for Fundamental Physics, Rutherford Appleton Laboratory, Chilton, Didcot, Oxon, OX11 0QX, U.K.

I. INTRODUCTION

Nonlinear effects, in which a given phenomenon affects its own evolution and dynamics, are prominent components in a large variety of physical, chemical, and biological systems. The examples range from optical and nerve fibers, and autocatalytic chemical reactions, to ocean waves (Scott, 2003). The field of hydrodynamics has been especially important for the development of nonlinear physics, both concerning analytical and computational tools, since there the nonlinear effects can play a major role in systems with important applications, e.g., meteorology. The subject of plasma physics is a natural generalization of the field of hydrodynamics, since it builds on the fluid or kinetic equations, while adding the electromagnetic interaction. The plasma state of matter is prominent in large regions of the Universe, such as our closest star, the Sun, accretion disks, and even interstellar clouds. It has since long also been noted within the field of plasma physics that both nonlinear effects and collective interactions can give rise to new physical effects, such as the ponderomotive force concept and Landau damping (Hasegawa, 1975). The low-frequency ponderomotive force, which arises due to nonlinear couplings between high-frequency electromagnetic fields, plays a central role in the physics of laser-plasma interactions. This force in an unmagnetized

plasma is expressed as the gradient of the electromagnetic field intensity, which pushes electrons locally and thereby creating large space-charge electric fields and plasma density cavities. Due to the radiation ponderomotive force, one opens the possibility of many interesting nonlinear phenomena in plasmas, e.g., the generation of intense wake fields, stimulated scattering of electromagnetic waves off plasmons and phonons, localization of electromagnetic fields, etc. (Eliezer, 2002). The momentum and energy transfer from the laser field to plasma particles can be harnessed in, e.g., inertial confinement fusion (Eliezer, 2002). Moreover, intense electromagnetic radiation generated in state-of-the-art lasers can be used to model certain astrophysical plasma conditions in a laboratory environment (Remington, 2005). Questions of astrophysical interest that can be approached within the field of high-energy-density laboratory astrophysics range from the equations of state of planetary interiors to supernova shock formation [see HEDLA (2005) for an overview]. In the next generation laser-plasma systems the influence of quantum electrodynamics will become important, and fundamental questions related to the nonlinearity of the quantum vacuum can be approached in laboratory systems (Mourou *et al.*, 2006).

Currently, lasers are capable of reaching intensities of 10^{21}–10^{22} W/cm^2 (Mourou *et al.*, 1998, 2006; Tajima and Mourou, 2002; Tajima, 2003; Bahk *et al.*, 2004). At such high field strengths, the quiver velocity of electrons is highly relativistic, and the radiation pressure, manifesting itself as a ponderomotive force term in the evolution equations for the plasma, gives rise to local electron expulsion. Moreover, at these intensities, the nonlinear relativistic dynamics of the laser-plasma system gives rise to a number of other interesting phenomena as well, such as soliton formation and pulse collapse (Shukla *et al.*, 1986). The latter could be of interest when using laser-plasma systems to generate electromagnetic field intensities approaching the Schwinger intensity limit (Bingham, 2003; Bulanov *et al.*, 2003; Bingham *et al.*, 2004; Cairns *et al.*, 2004; Shukla, Marklund, and Eliasson, 2004; Mourou *et al.*, 2006; Shukla *et al.*, 2005).

The event of future ultrashort (in the femtosecond range) intense (10^{23}–10^{25} W/cm^2) lasers (Mourou *et al.*, 1998, 2006; Tajima and Mourou, 2002; Tajima, 2003) could generate new physics within the next few years (see Fig. 1). This is based on the development of chirped pulse amplification, and the evolution of laser power is predicted to continue evolving for some time (Mourou *et al.*, 1998, 2006). The x-ray free-electron lasers (XFEL) under construction at SLAC (SLAC LCLS, 2005) and DESY (DESY XFEL, 2005) will be a major source of experimental data not achievable with today's systems, ranging from molecular properties (Patel, 2002) to astrophysical conditions (Chen, 2003), such as supernova shocks (Woolsey *et al.*, 2004). The XFEL focus is expected to reach intensities making the quantum vacuum directly accessible for observations (Ringwald, 2001a, 2001b, 2003; see Fig. 3). Moreover, combined effects of laser pulse collapse and ponderomotive force electron
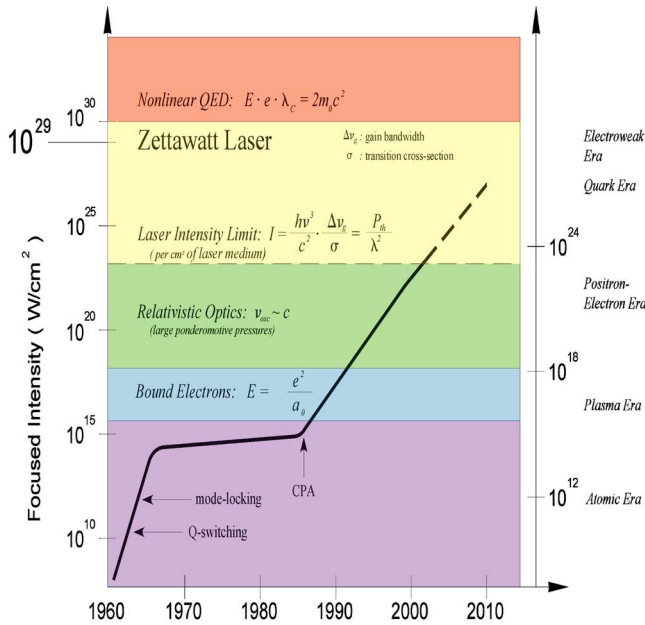
FIG. 1. (Color online) The evolution of laser intensity. Reprinted with permission from Tajima and Mourou, 2002.

FIG. 2. (Color online) The connection between different high-energy regions in physics and experiments. Reprinted with permission from Chen, 2003.

expulsion would create plasma channels in which ultra-high intensity field strengths are reached (Yu *et al.*, 1982), such that the nonlinear vacuum effect of elastic photon-photon scattering become important (Shen and Yu, 2003; Shen *et al.*, 2003).

A majority of studies have not taken into account the influence of electron-positron pair creation or elastic photon-photon scattering on the dynamics of laser-plasma systems [there are, however, important exceptions; see, e.g., Bulanov *et al.* (2005)]. Effects of this kind will be of the utmost importance when laser compression schemes approach the critical field strength

$$E_{\text{crit}} = \frac{m_e c^2}{e \lambda_e} \sim 10^{18} \text{ V/m}, \quad (1)$$

as the nonlinearity of the quantum vacuum becomes pronounced. Here m_e is the electron rest mass, c is the speed of light in vacuum, e is the magnitude of the electron charge, $\lambda_e = \hbar / m_e c$ is the Compton wavelength, and $\hbar$ is the Planck constant divided by 2π. Thus, for such extreme plasma systems, the concept of photon-photon scattering, both elastic and inelastic, has to be taken into account.

The interaction of high-intensity laser pulses with plasmas has applications to other fields of science, e.g., tabletop particle accelerators (Bingham, 2003). Also, achieving field strengths capable of producing pair plasmas in the laboratory could facilitate a means of producing antimatter on a more or less routine basis, as they currently are at high energy accelerators. However, it should be emphasized that the production of pairs from intense lasers requires that severe technical constraints can be overcome, such as phasing of two interacting short electromagnetic pulses. Even if routine pair production via laser systems is not to be reached within the near future, the possibility of directly detecting elastic photon-photon scattering is a fascinating possibility (Soljačić and Segev, 2000b; Brodin *et al.*, 2001). Furthermore, the creation of multidimensional high intensity electromagnetic pulses, using guiding structures (such as plasma boundaries), could result in pulse collapse (Brodin *et al.*, 2003; Shukla, Eliasson, and Marklund, 2004). Such pulse collapse would give rise to intensities close to the Schwinger critical field (1). Thus the combination of laser-plasma interactions and QED effects, such as pair production and photon-photon scattering, could spark new methods for producing conditions reminiscent of astrophysical environments in future experiments (see Fig. 2). In fact, the most pertinent fundamental physics research, such as the question of dark matter [e.g., through the effects of light pseudoscalar fields, such as the axion field, on QED interactions and light propagation, see Bernard (1999); Bradley *et al.* (2003); Dupays *et al.* (2005)], cosmic accelerators [such as through laboratory plasma wakefield accelerator tests (Chen, 2003)], and possible new high-density states of matter (Remington, 2005), are related to the high-energy events for which laboratory astrophysics would yield valuable insight. Thus it is of interest to study such high energy scenarios, e.g., photon-photons scattering in the context of laser-plasma systems (Bulanov, 2004), as these are, in the near future, likely to yield the right conditions for such events to take place.

A. Nonlinear quantum electrodynamics

In classical electrodynamics, as described by Maxwell's equations, photons are indifferent to each other as long as there is no material medium present. This is not so in quantum electrodynamics (QED). Due to the interaction of photons with virtual electron-positron pairs, QED offers the possibility of photon-photon scattering (Heisenberg and Euler, 1936; Schwinger, 1951). This is commonly expressed through the effective-field theory approach represented by the Heisenberg-Euler La-

grangian (Heisenberg and Euler, 1936; Weisskopf, 1936; Schwinger, 1951; Greiner *et al.*, 1985; Grib *et al.*, 1988; Fradkin *et al.*, 1991), neglecting dispersive effects. This Lagrangian [see Eq. (5) below] and its generalizations (Dittrich and Gies, 2000; Valluri *et al.*, 2003; Dunne, 2004) gives nonlinear corrections to Maxwell's vacuum equations, similar to self-interaction terms encountered in nonlinear optics due to the presence of a Kerr medium (Bloembergen, 1996; Agrawal, 2001) and higher-order corrections can be incorporated by taking into account higher vertex order diagrams. Since the lowest-order effective self-interaction term is proportional to the fine-structure constant squared, field strengths need to reach appreciable values until these effects become important, see Eq. (1) (Greiner *et al.*, 1985; Grib *et al.*, 1988; Fradkin *et al.*, 1991). The corrections give rise to single-particle effects, such as closed photon paths (Novello *et al.*, 2001), vacuum birefringence (Heyl and Hernquist, 1997a), photon splitting (Adler, 1971) and lensing effect in strong magnetic fields [see, e.g., Harding (1991); De Lorenci *et al.* (2000)], as well as collective effects, like the self-focusing of beams (Soljačić and Segev, 2000b) or the formation of light bullets (Brodin *et al.*, 2003). Recently, it has also been shown, using analytical means, that these effects give rise to collapsing structure in radiation gases (Marklund *et al.*, 2003), results that have been extended and confirmed by numerical simulations (Shukla and Eliasson, 2004). Possible detection techniques, as well as physical implications, of the effects of photon-photon scattering have attracted interest since first discussed [e.g., Erber (1966); Bialynicka-Birula and Bialynicki-Birula (1970); Tsai (1974a, 1974b); Greiner *et al.* (1985); Grib *et al.* (1988); Ding and Kaplan (1989); Fradkin *et al.* (1991); Latorre *et al.* (1995); Dicus *et al.* (1998); Kaplan and Ding (2000)], and the concept of self-trapping of photons due to vacuum nonlinearities was discussed independently by Rozanov (1993, 1998) and Soljačić and Segev (2000b) in the context of the nonlinear Schrödinger equation.

The above studies assume that the dispersive or diffractive effect of vacuum polarization is negligible, and this, of course, puts constraints on the allowed space and time variations of the fields (Soljačić and Segev, 2000b). In the context of pair creation, rapidly varying fields have been analyzed, since when individual photons pass the pair-creation energy threshold $2m_ec^2$, real electron-positron pairs may be created from the vacuum by a "down-conversion" process of photons. Similar processes are thought to be of importance in the neighborhood of strongly magnetized stars, where the magnetic field induces photon splitting (Erber, 1966; Adler *et al.*, 1970; Adler, 1971; Adler and Shubert, 1996; Baring and Harding, 2001), and may effectively absorb photons (Heyl and Hernquist, 1997a; Duncan, 2002). It has been suggested that the nontrivial refractive index due to photon-photon scattering could induce a lensing effect in the neighborhood of a magnetar (Shaviv *et al.*, 1999).

The physics of elastic photon-photon scattering has interested researchers for a long time, and several suggestions for ways to detect this scattering in the labora-

tory have been made during the last decades (Dewar, 1974; Alexandrov *et al.*, 1985), and the recent increase in available laser intensities have stimulated various schemes (Ding and Kaplan, 1992; Rozanov, 1993, 1998). It has been suggested by Brodin *et al.* (2001, 2002) that the effect of photon-photon scattering could be detected using fields significantly weaker (10 MV/m) than state-of-the-art laser fields.

Next, we present some physical systems in which the effects of photon-photon interactions may either be of importance (magnetars) or become important in the near future (such as state-of-the-art laser-plasma systems).

1. Intense field generation

a. Electromagnetic cavities

High performance, i.e., large electromagnetic fields combined with low dissipative losses, can be found in superconducting cavities, which among other things are used for particle acceleration (Graber, 1993). Waves that can be sustained within such a cavity can have a field strength $E \sim 10$ MV/m, i.e., close to the maximum that can be tolerated by the walls without field emissions. For such cavities, the different high intensity wave modes can act as pump waves for the quantum vacuum. Through the interaction between these waves and virtual electron-positron pairs, new modes with well-defined frequencies and wave numbers will be generated. Those satisfying the dispersion criteria for the given cavity could then also reflect within the cavity with very small losses, thus yielding a method for detection of the quantum vacuum nonlinearities. For example, for a cavity resistance $R \sim 1$ nΩ, corresponding to superconducting niobium at a temperature 1.4 K and a frequency $\omega \sim 2 \times 10^{10}$ rad/s of the wave mode generated via the nonlinear quantum vacuum, one finds that the saturated energy flux P_3 of the generated mode is of the order of 10^{-6} W/m^2 (see Secs. III.A.4 and IV.A.5) (Brodin *et al.*, 2001; Eriksson *et al.*, 2004). This energy flux is above the detection level by several orders of magnitude. However, one should note the importance of superconducting walls for the output level of the excited mode. For copper at room temperature, the cavity resistance increases by a factor $\sim 10^7$ as compared to the above example, and consequently the energy flux of the excited mode falls by a factor $\sim 10^{-14}$. In the latter case, it is questionable whether the excited signal can be detected. Concepts of cavity mode interactions and cavity experiments will be further discussed in Secs. III.A.4 and IV.A.5.

b. Laser development

The event of ultrashort (in the femtosecond range) intense (10^{22}–10^{24} W/cm^2) lasers (Mourou *et al.*, 1998, 2006; Tajima and Mourou, 2002; Tajima, 2003) holds the promise of generating large amounts of new physics within the next few years. This is based on the development of chirped pulse amplification, and the increase of

laser power is predicted to continue for some time (Mourou *et al.*, 1998, 2006). There are two ways for reaching high intensities within laser systems. The method most common is to shorten the pulse duration ($\lesssim 100$ fs), while keeping the energy content in each pulse rather modest (~ 1–10 J). Such pulse generation techniques can have high repetition rates, which can be advantageous in certain experiments where a large number of shots is needed. The other route is to increase the pulse contents while keeping the pulse duration of the order of 0.5–1 ps. Such a system has the advantage of providing a high signal-to-noise ratio for some experiments. The Nova Petawatt laser at the Lawrence Livermore National Laboratory, USA, used this principle, and each pulse, which had a duration of ~ 500 fs, had an energy content of ~ 500 J. Similar systems are operating at ILE/Osaka, Japan (ILE/Osaka, 2005) and the Rutherford Appleton Laboratory, UK, CCLRC (2005). The OMEGA EP laser under construction at the University of Rochester, USA, will also work according to the high-energy principle, and have pulse energies 1–2.6 kJ with durations 1–10 ps (OMEGA EP, 2005). Apart from being a tool for practical use, such as inertial confinement fusion and material science, intense laser facilities are now of international interest for basic research [such as at, e.g., the National Ignition Facility at the Lawrence Livermore National Laboratory (USA), the Laboratory for Laser Energetics at the University of Rochester (USA), the Advanced Photon Research Center (Japan), the Institute for Laser Engineering at Osaka University (Japan), LULI Laboratoire pour l'Utilisation des Lasers Intenses (France), LIL/Laser Mégajoule at CEA (France), or the Central Laser Facility, Rutherford Appleton Laboratory (UK)], and the increased laser output power also gives the opportunity to obtain astrophysical energy scales in a controlled laboratory setting (Chen, 2003; HEDLA, 2005; Remington, 2005).

The generation of high (electromagnetic) field strengths is at the heart of understanding a variety of phenomena, such as astrophysical shocks and jets, in a laboratory setting, and furthermore forms the basis for a number of applications, e.g., tabletop plasma accelerators. Thus schemes and mechanisms for generating such high fields, other than the direct laser pumping, will be of importance to the development of a wide range of scientific areas.

c. Free-electron laser

The x-ray free-electron laser (XFEL) is an alternative to the current laser generation techniques, and it has as its base the particle accelerator, where high-energy electrons are generated to obtain high-frequency radiation (DESY XFEL, 2005; SLAC LCLS, 2005). Within these lasers, a large number of coherent photons are generated (ten orders of magnitude more than regular synchrotron sources). The XFEL concept has a wide variety of interesting applications, among these the possibility to probe the structure of large molecules, commonly found within molecular biological systems (Patel, 2002).
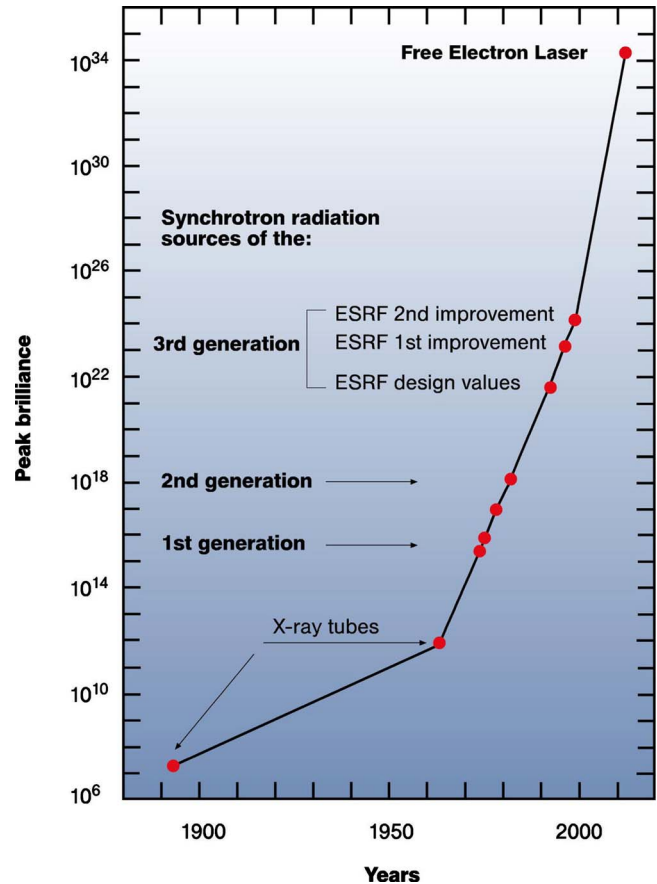
FIG. 3. (Color online) Evolution of peak brilliance, in units of photons/(s mrad^2 mm^2 0.1 % $\times$ bandwidth), of x-ray sources. Here, ESRF stands for the European Synchrotron Radiation Facility in Grenoble. (Source: DESY Hamburg, http://xfel.desy.de/)

It is also hoped that XFEL could form the basis of electron-positron pair creation (Alkhofer *et al.*, 2001; Ringwald, 2001a; Roberts *et al.*, 2002). Both at the TESLA collider at DESY and LCLS at SLAC, the energy density at the focus (with a spatial width $\sim 10^{-10}$ m and on the time scale 10^{-13} s) of the XFEL is expected to reach energy densities of 10^{29} J/m^3 (Ringwald, 2001a), see Fig. 3. This corresponds to electric-field strengths of the order 10^{20} V/m, i.e., two orders of magnitude above the Schwinger critical field (1), at which pair creation is expected to take place. The possibility to "fuel" the generation of electron-positron pairs by nonlinear effects is a promising prospect, and as some authors have noted this essentially amounts to "boiling the vacuum" (Ringwald, 2001b, 2003). Moreover, it is believed that nonlinear QED effects will be an important component of the interaction of XFEL generated radiation with dense media. Therefore it is of interest to achieve an understanding of the influence of those nonlinear effects within the parameter regime obtainable by the XFEL.

2. Laser-plasma systems

High laser powers generate enormous radiation pressures, and accelerate particles to relativistic velocities.

Fields generated by particles will therefore backscatter and create a nonlinear feedback, something which can give rise to, e.g., laser pulse compression and electron density cavitation. This may play a significant role in different proposed schemes of laser self-focusing (Bulanov *et al.*, 2003; Shorokhov *et al.*, 2003; Shukla *et al.*, 2005), completely changing the dynamics of suggested methods and altering final results in nontrivial ways. This serves as an important example of nonlinear effects in the evolution of laser-plasma systems.

The interaction of high power lasers, reaching intensities of 10^{20}–10^{22} W/cm^2, with plasmas has long been the backbone in different schemes for tabletop particle accelerators (Bingham, 2003), and is also essential for the concept of inertial confinement fusion (Eliezer, 2002). The ponderomotive force generated in high power laser-plasma systems due to laser intensity gradients may give rise to a plethora of phenomena, such as laser pulse self-focusing and filamentation, soliton formation, parametric instabilities, and magnetic-field generation [see Eliezer (2002), and references therein].

Laser-plasma systems have been suggested as sources of high intensity radiation. Due to the laser ponderomotive force plasma electrons will be pushed out of the path of the laser pulse, trapping and compressing the laser pulse, such that further electrons are pushed out. The plasma can sustain high-field strengths, and the pulse compression can therefore reach appreciable intensity values (Mourou *et al.*, 2006). In fact, using a Langmuir wave as a plasma "mirror" for the laser pulse, pulse intensities could reach, and even surpass, the Schwinger critical field (1) (Bulanov *et al.*, 2003; Mourou *et al.*, 2006). Thus the interaction between intense lasers and plasmas is an intriguing tool for generating pulse intensities above the laser limit (Mourou *et al.*, 1998).

3. Astrophysical and cosmological environments

Astrophysical environments and events display enormous energy releases. Supernova explosions, black-hole accretion, magnetar, and pulsar systems are a few examples of such extreme situations. Moreover, the energy scales in the early Universe are equally immense, or even greater, and our understanding of the origin of the Universe is hampered by the fact that the energy density scales are so far from anything that can be generated in a laboratory, except perhaps in relativistic heavy-ion collisions (RHIC, 2005). It is therefore not surprising that these environments can often act as laboratories for phenomena that we currently do not have technology to reproduce in Earth-based laboratories. Quantum electrodynamical nonlinear vacuum effects have received a fair amount of attention in strongly magnetized systems, such as pulsars (Curtis, 1982; Beskin *et al.*, 1993) and magnetar environments (Harding, 1991; Kouveliotou *et al.*, 1998). The magnetic-field strengths of magnetars can reach energy levels comparable to, or even surpassing, the energy corresponding to the Schwinger critical field strength 10^{18} V/m, thus making the vacuum truly nonlinear [nonlinear QED effects in the magnetized vacuum

are described in a number of publications, and for a representative but incomplete list, see Erber (1966); Adler *et al.* (1970); Adler (1971); Tsai (1974a, 1974b); Mentzel *et al.* (1994); Adler and Shubert (1996); Baier *et al.* (1996); Chistyakov *et al.* (1998), and references therein]. The effect of a nonlinear vacuum may even be of crucial importance for our understanding of these objects (Baring and Harding, 2001).

II. EFFECTIVE-FIELD THEORY OF PHOTON-PHOTON SCATTERING

The development of quantum electrodynamics was the result of a long and collective effort, and paved the way for an understanding of weak and strong forces as well. It has, since its advent, been confirmed to an unprecedented accuracy, compared to any physical theory. It solved some of the long-standing conceptual problems of relativistic quantum theory, as proposed by Dirac and others, and it furthermore changed the way we look at elementary interactions between particles and fields. The theoretical proposal, due to Dirac, of antimatter as a result of relativistic quantum theory was put on a firm foundation with QED.

The quantization of the vacuum has lead to remarkable insights and discoveries. Consider, for example, the Casimir effect (Casimir, 1948; Casimir and Polder, 1948),[1] in which two parallel conducting plates with area A are separated by a distance d. Due to the different boundary conditions between and outside the plates, there will be a net attractive force $F \propto A/d^4$ between the plates. In a heuristic sense, the vacuum between the plates is "emptier" than outside, since fewer states are allowed due to the finite distance between the plates. Related to this is the much debated Scharnhorst effect (Barton, 1990; Scharnhorst, 1990, 1998; Barton and Scharnhorst, 1993), at which the phase (and group) speed exceeds the speed of light c in vacuum. As demonstrated later, the opposite occurs in the electromagnetic vacuum, i.e., phase and group velocities decrease due to the electromagnetic influence on the quantum vacuum.

In conjunction with any description of photon-photon scattering, it should also be mentioned the large amount of literature and interest in finite-temperature effective-field theory effects. Thermal effects generalize the classical results of Schwinger in the weak-field limit (Heisenberg and Euler, 1936; Weisskopf, 1936; Schwinger, 1951). It was pioneered by Dittrich (1979) who investigated thermal effects in combination with an external mag-

---

[1]Casimir considered particle-particle and particle-plate (Casimir and Polder, 1948), and plate-plate systems (Casimir, 1948), since the problem stemmed from research on colloidal solutions, but is most clearly represented by the parallel plate example. The Casimir effect has since been confirmed by many different experiments [see, e.g., Sukenik *et al.* (1993); Mostepanenko and Trunov (1997); Lamoreaux (1998); Bordag *et al.* (2001); Bressi *et al.* (2002); Harber *et al.* (2005), and references therein].
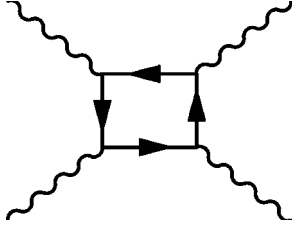
FIG. 4. The Feynman box diagram for the lowest-order photon-photon scattering at the one-loop level.

netic field, and later a comprehensive study using the real time formalism in the case of a general electromagnetic field background was performed by Elmfors and Skagerstam (1995) [see also Gies (1999a)]. The dispersion relation, including dispersive effects, was discussed by Gies (1999b), and it was later shown that in a thermal vacuum, in contrast to the nonthermal one, two-loop corrections dominate over one-loop effects (Gies, 2000). However, treating these studies (we have by no means exhausted the list of papers here) in detail is outside the scope of the present paper, and since we, moreover, are interested in the problem of collective effects, the treatment of thermal effects, although of interest, is left for a future review.

A. Concept of elastic scattering among photons

Photon-photon scattering is a nonclassical effect arising in quantum electrodynamics (QED) due to virtual electron-positron pairs in vacuum; see Fig. 4. In the low-energy limit, i.e., $\hbar\omega\ll m_ec^2$, the magnitude of photon-photon scattering can be described in terms of the differential cross section (Berestetskii *et al.*, 1982)

$$\frac{d\sigma_{\gamma\gamma}}{d\Omega} = \frac{139\alpha^2 r_e^2}{32\,400\pi^2}(3+\cos^2\theta)\left(\frac{\hbar\omega}{m_ec^2}\right)^6, \tag{2}$$

where ω is the photon frequency in the center-of-mass system, r_e is the classical electron radius, and $\alpha = e^2/4\pi\epsilon_0\hbar c \approx 1/137$ is the fine-structure constant. Integrating Eq. (2) gives the total cross section

$$\sigma_{\gamma\gamma} = \frac{973\alpha^2 r_e^2}{10\,125}\left(\frac{\hbar\omega}{m_ec^2}\right)^6 \approx 0.7\times10^{-65}\left(\frac{\hbar\omega}{1\text{ eV}}\right)^6\text{ cm}^2. \tag{3}$$

We note that the cross section decreases fast with decreasing photon energy. In the high-energy limit, the cross section, on the other hand, goes as ω^{-2}. The cross section reaches a maximum of $\sigma_{\gamma\gamma}\approx 2\times10^{-30}$ cm^2 for photon energies $\hbar\omega\sim m_ec^2$ (Berestetskii *et al.*, 1982), indeed a very small number.

Instead of a microscopic description, interactions of photons may be described by an effective-field theory. Formulated in terms of such an effective-field theory, using the Heisenberg-Euler Lagrangian [valid in the long-wavelength and weak-field limit, see Eq. (4)] (Heisenberg and Euler, 1936; Schwinger, 1951), this results in nonlinear corrections to Maxwell's vacuum equa-

tions, which to lowest order in the fine-structure constant are cubic in the electromagnetic (EM) field. These corrections take the same form as in nonlinear optics, where the material properties of, e.g., optical fibers, give rise to cubic nonlinear terms in Maxwell's equations, so-called Kerr nonlinearities (Agrawal, 2001; Kivshar and Agrawal, 2003). Since the effective self-interaction term is proportional to the fine-structure constant squared, this means that field strengths under most circumstances need to reach values close to the critical field (1) until these effects becomes important (Greiner *et al.*, 1985; Grib *et al.*, 1988; Fradkin *et al.*, 1991). With this at hand, we now focus on the concept of photon-photon scattering.

B. Weak-field limit

We first derive the general dispersion relation in the low photon energy and weak-field limit, assuming [see Eq. (1)]

$$\omega \ll \omega_e \equiv m_ec^2/\hbar \quad\text{and}\quad |\mathbf{E}| \ll E_{\text{crit}}, \tag{4}$$

where E_{crit} is given by Eq. (1), and $\omega_e\approx8\times10^{20}$ rad/s is the Compton frequency. When these constraints are valid, pair creation, due to both single photons and collective effects, will be unimportant, and the effective Lagrangian may therefore be treated solely in terms of its real part. It should be remembered that the second of these constraints comes from the pair-creation probability of Schwinger (Schwinger, 1951), which was derived for a pure electric field and may therefore not strictly be applied to the case of a radiation gas. Thus this investigation goes far beyond the description of the thermodynamics of nonlinearly interacting incoherent photons with a photon gas in a plasma environment (Tsintsadze and Mendonça, 1998).

Photon-photon scattering is a second-order effect (in terms of the fine-structure constant α), and for constant or weakly varying fields it can be formulated in standard notation using the Euler-Heisenberg Lagrangian density (Heisenberg and Euler, 1936; Schwinger, 1951)

$$\mathcal{L} = \mathcal{L}_0 + \mathcal{L}_c = \epsilon_0\mathcal{F} + \epsilon_0^2\kappa(4\mathcal{F}^2 + 7\mathcal{G}^2), \tag{5}$$

where

$$\kappa \equiv \frac{2\alpha^2\hbar^3}{45m_e^4c^5} = \frac{\alpha}{90\pi}\frac{1}{\epsilon_0 E_{\text{crit}}^2} \approx \frac{1}{3\times10^{29}\text{ J/m}^3}. \tag{6}$$

Moreover, the field invariants are defined in terms of the field tensor F_{ab} according to

$$\mathcal{F} \equiv \tfrac{1}{4}F_{ab}F^{ab} = \tfrac{1}{2}(c^2\mathbf{B}^2 - \mathbf{E}^2),$$

$$\mathcal{G} \equiv \tfrac{1}{4}F_{ab}\hat{F}^{ab} = -c\mathbf{E}\cdot\mathbf{B}, \tag{7}$$

$\hat{F}^{ab} = \epsilon^{abcd}F_{cd}/2$, and $\mathcal{F}^2$ and $\mathcal{G}^2$ are the lowest-order QED corrections. We note that $\mathcal{F}=\mathcal{G}=0$ in the limit of parallel propagating waves. The latter terms in Eq. (5) represent the effects of vacuum polarization and magne-

tization, and the QED corrected Maxwell's vacuum equations take the classical form, using

$$\mathbf{D} = \epsilon_0 \mathbf{E} + \mathbf{P}, \quad \mathbf{H} = \frac{1}{\mu_0} \mathbf{B} - \mathbf{M}, \tag{8}$$

where $\mathbf{P}$ and $\mathbf{M}$ are of third order in the field amplitudes $\mathbf{E}$ and $\mathbf{B}$ [see Eqs. (11) and (12) below], and $\mu_0 = 1/c^2\epsilon_0$. Furthermore, they contain terms $\mathcal{F}$ and $\mathcal{G}$ such that $\mathbf{P} = \mathbf{M} = 0$ in the limit of parallel propagating waves. It is therefore necessary to use nonparallel waves in order to obtain an effect from these QED corrections.

From the constituent relations (8) we can deduce the general wave equations for $\mathbf{E}$ and $\mathbf{B}$ according to

$$\frac{1}{c^2}\frac{\partial^2 \mathbf{E}}{\partial t^2} - \nabla^2 \mathbf{E} = -\mu_0 \left[\frac{\partial^2 \mathbf{P}}{\partial t^2} + c^2 \nabla(\nabla \cdot \mathbf{P}) + \frac{\partial}{\partial t}(\nabla \times \mathbf{M}) \right], \tag{9}$$

and

$$\frac{1}{c^2}\frac{\partial^2 \mathbf{B}}{\partial t^2} - \nabla^2 \mathbf{B} = \mu_0 \left[\nabla \times (\nabla \times \mathbf{M}) + \frac{\partial}{\partial t}(\nabla \times \mathbf{P}) \right]. \tag{10}$$

Furthermore, the effective polarization and magnetization, appearing in Eq. (8), in vacuum due to photon-photon scattering induced by the exchange of virtual electron-positron pairs can be obtained from the Lagrangian (5) and are given by [see, e.g., Soljačić and Segev (2000b)]

$$\mathbf{P} = 2\kappa\epsilon_0^2[2(E^2 - c^2B^2)\mathbf{E} + 7c^2(\mathbf{E} \cdot \mathbf{B})\mathbf{B}] \tag{11}$$

and

$$\mathbf{M} = 2\kappa\epsilon_0^2 c^2[-2(E^2 - c^2B^2)\mathbf{B} + 7(\mathbf{E} \cdot \mathbf{B})\mathbf{E}]. \tag{12}$$

Equations (9)–(12) offer the starting point for the study of a weakly nonlinear electromagnetic vacuum in terms of the classical field strength vectors $\mathbf{E}$ and $\mathbf{B}$.

The correction in the Lagrangian (5) is the power-series expansion in the field strengths of the full one-loop correction given by (Heisenberg and Euler, 1936; Weisskopf, 1936; Schwinger, 1951)

$$\mathcal{L}_c = -\frac{\alpha}{2\pi}\epsilon_0 E_{\text{crit}}^2 \int_0^{i\infty} \frac{dz}{z^3} e^{-z}$$

$$\times \left[z^2 \frac{ab}{E_{\text{crit}}^2} \coth\left(\frac{a}{E_{\text{crit}}}z\right) \cot\left(\frac{b}{E_{\text{crit}}}z\right) \right.$$

$$\left. - \frac{z^2}{3}\frac{(a^2 - b^2)}{E_{\text{crit}}^2} - 1 \right], \tag{13}$$

where

$$a = [(\mathcal{F}^2 + \mathcal{G}^2)^{1/2} + \mathcal{F}]^{1/2}, \quad b = [(\mathcal{F}^2 + \mathcal{G}^2)^{1/2} - \mathcal{F}]^{1/2}. \tag{14}$$

Thus $\mathcal{F} = (a^2 - b^2)/2$ and $|\mathcal{G}| = ab$. The Lagrangian correction (13) is the starting point of the effective-field theory analysis of a strongly nonlinear quantum vacuum, such as used in studies of photon splitting [see Dittrich and Gies (1998, 2000), and references therein], and defining

some of the properties of a strongly nonlinear gas of photons (Marklund, Shukla, and Eliasson, 2005).

C. Dispersion function

One may find the dispersion relation of photons in an arbitrary constant, or weakly varying, electromagnetic background (Bialynicka-Birula and Bialynicki-Birula, 1970; De Lorenci *et al.*, 2000; Thoma, 2000). Starting from the Lagrangian (5), introducing the four-potential A^b such that $F_{ab} = \partial_a A_b - \partial_b A_a$, the Maxwell equations resulting from the variation with respect to the four-potential becomes

$$\partial_a F^{ab} = 2\epsilon_0\kappa\partial_a[(F_{cd}F^{cd})F^{ab} + \tfrac{7}{4}(F_{cd}\hat{F}^{cd})\hat{F}^{ab}], \tag{15}$$

where we adopt the convention $(-1,1,1,1)$ for the metric η_{ab}, used for raising and lowering four-indices $a, b, \ldots = 0, 1, 2, 3$. Next, assuming that $F_{ab} = f_{ab} + \phi_{ab}$, where f_{ab} denotes the varying background field, and ϕ_{ab} ($\ll f_{ab}$) is a weak field propagating on this background, we find that the background satisfies $\partial_a f^{ab} = 0$, and $\partial_a \hat{F}^{ab} = 0$ is identically satisfied due to the definition of F_{ab} in terms of the four-potential A^b.

Linearizing Eq. (15) with respect to ϕ, and Fourier decomposing perturbations according to $\phi_{ab}(x) = (k_a\epsilon_b - k_b\epsilon_a)\exp(ik\cdot x) + \text{c.c.}$, where ϵ_a is the polarization vector, $k\cdot x \equiv k_a x^a$ and c.c. denotes the complex conjugate, we obtain the following algebraic set of equations for the polarization vector:

$$M_{ab}^0 \epsilon^b = [k^2 g_{ab} - k_a k_b - \kappa\epsilon_0(8a_a a_b + 14\hat{a}_a\hat{a}_b)]\epsilon^b = 0, \tag{16}$$

where $a_b \equiv f_{bc}k^c$ and $\hat{a}_b \equiv \hat{f}_{bc}k^c$ has the properties $k^b a_b = k^b \hat{a}_b 0$. From this it follows that $M_{ab}^0 k^b = 0$ and the polarization may therefore, without loss of generality, be taken to obey $\epsilon_b k^b = 0$, corresponding to the Lorentz gauge. In order to simplify the analysis, it is assumed that the background is slowly varying in spacetime compared to the perturbation. Using a_b and $\hat{a}_b$ as the polarization eigenvectors gives two equations,

$$k^2 = 8\kappa\epsilon_0 f_{ab}f^{ac}k^b k_c \quad \text{and} \quad k^2 = 14\kappa\epsilon_0 f_{ab}f^{ac}k^b k_c, \tag{17}$$

from Eq. (16) for the polarization a^a and $\hat{a}^a$, respectively. Since we can decompose $f_{ab} = u_a E_b - u_b E_a + \epsilon_{abc}B^c$ for an observer with four-velocity u^a, we have

$$a^2 = -(\mathbf{k} \cdot \mathbf{E})^2 - c^2(\mathbf{k} \cdot \mathbf{B})^2 + \omega^2\mathbf{E}^2 + c^2\mathbf{k}^2\mathbf{B}^2$$
$$- 2c\omega\mathbf{k} \cdot (\mathbf{E} \times \mathbf{B}) \tag{18}$$

and $\hat{a}^2 \approx a^2$. Equations (17) can be written in the clear and compact form (Bialynicka-Birula and Bialynicki-Birula, 1970),

$$\omega \approx c|\mathbf{k}|(1 - \tfrac{1}{2}\lambda|\mathbf{Q}|^2), \tag{19}$$

where λ is 8κ or 14κ, respectively, depending on the polarization state of the photon, and

$$|\mathbf{Q}|^2 \equiv \epsilon_0|\hat{\mathbf{k}} \times \mathbf{E} + c\hat{\mathbf{k}} \times (\hat{\mathbf{k}} \times \mathbf{B})|^2$$

$$= \epsilon_0[\mathbf{E}^2 + c^2\mathbf{B}^2 - (\hat{\mathbf{k}} \cdot \mathbf{E})^2 - c^2(\hat{\mathbf{k}} \cdot \mathbf{B})^2$$

$$- 2c\hat{\mathbf{k}} \cdot (\mathbf{E} \times \mathbf{B})]. \tag{20}$$

Here the hat denotes the unit vector. Equation (19) is valid for arbitrary, slowly varying background fields. It is straightforward to show that Eq. (20) vanishes in the case of a self-interacting plane-wave field. Two different possible polarization directions can be given in a similar manner [see Bialynicka-Birula and Bialynicki-Birula (1970)].

D. Corrections due to rapidly varying fields

As shown in the previous section, it is possible to derive a dispersion relation for photons moving in a given background field. However, field variations were neglected, and in order to take them into account a modified weak-field Lagrangian must be used.

It is well known that the weak-field theory of photon-photon scattering can be formulated using the effective Lagrangian density $\mathcal{L} = \mathcal{L}_0 + \mathcal{L}_{HE} + \mathcal{L}_D$, where $\mathcal{L}_0$ is the classical free-field Lagrangian $\mathcal{L}_{HE}$ is the Heisenberg-Euler correction as given in Eq. (5). The derivative corrections are given by (Mamaev $et\ al.$, 1981)

$$\mathcal{L}_D = \sigma\epsilon_0[(\partial_a F^{ab})(\partial_c F^c_b) - F_{ab} \square F^{ab}], \tag{21}$$

where $\square = \partial_a \partial^a$ and $\sigma = (2/15)\alpha c^2/\omega_e^2 \approx 1.4 \times 10^{-28}$ m^2. As we have seen in the dispersion relation (19), the parameter κ gives the nonlinear coupling. Here we find that the parameter σ gives dispersive effects in the polarized vacuum. Physically setting the parameter $\sigma \neq 0$ corresponds to taking correction due to rapidly varying perturbation into account. Since the Compton frequency is $\sim 10^{20}$ rad/s, we see that $\omega/\omega_e \ll 1$ in most applications. Thus the dispersive term is normally a small correction.

In the previous section, the requirement (4) was assumed to be satisfied. Here even though we include effects of the rapidly varying fields, we require that there is no electron-positron pair creation, neither by single photons nor by collective effects, i.e., the conditions (4) should still hold. Furthermore, dispersive or diffractive effects must be small, otherwise the limit of weak fields would imply unphysical branches in the dispersion relation (Rozanov, 1998).

As in the previous section, we set $F_{ab} = \partial_a A_b - \partial_b A_a$, and obtain field equations from the Euler-Lagrange equations $\partial_b[\partial\mathcal{L}/\partial F_{ab}] = 0$. Thus we have (Rozanov, 1998; Shukla, Marklund, Tskhakaya, $et\ al.$, 2004)

$$\tfrac{1}{2}(1 + 2\sigma \square)\partial_a F^{ab} = \epsilon_0\kappa\partial_a[(F_{cd}F^{cd})F^{ab}$$

$$+ \tfrac{7}{4}(F_{cd}\hat{F}^{cd})\hat{F}^{ab}]. \tag{22}$$

Equation (22) describes the nonlinear evolution of the electromagnetic field through the nonlinear dispersive vacuum. We note that when $\sigma, \kappa \to 0$, we obtain the classical Maxwell's equations, as we should.

Repeating the procedure leading up to Eq. (16), we find the corresponding expression in the case of a dispersive vacuum,

$$M_{ab}\epsilon^b = [M^0_{ab} - 2\sigma k^2(k^2 g_{ab} - k_a k_b)]\epsilon^b = 0, \tag{23}$$

where M^0_{ab} is given by Eq. (16). With a_b and $\hat{a}_b$ as the principal polarization direction, Eq. (23) yields

$$(1 - 2\sigma k^2)k^2 = 8\kappa\epsilon_0 f_{ab}f^{ac}k^b k_c \tag{24a}$$

and

$$(1 - 2\sigma k^2)k^2 = 14\kappa\epsilon_0 f_{ab}f^{ac}k^b k_c, \tag{24b}$$

for the two different polarizations a_b and $\hat{a}_b$, respectively. When $\sigma = 0$, Eqs. (24) reduce to Eqs. (17), which yield the dispersion relation (19). With $\sigma \neq 0$, we may use Eq. (19) in the dispersive term of Eqs. (24). Thus the final dispersion relation is of the form (Rozanov, 1998; Shukla, Marklund, Tskhakaya, $et\ al.$, 2004)

$$\omega \approx c|\mathbf{k}|[1 - \tfrac{1}{2}\lambda|\mathbf{Q}|^2(1 + 2\sigma\lambda|\mathbf{Q}|^2|\mathbf{k}|^2)], \tag{25}$$

where $|\mathbf{Q}|^2$ is given by Eq. (20). Thus we see that the effect of the dispersive parameter is, as expected, to make ω a nonlinear function of $\mathbf{k}$.

E. Special cases of weak-field dispersion

1. Magnetized background

In the case of a background magnetic field $\mathbf{B}_0$, the dispersion relation (19) becomes (Erber, 1966; Adler $et\ al.$, 1970; Adler, 1971; Adler and Shubert, 1996; Dittrich and Gies, 1998)

$$\omega \approx c|\mathbf{k}|(1 - \tfrac{1}{2}\lambda\epsilon_0 c^2|\mathbf{B}_0|^2\sin^2\theta), \tag{26}$$

where θ is the angle between the background magnetic field $\mathbf{B}_0$ and the wave vector $\mathbf{k}$. Thus photons propagating parallel to the background magnetic field will not experience any refractive effects, while a maximum refraction is obtained for perpendicular propagation. This dispersion relation will be relevant for photon propagation in pulsar magnetospheres and in magnetar environments, where, for example, the vacuum becomes birefringent (Tsai and Erber, 1975; Heyl and Hernquist, 1997a). This in turn may affect the optical depth of neutron star thermal emission, and thereby also influence the interpretation of pulsar observations (Lodenqual $et\ al.$, 1974; Ventura, 1979; Heyl and Shaviv, 2002; Heyl $et\ al.$, 2003).

For a magnetar with surface field strength $|\mathbf{B}_0| = 10^{11}$ T (Kouveliotou $et\ al.$, 1998), the field has the energy density $\epsilon_0 c^2|\mathbf{B}_0|^2 \approx 8 \times 10^{27}$ J/m^3. Since $\lambda \sim 10\kappa \approx 1/(3 \times 10^{28}$ J/m$^3)$ [see Eqs. (6) and (19)], we find from Eq. (26) that the phase velocity $v = \omega/|\mathbf{k}|$ satisfies $v/c \approx 1 - 0.13 \sin^2\theta$. However, the magnetar field strength does not qualify as a weak field, and one may question if it is appropriate to use Eq. (26) in this case (see Sec. II.F.1).

2. Random photons in a magnetic field

From the previous example, the effect of a magnetic field on the thermal or random distribution of photons could be observationally important. Thus for a random ensemble of photons in a strong magnetic field we have a direction-independent dispersion relation

$$\omega \approx c|\mathbf{k}|(1 - \tfrac{1}{3}\lambda\epsilon_0 c^2|\mathbf{B}_0|^2). \tag{27}$$

We note that the value of the effective action charge λ depends on the polarization of thermal photons. As the crust of magnetars is subject to enormous stresses due to immense field strengths [$\sim 10^{10}$–10^{11} T (Kouveliotou *et al.*, 1998)], it will suffer from crust quakes, at which bursts of low-frequency random photons are released (Kondratyev, 2002). In such a scenario, the above dispersion relation may be of relevance.

3. Random photons in a plane-wave field

Analogously, we may treat the case of incoherent photons on an intense plane-wave background $\mathbf{E}_p$. Then, in the equilibrium state of the radiation gas the propagation directions of the photons in the gas are random and the EM pulse is a superposition of unidirectional plane waves such that $\mathbf{B}_p = \hat{\mathbf{k}}_p \times \mathbf{E}_p/c$. Thus we obtain the direction-independent dispersion relation

$$\omega \approx c|\mathbf{k}|(1 - \tfrac{2}{3}\lambda\epsilon_0|\mathbf{E}_p|^2). \tag{28}$$

Equation (28) is the proper dispersion relation to use in some laser-plasma interaction applications, where a large number of incoherent photons are produced (Bingham, 2003; Bingham *et al.*, 2004; Cairns *et al.*, 2004).

4. Radiation gas background

Consider a single photon transversing a dense background radiation gas with energy density $\mathcal{E}$. Then the dispersion relation can be written as (Dittrich and Gies, 2000; Marklund *et al.*, 2003)

$$\omega \approx c|\mathbf{k}|(1 - \tfrac{2}{3}\lambda\mathcal{E}). \tag{29}$$

As one considers higher redshifts z, the cosmic microwave background will increase in energy density, since $\mathcal{E}(z) = (1+z)^4 \mathcal{E}_0$ [we note that radiation decouples from matter at a redshift $\sim 10^3$ (Peacock, 1998)], where $\mathcal{E}_0 = aT_0^4$ denotes the current energy density and $a = 8\pi^5 k_B^4/15h^3c^3 \approx 7.6\times10^{-16}$ J/m^3 K^4 is the radiation constant. Thus Eq. (29) gives $v/c = 1 - (2/3)\lambda a(1+z)^4 T_0^4$, for the phase velocity v. Using $T_0 = 2.7$ K, a correction of 10% to the phase velocity in vacuum is obtained for a redshift $z_c \sim 10^{10}$, i.e., roughly at the time for neutrino-matter decoupling (Peacock, 1998).

Including the dispersive correction, as given by Eq. (25), the dispersion relation for a background of incoherent photons takes the form

$$\omega \approx c|\mathbf{k}|[1 - \tfrac{2}{3}\lambda\mathcal{E}(1 + \tfrac{8}{3}\sigma\lambda\mathcal{E}|\mathbf{k}|^2)], \tag{30}$$

i.e., high-frequency pulses may suffer spectral dilution when propagating through a radiation gas.

5. Other field configurations
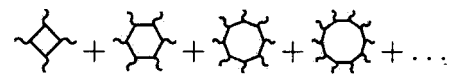
Similar dispersion relations can be found for other background field configurations, e.g., plane-wave backgrounds or partially coherent electromagnetic fields, as is relevant in ultrahigh intensity laser applications. Of special interest for detection purposes is the configuration of photon propagation perpendicular to a collection of constant electric and magnetic fields (Bakalov *et al.*, 1998; Rikken and Rizzo, 2000, 2003).

We should also note that in the above cases the group and phase velocities of test photons are subluminal, as expected, since we have excited the quantum vacuum by using electromagnetic fields, analogous to a normal dispersive material medium. This can be contrasted with the Scharnhorst effect (Barton, 1990; Scharnhorst, 1990, 1998; Barton and Scharnhorst, 1993), for which we obtain superluminal phase and group velocities between two conducting plates. This can be traced back to the Casimir effect (Casimir, 1948; Casimir and Polder, 1948), where the quantization between two conducting plates allows fewer states than for fields with boundary conditions at infinity. Thus, in this sense, the vacuum between the plates is "emptier" than outside, giving rise to super-luminal velocity.

F. Ultraintense fields

The dispersion relations treated so far have used the weak-field expansion of the general Heisenberg-Euler correction (13). However, both from an application point of view and due to theoretical issues, the inclusion of fully nonlinear vacuum effects deserves attention [see also Dittrich and Gies (2000) for a thorough discussion of the strong magnetic-field case].

Within astrophysical and cosmological settings, such as neutron stars and magnetars (Kouveliotou *et al.*, 1998), strong-field conditions can be met. Even in laboratory environments, such conditions could be encountered in future high-energy laser configurations. While today's lasers can produce 10^{21}–10^{22} W/cm^2 (Mourou *et al.*, 1998), it is expected that the next generation laser-plasma systems could reach 10^{25} W/cm^2 (Bingham, 2003; Bingham *et al.*, 2004; Cairns *et al.*, 2004), where field strengths close to the Schwinger critical value could be reached (Bulanov *et al.*, 2003). Thus nonlinear effects introduced by photon-photon scattering will be significant, and the weak-field approximation no longer holds. In terms of Feynman diagrams the discussion to follow will consider the full one-loop correction,

$$\tag{31}$$

The general dispersion relation for a test photon in a vacuum dressed by a strong electromagnetic field is given by (Dittrich and Gies, 1998)

$$[1 + \tfrac{1}{2}\lambda\epsilon_0(\mathbf{E}^2 + c^2\mathbf{B}^2)]\frac{v^2}{c^2} - 2\lambda\epsilon_0 c\hat{\mathbf{k}} \cdot (\mathbf{E} \times \mathbf{B})\frac{v}{c}$$

$$+ \lambda\epsilon_0[\tfrac{1}{2}(\mathbf{E}^2 + c^2\mathbf{B}^2) - (\hat{\mathbf{k}} \cdot \mathbf{E})^2 - c^2(\hat{\mathbf{k}} \cdot \mathbf{B})^2] = 1, \tag{32}$$

where $v = \omega/|\mathbf{k}| \equiv c/n$ is the photon phase velocity and n is the refractive index. The effective action charge λ is no longer a constant, but instead defined through (Dittrich and Gies, 1998)

$$\lambda = \frac{1}{\epsilon_0}\frac{(\partial_\mathcal{F}^2 + \partial_\mathcal{G}^2)\mathcal{L}}{-2\partial_\mathcal{F}\mathcal{L} + \mathcal{F}(\partial_\mathcal{F}^2 + \partial_\mathcal{G}^2)\mathcal{L} - 2(\mathcal{F}\partial_\mathcal{F}^2 + \mathcal{G}\partial_{\mathcal{F}\mathcal{G}}^2)\mathcal{L}}. \tag{33}$$

In many cases, the part of the denominator of Eq. (33) stemming from the nonlinear QED correction (13) can be neglected, since it will be much smaller than the remaining terms, even for fields $\gg E_{\mathrm{crit}}$.

1. Pure magnetic field

The case of pure magnetic fields enables a simplification of the evaluation of the Lagrangian (13). The refractive index for a strongly magnetized vacuum can be determined in terms of special functions. For a pure magnetic field $\mathbf{B}_0$, we obtain using Eq. (14) that $a = c|\mathbf{B}_0|$ and $b = 0$, respectively. Dittrich and Gies (1998) [see also Dittrich and Gies (2000)], starting from the Lagrangian (13), devised the general expression (33) for the effective action charge λ [also found in the work of, e.g., Bialynicka-Birula and Bialynicki-Birula (1970)].

Using $a = c|\mathbf{B}_0|$, $b = 0$, and the approximation $\lambda \approx (\partial_\mathcal{F}^2 + \partial_\mathcal{G}^2)\mathcal{L}/2\epsilon_0$ [see Eq. (33)], the effective action charge takes the form

$$\lambda = \frac{\alpha}{2\pi\epsilon_0 c^2|\mathbf{B}_0|^2}\left[\left(2x^2 - \frac{1}{3}\right)\psi(1 + x) - x - 3x^2\right.$$

$$\left. - 4x\ln\Gamma(x) + 2x\ln 2\pi + \frac{1}{6} + 4\zeta'(-1, 4x) + \frac{1}{6x}\right], \tag{34}$$

where $x = E_{\mathrm{crit}}/2c|\mathbf{B}_0|$, ψ is the logarithmic derivative of the Γ function, and ζ' is the derivative of the Hurwitz zeta function with respect to the first index. Thus the refractive index, given in Eq. (32), becomes

$$n^{-2} \approx 1 - \lambda\epsilon_0 c^2|\mathbf{B}_0|^2\sin^2\theta \geq 0, \tag{35}$$

where higher-order terms in the fine-structure constant α have been neglected, and θ is the angle between the background magnetic field $\mathbf{B}_0$ and the wave vector $\mathbf{k}$.

Refractive effects of a superstrong magnetic field are of interest in neutron stars and in magnetar environments, since they generate extreme conditions in terms of the field strength. Comparing with the case presented in Sec. II.E.1 we see that given the magnetic-field strength $|\mathbf{B}_0| \sim 10^{11}$ T we have $\lambda\epsilon_0 c^2|\mathbf{B}_0|^2 \approx 15\alpha/\pi \approx 0.03$. Thus the effect of the magnetic field on the refractive index is weaker than predicted by the lowest-order calculation.

2. Crossed field background

For a crossed field configuration, i.e., $|\mathbf{E}| = c|\mathbf{B}|$ and $\mathbf{E} \cdot \mathbf{B} = 0$, it immediately follows that $a = b = 0$. For a test photon belonging to an ensemble of random photons (such as in a photon gas), we obtain (Marklund, Shukla, and Eliasson, 2005)

$$n = \left(\frac{1 + \lambda\epsilon_0|\mathbf{E}|^2}{1 - \tfrac{1}{3}\lambda\epsilon_0|\mathbf{E}|^2}\right)^{1/2}, \tag{36}$$

from Eq. (32), where the effective action charge in Eq. (33) is a constant due to the random properties of test photons, $\lambda^{-1} = (45/22)(4\pi/\alpha)\epsilon_0 E_{\mathrm{crit}}^2$. Note that this is the same charge as the geometrical average of the coefficient obtained from the polarization tensor in the weak-field limit (Bialynicka-Birula and Bialynicki-Birula, 1970), i.e., an average over polarization states. The refractive index diverges as $\epsilon_0|\mathbf{E}|^2 \to 3\lambda^{-1}$. As these field strengths are reached, it is not correct that the test radiation gas is in thermodynamical equilibrium, and the assumptions behind the derivation of Eq. (36) are no longer valid.

3. Incoherent radiation background

We may characterize single photons in terms of plane electromagnetic waves. Thus for an electromagnetic wave moving in an isotropic and homogeneous medium with the refractive index n we have $|\mathbf{B}| = n|\mathbf{E}|/c$, $\mathcal{G} = -c\mathbf{E} \cdot \mathbf{B} = 0$, and $\mathcal{F} = \tfrac{1}{2}(n^2 - 1)|\mathbf{E}|^2 \geq 0$. Here we have assumed that $n > 1$, which implies $a = [(n^2 - 1)\mathcal{E}/\epsilon_0]^{1/2} \neq 0$ and $b = 0$, while for superluminal velocities we have $a = 0$ and $b \neq 0$, which allows for spontaneous pair production (Schwinger, 1951). The $n > 1$ assumption is consistent with elastic photon-photon scattering. The vacuum is now treated nonlinearly so we have to take into account the backreaction of the random photons onto themselves, an interaction mediated by the refractive index. The effective action charge (33) will therefore depend on both the field strength and the refractive index. Since the refractive index itself depends on the effective action charge λ, it will be nonlinearly determined via Eq. (32). For incoherent photons the Poynting flux in the gas rest frame vanishes, and we may uniquely characterize the gas by its energy density $\mathcal{E}$. From Eq. (32) we then obtain (Marklund, Shukla, and Eliasson, 2005)

$$\frac{1}{n^2} = \frac{1 - \tfrac{2}{3}\lambda\mathcal{E} + \sqrt{1 - 2\lambda\mathcal{E} + \tfrac{1}{9}(\lambda\mathcal{E})^2}}{2 + \lambda\mathcal{E}}, \tag{37}$$

while the effective action charge takes the form

$$\lambda = \frac{\alpha}{4\pi\epsilon_0 a^2}\frac{F(a/E_{\mathrm{crit}})}{2 + (\alpha/8\pi)[F(a/E_{\mathrm{crit}}) + G(a/E_{\mathrm{crit}})]}. \tag{38}$$
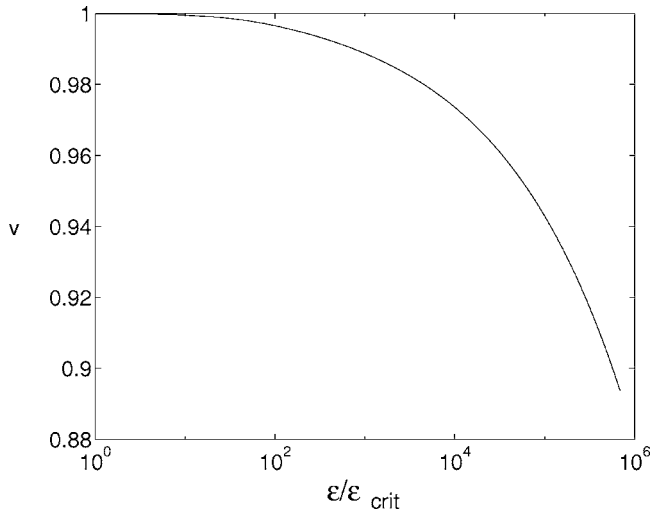
Here

FIG. 5. The phase velocity v in units of c, as given by Eqs. (37) and (38), plotted as a function of the normalized energy density $\mathcal{E}/\mathcal{E}_{\mathrm{crit}}$ Reprinted with permission from Marklund, Shukla, and Eliasson, 2005.

$$F(a/E_{\mathrm{crit}}) = \frac{4\pi}{\alpha\epsilon_0}a^2\lim_{b\to 0}(\partial_{\mathcal{F}}^2 + \partial_{\mathcal{G}}^2)\mathcal{L}$$
$$= \frac{1}{4\pi}\int_0^{i\infty}\frac{dz}{z}e^{-E_{\mathrm{crit}}z/a}\left(\frac{1 - z\coth z}{\sinh^2 z} + \frac{1}{3}z\coth z\right)$$

$$\tag{39}$$

and

$$G(a/E_{\mathrm{crit}}) = \frac{8\pi}{\alpha\epsilon_0}\lim_{b\to 0}[-2\partial_{\mathcal{F}}\mathcal{L}_c - a^2\partial_{\mathcal{F}}^2\mathcal{L}_c]. \tag{40}$$

Note that the latter function gives only a small correction to the effective action charge, and can in most cases safely be neglected. Moreover, the function F may be expressed in terms of special functions, see Eq. (34) (Dittrich and Gies, 2000).

The weak-field limit of Eqs. (37) and (38) takes the form (29) (Bialynicka-Birula and Bialynicki-Birula, 1970; Dittrich and Gies, 1998; Marklund *et al.*, 2003). On the other hand, in the ultrastrong-field limit ($\mathcal{E}/\epsilon_0 E_{\mathrm{crit}}^2 \to \infty$), we obtain the asymptotic constant phase velocity (Marklund, Shukla, and Eliasson, 2005)

$$v_\infty = c/\sqrt{5} \approx 0.45c, \tag{41}$$

valid in the low-frequency approximation. Thus for very high radiation densities, we expect the phase and group velocities to be approximately half that of the speed of light in vacuum. In this limit, one-loop radiation gas essentially evolves by free streaming, and it is therefore likely that higher-order loop corrections are important (Ritus, 1976). The phase velocity as a function of intensity is depicted in Fig. 5.

Under most circumstances, the contribution proportional to α in the denominator of Eq. (38) is small and

may be neglected. When $\mathcal{E} \gtrsim \epsilon_0 E_{\mathrm{crit}}^2$, we obtain $F \approx a/3E_{\mathrm{crit}}$ from Eq. (39), and we have (Marklund, Shukla, and Eliasson, 2005)

$$\lambda \approx \frac{\alpha}{8\pi\epsilon_0 a^2}F(a/E_{\mathrm{crit}}) \approx \frac{\alpha}{24\pi\epsilon_0^{1/2}E_{\mathrm{crit}}}\frac{1}{\sqrt{n^2 - 1}}\frac{1}{\sqrt{\mathcal{E}}}. \tag{42}$$

This expression for the effective action charge can be used in conjunction with Eq. (37) to analyze the propagation of single photons in a radiation gas where the energy density is in the intermediate range.

III. NONLINEAR COLLECTIVE PHOTON INTERACTIONS

In the preceding section, we presented dispersion relations for special cases of single photons interacting nonlinearly with the vacuum. The single-photon picture contains many interesting physical phenomena, such as photon splitting and the birefringence of the quantum vacuum. However, in many applications, collective effects among photons may be dominant (Mendonça, 2001).

A. Coherent field interactions

The formulation of the interaction between coherent electromagnetic waves and possible background field configurations is a starting point for the discussion concerning possible detection techniques of elastic photon-photon collisions. Experiments for detecting elastic photon-photon scattering are important tests of QED, and constitute a new type of tests of, e.g., Lorentz invariance in extensions of the Standard Model such as supersymmetric field theories (Colladay and Kostelecký, 1998; Jackiw and Kostelecký, 1999; Lipa *et al.*, 2003; Nibbelink and Pospelov, 2005).

The Maxwell equations that results from the weak-field Heisenberg-Euler corrected electromagnetic Lagrangian (5) are

$$\nabla\cdot\mathbf{E} = (\rho - \nabla\cdot\mathbf{P})/\epsilon_0, \tag{43a}$$

$$\nabla\cdot\mathbf{B} = 0, \tag{43b}$$

$$\frac{\partial\mathbf{B}}{\partial t} + \nabla\times\mathbf{E} = 0, \tag{43c}$$

$$\frac{1}{c^2}\frac{\partial\mathbf{E}}{\partial t} - \nabla\times\mathbf{B} = -\mu_0\left(\mathbf{j} + \frac{\partial\mathbf{P}}{\partial t} + \nabla\times\mathbf{M}\right), \tag{43d}$$

where the vacuum polarization and magnetization are given by Eqs. (11) and (12), respectively, and ρ and $\mathbf{j}$ are the charge and current densities, respectively. From these it is straightforward to derive the wave equations (9) and (10). These may in turn be used to derive the dispersion function for the appropriate wave field on a given background.

As noted above, the interaction between waves in parallel propagation does not yield any interaction due to the vacuum dispersion function $D_{\mathrm{vac}} = \omega^2 - |\mathbf{k}|^2 c^2$ appear-

ing as an overall factor in the wave equations (9) and (10). Thus dispersive effects need to be introduced in the wave propagation. This can be done in a multitude of ways, such as crossing light beams (Soljačić and Segev, 2000b), photon propagation on a constant coherent field background (Ding and Kaplan, 1989, 1992; Rozanov, 1993, 1998; Bakalov *et al.*, 1998; Kaplan and Ding, 2000; Rikken and Rizzo, 2000, 2003),[2] cavity fields (Brodin *et al.*, 2001, 2002), waveguide propagation (Brodin *et al.*, 2003; Shen and Yu, 2003; Shen *et al.*, 2003; Shukla, Eliasson, and Marklund, 2004), plasma interactions (Shen and Yu, 2003; Shen *et al.*, 2003; Marklund *et al.*, 2004a, 2005d; Stenflo *et al.*, 2005), and interaction between coherent and incoherent photons (Marklund *et al.*, 2003, 2004b; Marklund, Eliasson, and Shukla, 2004; Shukla and Eliasson, 2004; Shukla, Marklund, Brodin, *et al.*, 2004; Shukla, Marklund, Tskhakaya, *et al.*, 2004; Marklund, Shukla, Brodin, *et al.*, 2005).

1. Nonlinear vacuum magneto-optics

We have seen that the propagation of photons on a magnetized background can be expressed according to the dispersion relation (26). We may also start from the constituent relations (8) together with Eqs. (11) and (12) for the polarization and magnetization, respectively. This was first done by Klein and Nigam (1964a, 1964b), and later for arbitrary intensities by Heyl and Hernquist (1997a). If we denote the slowly varying background magnetic field by $\mathbf{B}_0$, and the perturbation fields by $\mathbf{E}$ and $\mathbf{B}$, then we find that $D_i = \epsilon_{ij} E_j$ and $H_i = \mu_{ij} B_j$, where the quantum vacuum electric permittivity and magnetic permeability are given by

$$\epsilon_{ij} = \epsilon_0 [\delta_{ij} + 4\kappa \mathcal{B}_0 (-\delta_{ij} + \tfrac{7}{2} b_i b_j)], \qquad (44)$$

$$\mu_{ij} = \mu_0 [\delta_{ij} + 4\kappa \mathcal{B}_0 (\delta_{ij} + 2 b_i b_j)], \qquad (45)$$

respectively. Here we have introduced the background magnetic-field energy density $\mathcal{B}_0 = |\mathbf{B}_0|^2/\mu_0$ and the background magnetic-field direction $\mathbf{b} = \mathbf{B}_0/|\mathbf{B}_0|$. Thus the permittivity and permeability are diagonal when using the magneto-optical axis as the eigendirection. Denoting this direction by z, we have $\epsilon_{xx} = \epsilon_{yy} = \epsilon_0 (1 - 4\kappa \mathcal{B}_0)$ and $\epsilon_{zz} = \epsilon_0 (1 + 10\kappa \mathcal{B}_0)$, while $\mu_{xx} = \mu_{yy} = \mu_0 (1 + 4\kappa \mathcal{B}_0)$ and $\mu_{zz} = \mu_0 (1 + 12\kappa \mathcal{B}_0)$.

For an electromagnetic wave propagating perpendicular to $\mathbf{B}_0$, there are essentially two different polarization states, and we may write $\epsilon_{ij} = \epsilon \delta_{ij}$, $\mu_{ij} = \mu \delta_{ij}$. When $\mathbf{E} \perp \mathbf{B}_0$, we have $\epsilon = \epsilon_\perp$, $\mu = \mu_\perp$ according to

$$\epsilon_\perp = \epsilon_0 (1 - 4\kappa \mathcal{B}_0) \quad \text{and} \quad \mu_\perp = \mu_0 (1 + 12\kappa \mathcal{B}_0), \qquad (46)$$

while if $\mathbf{E} \parallel \mathbf{B}_0$, we find $\epsilon = \epsilon_\parallel$, $\mu = \mu_\parallel$, where

---

[2]Here it should be noted that the paper by Bakalov *et al.* (1998) is a progress report to one of the few actual experimental setups within photon-photon scattering, and their detection techniques are based on the work by Iacopini and Zavattini (1979) and Bakalov *et al.* (1994).

$$\epsilon = \epsilon_0 (1 + 10\kappa \mathcal{B}_0) \quad \text{and} \quad \mu = \mu_0 (1 + 4\kappa \mathcal{B}_0). \qquad (47)$$

Thus we see that for strong magnetic fields there is a significant difference in the behavior of the two polarization modes. This has been exploited in various scenarios [e.g., Ding and Kaplan (1989, 1992); Bakalov *et al.* (1994, 1998); Heyl and Hernquist (1997a); Kaplan and Ding (2000); Rikken and Rizzo (2000, 2003)]. The procedure is straightforward to perform for other unidirectional background field configurations.

2. Nonlinear self-interactions

Based on these results, the self-action of an electromagnetic pulse on a given background can also be considered. Taking into account the lowest-order cubic nonlinear terms of the (complex) pulse amplitude E, and employing the slowly varying envelope approximation (Hasegawa, 1975; Kivshar and Agrawal, 2003), one can derive a nonlinear Schrödinger equation (NLSE) for E. Letting $E = \int E_k \exp[i(\mathbf{k} - \mathbf{k}_0) \cdot \mathbf{r} - i(\omega - \omega_0) t] d\mathbf{k}$, and expanding the frequency around the background values (denoted by 0), we obtain

$$\omega \approx \omega_0 + \frac{\partial \omega}{\partial k_i}\bigg|_0 (k_i - k_{0i}) + \frac{1}{2} \frac{\partial^2 \omega}{\partial k_i \partial k_j}\bigg|_0 (k_i - k_{0i})$$
$$\times (k_j - k_{0j}) + \frac{\partial \omega}{\partial |\mathbf{Q}|^2}\bigg|_0 (|\mathbf{Q}|^2 - |\mathbf{Q}_0|^2), \qquad (48)$$

where $|\mathbf{Q}|^2$ is given by Eq. (20). Thus the envelope will satisfy the NLSE,

$$i \left(\frac{\partial}{\partial t} + v_{gi} \nabla_i \right) E + \frac{1}{2} \frac{\partial v_{gi}}{\partial k_{0j}} \nabla_i \nabla_j E + \frac{1}{2} \lambda k_0 c I(|\mathbf{Q}|^2) = 0,$$
$$(49)$$

where $\mathbf{v}_g$ is the group velocity and $I(|\mathbf{Q}|^2) = \int E_k (|\mathbf{Q}|^2 - |\mathbf{Q}_0|^2) \exp[i(\mathbf{k} - \mathbf{k}_0) \cdot \mathbf{r} - i(\omega - \omega_0) t] d\mathbf{k}$ is the nonlinear response. We note that the term containing $|\mathbf{Q}_0|^2$ represents a phase shift, and can be removed by a transformation. When high-frequency corrections are added, the NLSE will attain a second-order derivative along the propagation direction. The group velocity $\mathbf{v}_g = \partial \omega / \partial \mathbf{k}$ on an arbitrary background can be written as (Bialynicka-Birula and Bialynicki-Birula, 1970)

$$\mathbf{v}_g = c\hat{\mathbf{k}} - (c\lambda \epsilon_0/2)[|\mathbf{E}|^2 + c^2 |\mathbf{B}|^2 + (\hat{\mathbf{k}} \cdot \mathbf{E})^2$$
$$+ c^2 (\hat{\mathbf{k}} \cdot \mathbf{B})^2]\hat{\mathbf{k}} - c\lambda \epsilon_0 [(\hat{\mathbf{k}} \cdot \mathbf{E})\mathbf{E} + c^2 (\hat{\mathbf{k}} \cdot \mathbf{B})\mathbf{B}$$
$$+ c\mathbf{E} \times \mathbf{B}]$$

in the weak-field case. We note that $|\mathbf{v}_g| = \omega/k < c$. We now discuss some special cases.

a. Constant background fields

For a constant background configuration, the back-reaction of the photon propagation may, in some cases, be neglected. Then the nonlinear contribution to the self-interaction of the pulse occurs via a coupling of higher order in the parameter λ.

Rozanov (1998) considered the perpendicular propagation of high intensity laser pulses on a background $\mathbf{E}_0 = E_0\hat{\mathbf{x}}$, $\mathbf{B}_0 = B_0\hat{\mathbf{y}}$. By choosing the polarization directions of the laser pulse in the direction of the background fields, one obtains the NLSE,[3]

$$i\left(\frac{\partial}{\partial t} + v_g\frac{\partial}{\partial z}\right)E + \frac{1}{2}v_g'\nabla_\perp^2 E + \xi|E|^2 E = 0, \qquad (50)$$

where $v_g' = c(1 - \lambda|\mathbf{Q}_0|^2/2)/k_0$ is the group velocity dispersion, $\xi = k_0 c\epsilon_0\lambda^3|\mathbf{Q}_0|^4/8$, and $|\mathbf{Q}_0|^2 = \epsilon_0(E_0 - cB_0)^2$. The NLSE (50) could be of interest for laboratory applications, when studying high intensity laser pulse propagation in given background electromagnetic fields.

b. Crossing beams

When the background is given by the source itself, the nonlinear self-interaction term will be of first order in λ, thus requiring weaker background conditions.

Soljačić and Segev (2000b) derived a NLSE for the dynamics of the envelope $A(x)$ of the interaction region due to crossing laser beams. By symmetry arguments concerning the QED corrected Maxwell's equations, they reduce the problem to a 1D stationary NLSE,

$$\frac{d^2 A}{dx^2} + \Gamma A + \frac{1}{2}k^2\kappa\epsilon_0 A^3 = 0, \qquad (51)$$

where k is the wave number of the laser beam, Γ is the eigenvalue of the equation, and the beams are assumed to be polarized in the x direction. The lowest-order solitary wave solution is given by (Kivshar and Agrawal, 2003) $A(x) = A_0\,\mathrm{sech}(\sqrt{-2\Gamma}z)$, where we have denoted the eigenvalue $\Gamma = -k^2\kappa\epsilon_0 A_0^2/8$. This one-dimensional soliton solution is stable, as opposed to higher dimensional solitons (Berge and Rasmussen, 1996; Kivshar and Agrawal, 2003). Furthermore, Soljačić and Segev (2000b) suggested the possibility of higher dimensional soliton formation, e.g., necklace solitons (Soljačić et al., 1998; Soljačić and Segev, 2000a).

3. Propagation between conducting planes

Similar to the case of a Casimir vacuum, one of the simplest geometries where dispersive effects makes the presence of QED vacuum nonlinearities apparent is given by two parallel conducting planes. They are the first example where multidimensional photon configurations can self-compress to reach intensities above the laser limit (Mourou et al., 1998; Brodin et al., 2003; Shukla et al., 2004).

a. Variational formulation

Consider the propagation between two parallel conducting planes with spacing x_0 of one $\mathrm{TE}_{\ell 0}$ mode ($\ell = 1, 2, \ldots$) given by

---

[3]We note that Rozanov (1998) obtained the NLSE (50) with the dispersive correction.

$$\mathbf{A} = A\sin\left(\frac{\ell\pi x}{x_0}\right)\exp[i(kz - \omega t)]\hat{\mathbf{y}} + \text{c.c.} \qquad (52)$$

in the radiation gauge ($\phi = 0$). The linear dispersion relation is $\omega^2/c^2 - k^2 - \ell^2\pi^2/x_0^2 = 0$. From Maxwell's equations (43) a nonlinear dispersion relation can be derived by inserting the linear expression for the fields and separating into orthogonal trigonometric functions. The coefficients in the NLSE can be found from the resulting equation. One may also start from the Heisenberg-Euler Lagrangian (5), and minimize the resulting expression for the action. This may appear more elegant and gives the same result (Brodin et al., 2003).

We follow the results of Brodin et al. (2003). Let $A = A(t, y, z)$ and assume A to be weakly modulated so that $|\partial A/\partial t| \ll |\omega A|$, $|\partial A/\partial z| \ll |kA|$. To lowest order, nonlinear terms and slow derivatives in $\mathcal{L}$ are omitted. Averaging over the plate spacing x_0 shows that this lowest order Lagrangian is identically zero due to the dispersion relation. To the next order of approximation in the Lagrangian, first-order slow derivatives are included. After variation of the corresponding action, this leads to an equation where the envelope moves with the group velocity. The next order and final approximation includes second-order slow derivatives. After performing the averaging between the plate interspacing, the final expression for the Lagrangian is

$$\mathcal{L} = i\omega\varepsilon_0\left(\frac{\partial A}{\partial t}A^* - \frac{\partial A^*}{\partial t}A\right) - ikc^2\varepsilon_0\left(\frac{\partial A}{\partial z}A^* - \frac{\partial A^*}{\partial z}A\right)$$
$$+ (c^2 - v_g^2)\varepsilon_0\left|\frac{\partial A}{\partial z}\right|^2 + \frac{3\ell^4 c^4\pi^4\epsilon_0^2\kappa}{x_0^4}|A|^4. \qquad (53)$$

The variation of the action due to the Lagrangian (53) with respect to A^* leads to the NLSE

$$i\left(\frac{\partial}{\partial t} + v_g\frac{\partial}{\partial z}\right)A + \frac{c^2}{2\omega}\frac{\partial^2 A}{\partial y^2} + \frac{v_g'}{2}\frac{\partial^2 A}{\partial z^2} + L^2|A|^2 A = 0,$$
$$(54)$$

where v_g and $v_g' = \partial v_g/\partial k$ follow from the linear dispersion relation and $L^2 = 3\ell^4 c^4\pi^4\kappa\epsilon_0/\omega x_0^4$. The nonlinear correction in Eq. (54) is due to the self-interaction of the $\mathrm{TE}_{\ell 0}$ mode (52) via the quantum vacuum. In one space dimension, i.e., $\partial^2 A/\partial y^2 = 0$, Eq. (54) reduces to the cubic Schrödinger equation having an envelope soliton solution (Kivshar and Agrawal, 2003).

Changing to a system moving with the group velocity while rescaling the coordinates and the amplitude according to $\tau = \omega t/2$, $\upsilon = \omega y/c$, $\zeta = (\omega/v_g')^{1/2}(z - v_g t)$, and $a = \sqrt{2}LA$, and assuming cylindrical symmetry, Eq. (54) takes the form

$$i\frac{\partial a}{\partial \tau} + \frac{1}{\rho}\frac{\partial}{\partial \rho}\left(\rho\frac{\partial a}{\partial \rho}\right) + |a|^2 a = 0, \qquad (55)$$

where $a = a(t, \rho)$ and $\rho^2 = \upsilon^2 + \zeta^2$.

Equation (55) is a two-dimensional radially symmetric NLSE, to which exact solutions are not available. However, an accurate analytical approximation of pulselike

solutions of Eq. (55) can be obtained by means of Rayleigh-Ritz optimization based on suitably chosen trial functions [see, e.g., Desaix *et al.* (1991); Anderson, Cattani, and Lisak (1999), and references therein]. An accurate approximate solution, mimicking the solitary behavior as well as capturing the collapse properties of Eq. (55), is given by (Desaix *et al.*, 1991)

$$a_T(\tau,\rho) = F(\tau)\mathrm{sech}\left[\frac{\rho}{f(\tau)}\right]\exp[ib(\tau)\rho^2], \qquad (56)$$

where[4] $f(\tau) = [f^2(0) + \gamma(1 - I_0/I_c)\tau^2]^{1/2}$, showing the instability of the stationary solution $I_0 = I_c$, either collapsing to zero width in a finite time when $I_0 > I_c$ or diffracting monotonously towards infinite width when $I_0 < I_c$.

In the next section, a perturbation analysis shows that the exact equations produced unstable solutions.

b. Instability analysis

Following Shukla, Eliasson, and Marklund (2004), a rescaling of Eq. (54) gives the dimensionless equation

$$i\left(\frac{\partial}{\partial t} + \sqrt{1-\beta^2}\frac{\partial}{\partial z}\right)A + \frac{1}{2}\frac{\partial^2 A}{\partial y^2} + \frac{\beta^2}{2}\frac{\partial^2 A}{\partial z^2} + |A|^2 A = 0,$$

$$(57)$$

where $\beta = \ell\pi c/x_0\omega$ and the time is scaled by ω^{-1}, the spatial variables by c/ω, and the vector potential by $(\kappa\epsilon_0/2\omega^2)^{1/2}$.

Conditions for the modulational and filamentation instabilities can be obtained as follows. Let $A = [A_0 + A_1\exp(i\phi) + A_2\exp(-i\phi)]\exp(-i\omega_0 t)$, where $\phi = \mathbf{K}\cdot\mathbf{r} - \Omega t$ is a phase, ω_0 is a constant frequency, and the constants A_0, A_1, and A_2 are the complex amplitudes of the pump wave and the two electromagnetic sidebands, respectively. The wave vector and the frequency of modulating perturbations are denoted by $\mathbf{K} = \hat{\mathbf{y}}K_y + \hat{\mathbf{z}}K_z$ and Ω, respectively, where $\hat{\mathbf{y}}$ and $\hat{\mathbf{z}}$ are unit vectors along x and y axes, respectively. Following the standard procedure of the modulational and filamentational instability (Shukla *et al.*, 1986; Anderson, Fedele, *et al.*, 1999), the nonlinear dispersion relation becomes

$$(\Omega - K_z\sqrt{1-\beta^2})^2 + [|A_0|^2 - \tfrac{1}{4}(K_y^2 + \beta^2 K_z^2)]$$

$$\times(K_y^2 + \beta^2 K_z^2) = 0. \qquad (58)$$

Letting $\Omega = K_z\sqrt{1-\beta^2} + i\gamma$ in Eq. (58), one obtains the modulational instability growth rate

$$\gamma = [|A_0|^2 - \tfrac{1}{4}(K_y^2 + \beta^2 K_z^2)]^{1/2}(K_y^2 + \beta^2 K_z^2)^{1/2}. \qquad (59)$$

The instability grows quadratically with the amplitude A_0, and attains a maximum value at a critical wave number. The values of β different from unity make the instability region asymmetric with respect to K_y and K_z. On

---

[4] The complex amplitude $F(\tau)$ and the phase function $b(\tau)$ can be expressed in terms of the pulse width $f(\tau)$ (Desaix *et al.*, 1991). Here $\gamma = 4(\ln 4 + 1)/27\zeta(3) \approx 0.29$, $I(\tau) = f^2(\tau)|F(\tau)|^2 = f^2(0)|F(0)|^2 = I_0$, and $I_c = (2\ln 2 + 1)/(4\ln 2 - 1) \approx 1.35$.
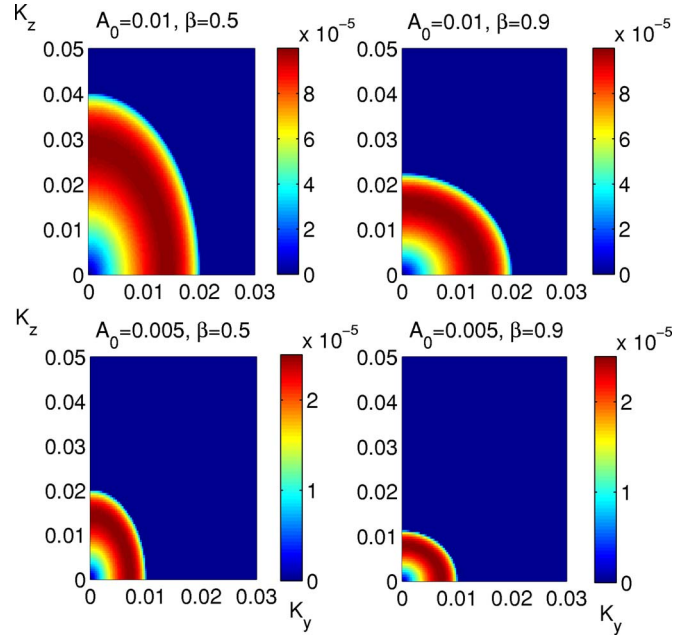
FIG. 6. (Color online) The growth rate γ given by Eq. (59) of the modulational instability for an initially homogeneous radiation field as a function of the wave number (K_y, K_z), for different values of β and pump strength A_0. Reprinted from Shukla, Eliasson, and Marklund, 2004. Copyright 2004, with permission from Elsevier.

the other hand, the spatial amplification rate $\Gamma = iK_z$ of the filamentation instability in the quasistationary limit (viz., $\Omega = 0$), and for $\beta^2\Gamma^2 \ll K_y^2$, is

$$\Gamma = \left(|A_0|^2 - \tfrac{1}{4}K_y^2\right)^{1/2}\frac{K_y}{\sqrt{1-\beta^2}}. \qquad (60)$$

Shukla, Eliasson, and Marklund (2004) performed a numerical study of Eq. (58) showing the instabilities indicated by the approximate solution (56); see Fig. 6. Using the normalized Eq. (57) an initially Gaussian pulse was shown to collapse or disperse in accordance to the collapse criterion presented in Brodin *et al.* (2003); see Fig. 7. The collapse is unbounded in the weakly nonlinear model given by Eq. (57). As the collapse pursues, the intensity of the pulse will reach values at which the weakly nonlinear theory breaks down and higher order effects (Bialynicka-Birula and Bialynicki-Birula, 1970; Marklund, Shukla, and Eliasson, 2005), and possible pair-creation processes (Schwinger, 1951), has to be taken into account. For the latter, a significant energy dissipation into the electron-positron plasma will take place.

In practice, the trapping of an electromagnetic pulse can be achieved by two highly conduction layers. As an example, consider the generation of two-dimensional plasma channels due to the interaction of a plasma with high-intensity lasers (Shen *et al.*, 2003). In this case, a vacuum will be created within the plasma due to the complete evacuation of electrons by the ponderomotive force of intense laser beams. The resulting plasma waveguides can sustain very high-field intensities (Bing-

FIG. 7. (Color online) The time evolution of $|A|^2$ given by Eq. (57) for an initially Gaussian shaped electromagnetic pulse. The puls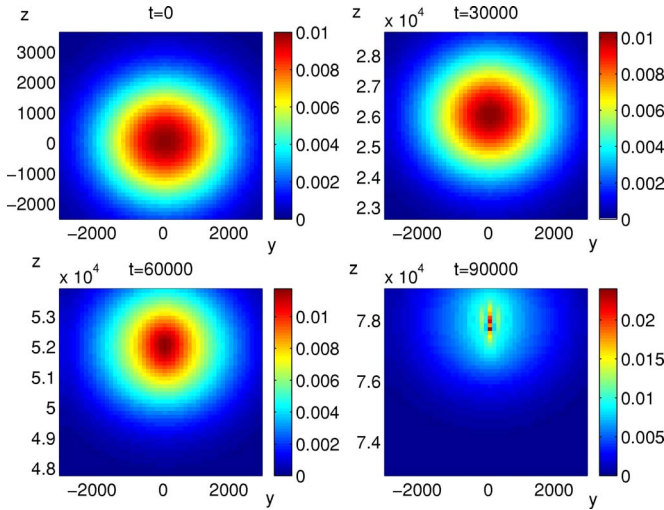e slowly self-focuses and finally collapses. Here $\beta = 0.5$ and a Gaussian pulse $A = 10^{-2} \exp[-(y^2 + z^2)/(2 \times 10^3)^2]$ is used. In the upper-right and lower-left panels, the pulse self-compresses and in the lower-right panel the field strength of the pulse has reached a critical limit where Eq. (57) is no longer valid. Reprinted from Shukla, Eliasson, and Marklund, 2004. Copyright 2004, with permission from Elsevier.

ham, 2003), and with future laser systems (Mourou *et al.*, 1998, 2006) the intensities could surpass even the theoretical laser limit (Mourou *et al.*, 1998; Shen and Yu, 2002; Shorokhov *et al.*, 2003). The trapping of intense laser fields could yield the right conditions for electromagnetic modes to self-interact via the nonlinear quantum vacuum, giving rise to pulse evolution according to Eq. (57).

4. Cavity mode interactions

Wave-wave interactions give rise to a host of interesting phenomena, well known in optics and plasma physics (Weiland and Wilhelmsson, 1977; Agrawal, 2001; Kivshar and Agrawal, 2003). As cubic nonlinearities act within a cavity environment, they produce wave-wave couplings, and given certain resonance conditions a new mode will be generated that will satisfy the cavity dispersion relation. Brodin *et al.* (2001) showed that these new modes could reach detectable levels within state-of-the-art cavities, and Brodin *et al.* (2002) were able to derive a NLSE for the self-interaction of a single mode in a rectangular cavity.

Calculations of the three-wave coupling strength between various eigenmodes can be done including the nonlinear polarization (11) and magnetization (12); see, e.g., Brodin *et al.* (2001). However, a more convenient and elegant approach, which was pioneered by Brodin *et al.* (2003) and gives the same result, starts directly with the Lagrangian density (5).

A general procedure for finding the cavity eigenmode coupling and saturated amplitudes of the excited mode can be formulated (Weiland and Wilhelmsson, 1977;

Brodin *et al.*, 2001, 2002; Eriksson *et al.*, 2004):

(1) Determine the linear eigenmodes of the cavity in terms of the vector potential.

(2) Choose resonant eigenmodes fulfilling frequency matching conditions for modes 1, 2, and 3, such as

$$\omega_3 = 2\omega_1 - \omega_2. \tag{61}$$

(3) Assume a slowly varying amplitude of the vector potential eigenmode amplitudes and minimize the effective action obtained from the Lagrangian (5) and follow steps (1) and (2). The lowest-order linear terms vanish, since the dispersion relation of each mode is fulfilled.

(4) In the absence of dissipation, the mode coupling equations imply steady growth of mode 3, until the energy of that mode is comparable to that of the pump modes. A damping mechanism, such as finite conductivity of the cavity walls, may be inserted on phenomenological grounds. This saturates the amplitude at a level depending on the mode-coupling growth versus losses.

a. Rectangular cavities

For a rectangular prism cavity with dimensions (x_0, y_0, z_0), choosing the radiation gauge, the pump modes have vector potentials of the form

$$\mathbf{A}_j = A_j \sin\left(\frac{\pi x_j}{x_{j0}}\right) \sin\left(\frac{\ell_j \pi z}{z_0}\right) \exp(-i\omega_j t)\hat{\mathbf{y}} + \text{c.c.}, \tag{62}$$

where $j = 1, 2$, $\ell_j = 1, 2, 3, \ldots$ are the mode numbers for pump waves, and $x_1 = x$, $x_2 = y$, $x_{10} = x_0$, and $x_{20} = y_0$. The dispersion relations are

$$\omega_j^2 = \frac{\ell_j^2 \pi^2 c^2}{z_0^2} + \frac{\pi^2 c^2}{x_{j0}^2}. \tag{63}$$

The mode excited due to the QED nonlinearities is given by

$$\mathbf{A}_3 = A_3 \sin\left(\frac{\pi y}{y_0}\right) \sin\left(\frac{\ell_3 \pi z}{z_0}\right) \exp(-i\omega_3 t)\hat{\mathbf{x}} + \text{c.c.}, \tag{64}$$

where

$$\omega_3^2 = \frac{\ell_3^2 \pi^2 c^2}{z_0^2} + \frac{\pi^2 c^2}{y_0^2}. \tag{65}$$

Following the scheme given by Brodin *et al.* (2001, 2003) and Eriksson *et al.* (2004), with the resonance condition $\omega_3 = 2\omega_1 - \omega_2$, one obtains the following evolution equation for mode 3:

$$\frac{dA_3}{dt} = -\frac{i\varepsilon_0 \kappa \omega_3^3}{8} K_{\text{rec}} A_1^2 A_2^*, \tag{66}$$

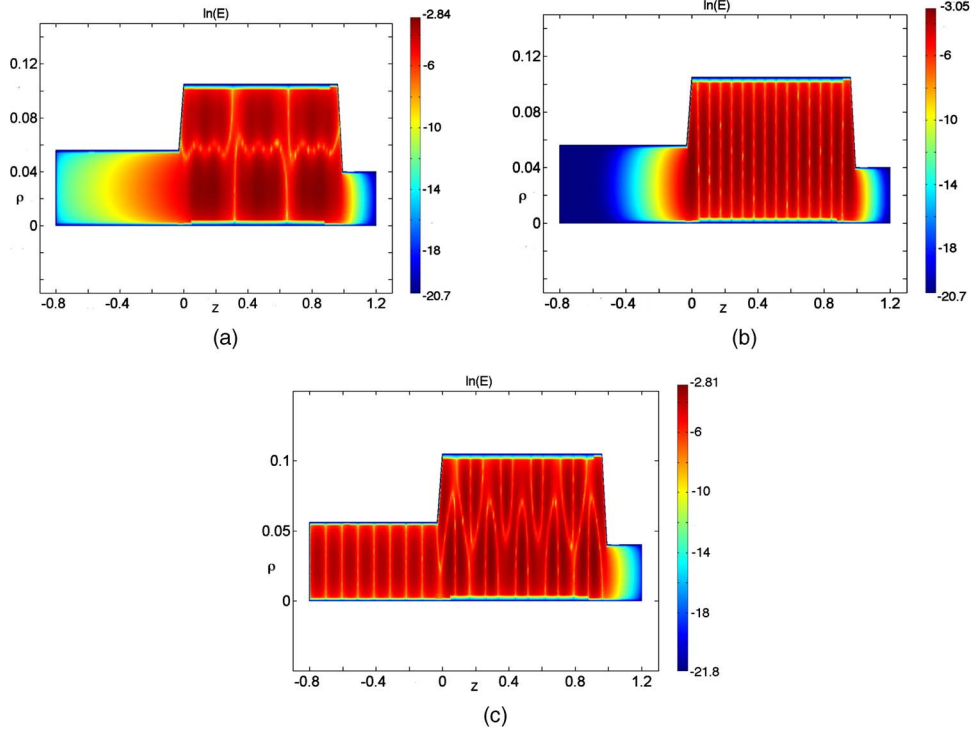where the dimensionless coupling coefficient K_{rec} is

FIG. 8. (Color online) The mode structure for the filtering geometry. The small region to the right is the entrance region, the large middle region is where the interaction takes place, and the region to the left is the filtering region. Here $\ln|E|$ is plotted using an arbitrary normalization. We have the cavity distance z and the cylindrical radius ρ in units of meter. (a) Pump mode 1: We see that spatial exponential decay has diminished the amplitude by a factor 10^{-6} in the filtered region to the left. (b) Pump mode 2: As for mode 1, exponential decay diminishes the amplitude in the filtering region, here by a factor 10^{-8}. (c) Excited mode: The amplitude of the mode excited by the QED vacuum nonlinearities is almost unaffected when passing into the filtering region. Figure adopted from Eriksson *et al.*, 2004.

$$K_{\text{rec}} = \frac{\pi^2 c^2}{\omega_3^4}\left\{(-,-,+)\left[\frac{8\pi^2 c^2}{x_0^2 y_0^2} + \left(\frac{4}{x_0^2} + \frac{7\ell_1^2}{z_0^2}\right)\omega_2\omega_3\right]\right.$$
$$+ \frac{\ell_2\ell_3\pi^2 c^2}{z_0^2}\left(\frac{7\ell_1^2}{z_0^2} - \frac{3}{x_0^2}\right) + \frac{7\omega_1\ell_1}{z_0^2}$$
$$\left.\times[(-,+,-)\omega_2\ell_3(+,-,-)\omega_3\ell_2]\right\}. \quad (67)$$

The different signs in Eq. (67) for the coupling strength correspond to the mode number matchings $2\ell_1 - \ell_2 + \ell_3 = 0$, $2\ell_1 + \ell_2 - \ell_3 = 0$, and $2\ell_1 - \ell_2 - \ell_3 = 0$ that must be fulfilled for nonzero coupling. The coupling coefficient for specific mode numbers and geometries can thus be evaluated. If a saturation mechanism is included in Eq. (66), one may solve for the steady-state value of A_3.

b. Cylindrical cavities

As shown by Eriksson *et al.* (2004), the efficiency of the mode conversion can be slightly improved by the choice of a cylindrical cavity. The results can be obtained along the lines of the previous example. For TE modes with no angular dependence, the vector potential

$$\mathbf{A} = AJ_1(\rho\beta/a)\sin\left(\frac{\ell\pi z}{z_0}\right)\exp(-i\omega t)\hat{\varphi} + \text{c.c.} \quad (68)$$

gives a complete description of the fields. Here a is the cylinder radius, z_0 the length of the cavity, J_1 the first-order Bessel function, ℓ the mode number, and β one of its zeros. The cylinder occupies the region $0 \leq z \leq z_0$ centered around the z axis. We have introduced here cylindrical coordinates ρ and z as well as the unit vector $\hat{\varphi}$ in the azimuthal direction. The eigenfrequency is given by $\omega^2 = c^2[(\beta/a)^2 + (\ell\pi/z_0)^2]$, for all modes $\omega = \omega_{1,2,3}$. From the matching condition $\omega_3 = 2\omega_1 - \omega_2$ it follows that the eigenmodes cannot have the same order of their respective β, and one thus introduces $\beta = \beta_{1,2,3}$. Proceeding along the lines of the previous section, one obtains

$$\frac{dA_3}{dt} = -\frac{i\varepsilon_0\kappa\omega_3^3}{8}K_{\text{cyl}}A_1^2 A_2^* \quad (69)$$

for the mode number matching $\ell_3 = 2\ell_1 + \ell_2$. Here the cylindrical coupling coefficient K_{cyl} is defined in terms of integrals of Bessel functions and can be found in Eriksson *et al.* (2004). As in the case of a rectangular geometry, the linear growth of A_3 as dictated by Eq. (69) will be saturated by dissipative mechanisms. The intensity of the generated field amplitudes and the pump field amplitudes is shown in Fig. 8.

B. Incoherent field interactions

We have considered the interaction via the nonlinear quantum vacuum between coherent electromagnetic waves. However, in many situations where the Heisenberg-Euler Lagrangian is important, such as in astrophysical and laser-plasma applications, there can be intense incoherent electromagnetic fields present. We will below study two scenarios. First, a plane-wave pulse propagating on a vacuum dressed by an intense gas of incoherent photons is analyzed, and, second, effects on a radiation gas by the quantum vacuum excited by an intense electromagnetic (EM) pulse is investigated. These two results are then used in conjunction to obtain the relevant equations governing the nonlinear interaction between the pulse and the radiation gas.

1. Coherent pulse interaction with incoherent photons

The dispersion relation (30) represents the propagation of test photons in an intense incoherent radiation background. Using standard methods for slowly varying envelopes (Hasegawa, 1975) in conjunction with Eq. (30), we obtain the special case of Eq. (49), for a pulse in an intense photon gas background (Marklund *et al.*, 2003; Marklund, Eliasson, and Shukla, 2004; Shukla, Marklund, Tskhakaya, *et al.*, 2004) [see also Rozanov (1998) for a similar result using a different strong background field],

$$i\left(\frac{\partial}{\partial t} + v_g \frac{\partial}{\partial z}\right)E_p + \frac{v_g}{2k_0}\left(\nabla_\perp^2 - \beta_z \frac{\partial^2}{\partial z^2}\right)E_p + \mu\delta\mathcal{E}E_p = 0,$$

(70)

where $\delta\mathcal{E} = \mathcal{E} - \mathcal{E}_0$ is a radiation gas perturbation due to the pulse propagation and $\mathcal{E}_0$ is the unperturbed background radiation energy density. Here we have adapted coordinates such that $\mathbf{k}_0 = k_0\hat{\mathbf{z}}$, $\mathbf{k}_0$ being the background wave vector of the pulse, included the high-frequency correction represented by β_z, and denoted the (complex) pulse amplitude by E_p. Moreover, $\mathbf{v}_g = (\partial\omega/\partial\mathbf{k})_0$ is the group velocity on the background, $\beta_z = (32/3)\sigma\lambda^2\mathcal{E}_0^2 k_0^2$ is the vacuum dispersion parameter, $\mu = (2/3)ck_0\lambda[1 + (16/3)\sigma\lambda\mathcal{E}_0 k_0^2]$ is the nonlinear refraction parameter, $\nabla_\perp^2 = \nabla^2 - (\hat{\mathbf{k}}_0 \cdot \nabla)^2$, and $\lambda = 8\kappa$ of 14κ depending on the polarization of the pulse (see Sec. II.C).

2. Radiation gas response of pulse propagation

We have seen that the effects of a plane wave on incoherent photons can be expressed via the dispersion relation (28). Following Marklund *et al.* (2003), the response of the radiation gas can be determined using a kinetic theory. For a dispersion relation $\omega = ck/n(\mathbf{r},t)$, where n is the spacetime-dependent refractive index, we have the Hamiltonian ray equations

$$\dot{\mathbf{r}} = \frac{\partial\omega}{\partial\mathbf{k}} = \frac{c}{n}\hat{\mathbf{k}} \quad \text{and} \quad \dot{\mathbf{k}} = -\nabla\omega = \frac{\omega}{n}\nabla n,$$

(71)

where $\dot{\mathbf{r}}$ denotes the group velocity of the photon, $\dot{\mathbf{k}}$ the force on a photon, and the dot denotes a time derivative.

The equation for the collective interaction of photons can then be formulated as (Mendonça, 2001)

$$\frac{\partial f(\mathbf{k},\mathbf{r},t)}{\partial t} + \nabla \cdot [\dot{\mathbf{r}}f(\mathbf{k},\mathbf{r},t)] + \frac{\partial}{\partial\mathbf{k}} \cdot [\dot{\mathbf{k}}f(\mathbf{k},\mathbf{r},t)] = 0,$$

(72)

where the distribution function $f(\mathbf{k},\mathbf{r},t)$ has been normalized such that $\int f(\mathbf{k},\mathbf{r},t)d\mathbf{k}$ gives the photon gas number density. In what follows, we neglect dispersive effects on the evolution of the radiation gas.[5] Taking the moments of the kinetic equation (72) (Marklund, Eliasson, and Shukla, 2004), we obtain the energy conservation equation

$$\frac{\partial\mathcal{E}}{\partial t} + \nabla \cdot (\mathcal{E}\mathbf{u} + \mathbf{q}) = -\frac{\mathcal{E}}{n}\frac{\partial n}{\partial t},$$

(73a)

where $\mathcal{E}(\mathbf{r},t) = \int\hbar\omega f d\mathbf{k}$ is the energy density and $\mathbf{q}(\mathbf{r},t) = \int\hbar\omega\mathbf{w}f d\mathbf{k}$ is the energy (or Poynting) flux. Here we have introduced $\dot{\mathbf{r}} = \mathbf{u} + \mathbf{w}$, where $\int\mathbf{w}f d\mathbf{k} = 0$. Thus $\mathbf{w}$ represents the random velocity of the photons. Equation (73a) is coupled to the momentum conservation equation

$$\frac{\partial\mathbf{\Pi}}{\partial t} + \nabla \cdot [\mathbf{u} \otimes \mathbf{\Pi} + \mathbf{P}] = \frac{\mathcal{E}}{n}\nabla n,$$

(73b)

where $\mathbf{\Pi} = \int\hbar\mathbf{k}f d\mathbf{k}$ is the momentum density and $\mathbf{P} = \int\mathbf{w} \otimes (\hbar\mathbf{k})f d\mathbf{k}$ is the pressure tensor. It follows from the definition of the pressure tensor that the trace satisfies $\text{Tr}\,\mathbf{P} = \int\hbar k\mathbf{w} \cdot \hat{\mathbf{k}}f d\mathbf{k} = (n/c)\int\hbar\omega\mathbf{w} \cdot \hat{\mathbf{k}}f d\mathbf{k}$. For an observer comoving with the fluid, i.e., a system in which $(\mathbf{u})_0 = 0$ (the 0 denoting the comoving system), Eq. (71) shows that $(\mathbf{w} \cdot \hat{\mathbf{k}})_0 = (n)_0/c$, so that the trace of the pressure tensor in the comoving system becomes $(\text{Tr}\,\mathbf{P})_0 = (\mathcal{E})_0$. For an isotropic distribution function, the pressure can be expressed in terms of the scalar function $P = \text{Tr}\,\mathbf{P}/3$, satisfying the equation of state $P = \mathcal{E}/3$. We will henceforth adopt the comoving frame, in which $\mathbf{u} = 0$, and the equation of state $\mathbf{P}_{ij} = P\delta_{ij}\mathcal{E}/3$, in order to achieve closure of the fluid equations.

3. Quasilinear theory

We now assume that the radiation gas is perturbed around the equilibrium state $\mathcal{E}_0 = $ const and $\mathbf{\Pi}_0 = \mathbf{0}$, letting $\mathcal{E} = \mathcal{E}_0 + \delta\mathcal{E}$, where $|\delta\mathcal{E}| \ll \mathcal{E}_0$. Then, using Eqs. (73) we obtain an acoustic equation

---

[5]The dispersive correction, due to the variations in the photon field, will give rise to higher-order effects in the final fluid equation for the energy density of the radiation gas. Thus we may at this stage neglect the dispersive term from the fluid equations.

$$\left(\frac{\partial^2}{\partial t^2} - \frac{c^2}{3}\nabla^2 \right)\delta\mathcal{E} = -\frac{2\lambda\epsilon_0\mathcal{E}_0}{3}\left(\frac{\partial^2}{\partial t^2} + c^2\nabla^2 \right)|E_p|^2, \qquad (74)$$

to lowest order in $\delta\mathcal{E}$. This gives the dynamics of a radiation gas due to the pulse propagation (Marklund, Eliasson, and Shukla, 2004). Equations (70) and (74) were first presented by Marklund, Eliasson, and Shukla (2004), and generalize the Marklund-Brodin-Stenflo equations (Marklund *et al.*, 2003), to the case of a dispersive vacuum. The Marklund-Brodin-Stenflo equations are different from the Karpman equations (Karpman, 1971, 1998) that govern the dynamics of small amplitude nonlinearly interacting electromagnetic waves and ion-sound waves driven by the radiation pressure in an electron-ion plasma, due to the difference in the driving term on the right-hand side of Eq. (74).

The dispersion-free case admits pulse collapse (Marklund *et al.*, 2003; Shukla and Eliasson, 2004), and similar features appear within the dispersive case, with the difference that pulse splitting may occur, resulting in a train of ultrashort pulses. If the time response of the radiation background is slow, Eq. (74) may be integrated to yield $\delta\mathcal{E} \approx 2\lambda\mathcal{E}_0\epsilon_0|E_p|^2$, and from Eq. (70) we obtain the standard equation for analyzing ultrashort intense pulses in normal dispersive focusing media; see Chernev and Petrov (1992); Rothenberg (1992); Gaeta (2003); Kivshar and Agrawal (2003); Zharova *et al.* (2003), and references therein. It is well known that the evolution of a pulse within this equation displays first self-focusing, then pulse splitting (Chernev and Petrov, 1992; Rothenberg, 1992), and the approximate description of the solutions can be given as a product of bright and dark soliton solutions (Hayata and Koshiba, 1993). A modulational instability can be found as well (Kivshar and Agrawal, 2003).

4. Instability analysis

a. Two-dimensional case

As β_z goes to zero in Eq. (70), we regain the Marklund-Brodin-Stenflo equations (Marklund *et al.*, 2003). In this case, the dispersion relation for the modulational and filamentational instabilities of a constant amplitude photon pump $(\omega_0, \mathbf{k}_0)$ can be found by linearizing the simplified set of Eqs. (70) and (74) around the unperturbed state $E_p = E_0 = \text{const}$ and $\delta\mathcal{E} = 0$. Following the standard procedure of parametric instability analysis (Shukla, 1992; Kivshar and Agrawal, 2003) (see also next section), we consider perturbations varying according to $\exp[i(\mathbf{K}\cdot\mathbf{r} - \Omega t)]$. Here Ω and $\mathbf{K}$ are the frequency and wave vector of the acousticlike disturbances. Then, Eqs. (70) and (74) yield the nonlinear dispersion relation (Shukla and Eliasson, 2004; Shukla, Marklund, Tskhakaya, *et al.*, 2004)
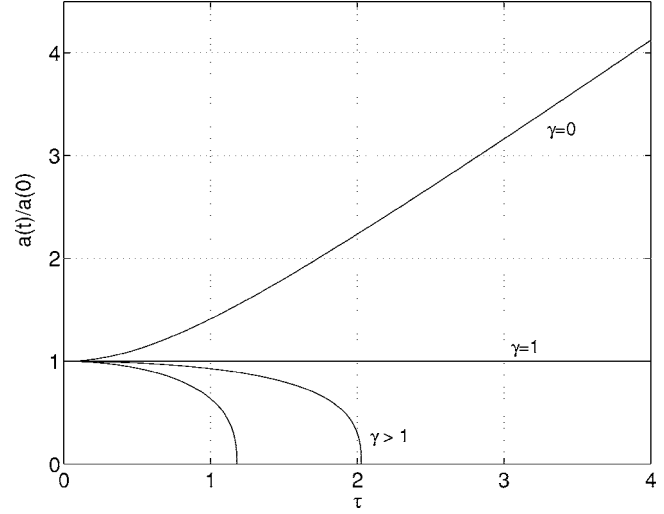
FIG. 9. The pulse width as a function of normalized time ($\tau \rightarrow ck_0\tau$) in the two-dimensional case. Note that the solitary solution ($\gamma = 1$) is unstable.

$$\left[(\Omega - c\hat{\mathbf{k}}_0 \cdot \mathbf{K})^2 - \frac{K_\perp^4 c^2}{4k_0^2} \right](3\Omega^2 - K^2c^2)$$

$$= \frac{4K_\perp^2 c^2}{3}(\Omega^2 + K^2c^2)\lambda^2\mathcal{E}_0\epsilon_0 E_0^2, \qquad (75)$$

where $K^2 = K_x^2 + K_y^2 + K_z^2 \equiv K_\perp^2 + K_z^2$. Defining $\Omega = cK_z + i\gamma_{2D}$, $|\gamma_{2D}| \ll cK_z$, we obtain the approximate modulational instability growth rate

$$\gamma_{2D} \approx \left\{ \frac{c}{2k_0}K_\perp^2 \left[\chi_{2D}\frac{K_\perp^2 + 2K_z^2}{K_\perp^2 - 2K_z^2} - \frac{c}{2k_0}K_\perp^2 \right] \right\}^{1/2}, \qquad (76)$$

where $\chi_{2D} = (8/3)ck_0\lambda^2\mathcal{E}_0\epsilon_0 E_0^2$.

Similarly, in the quasistationary limit $\Omega = 0$ a filamentational instability may occur. For $K_z \ll K_\perp$, we obtain

$$K_z^2 = \frac{K_\perp^4}{4k_0^2} - \frac{4}{3}K_\perp^2\lambda^2\mathcal{E}_0\epsilon_0 E_0^2. \qquad (77)$$

Thus filamentation of an intense photon beam on a radiation background takes place when $\epsilon_0|E_{p0}|^2 > 3K_\perp^2/16k_0^2\lambda^2\mathcal{E}_0$, due to elastic photon-photon scattering.

In the case of a slow acoustic response, we integrate Eq. (74) in comoving coordinates, to obtain a relation between the radiation gas perturbation and pulse intensity. By inserting the relation into Eq. (70) (with $\beta_z = 0$), we obtain

$$i\frac{\partial E_p}{\partial\tau} + \frac{c}{2k_0}\nabla_\perp^2 E_p + \frac{4}{3}\lambda^2 ck_0\varepsilon_0\mathcal{E}_0|E_p|^2 E_p = 0. \qquad (78)$$

The collapse properties of Eq. (78) can be obtained by approximate analytical means. Starting from a two-dimensional approximately Gaussian pulse $E_p = A(\tau)\text{sech}[r_\perp/a(\tau)]\exp[ib(\tau)r_\perp^2]$, where $r_\perp^2 = x^2 + y^2$, an approximate solution can be found (Desaix *et al.*, 1991). The relation $|A|/|A_0| = a_0/a$ is found, where the 0 denotes the initial value. Moreover, the parameter γ

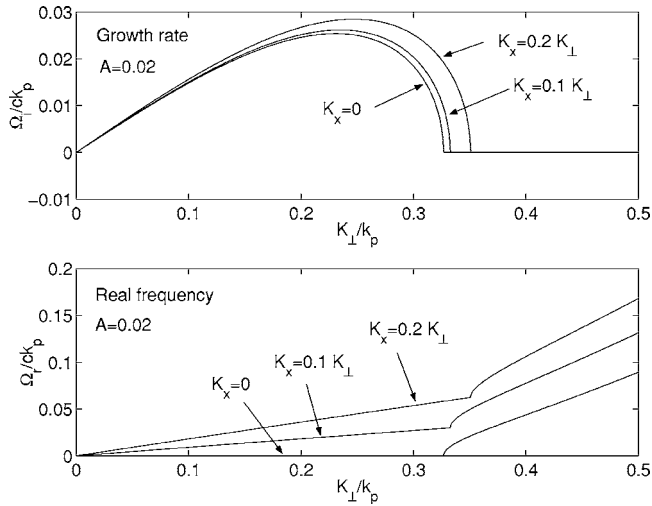FIG. 10. The growth rate and real part of the frequency, respectively, as a function of the orthogonal wave number for different values of the parallel wave number [see Eq. (76)]. The dimensionless pump strength is $A = \lambda^2 \mathcal{E}_0 \epsilon_0 E_0^2 = 0.02$. Reprinted with permission from Shukla and Eliasson, 2004.

$$= (4/3)\lambda^2 \epsilon_0 \mathcal{E}_0 k_0^2 |A_0|^2 a_0^2 (I_1/I_2), \quad \text{where} \quad I_1 = \int_0^\infty x \, \text{sech}^4(x) dx$$

$= (4 \ln 2 - 1)/6$ and $I_2 = \int_0^\infty x^3 \text{sech}^2(x) dx = 9\zeta(3)/8$, and ζ is the Riemann zeta function, characterizes the critical behavior of the solution in terms of the initial data. The collapse criteria can be seen in Fig. 9.

    Exact results regarding the two-dimensional modulational and filamentational instabilities were found by Shukla and Eliasson (2004), where numerical solutions of Eq. (75) were presented; see Figs. 10 and 11. The growth of random seeds on a radiation gas background was also investigated and is shown in Fig. 12.

b. The three-dimensional case

    We now show the presence of modulational and filamentational unstable modes for the three-dimensional
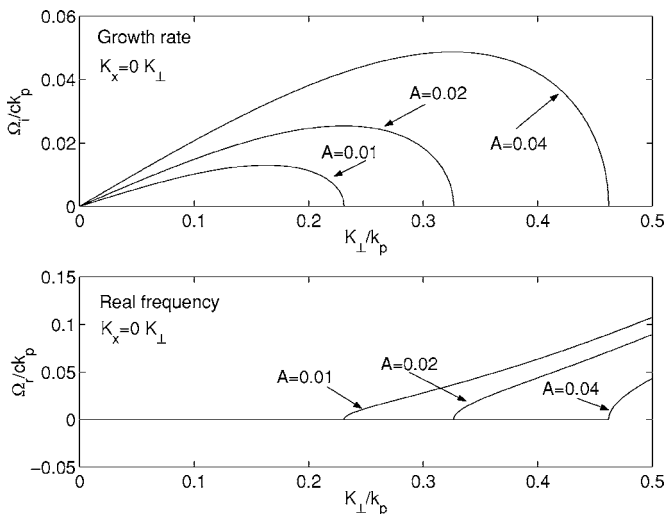
FIG. 11. The growth rate and real part of the frequency, respectively, as a function the orthogonal wave number for different dimensionless pump strengths $A = \lambda^2 \mathcal{E}_0 \epsilon_0 E_0^2$ [see Eq. (76)]. Reprinted with permission from Shukla and Eliasson, 2004.
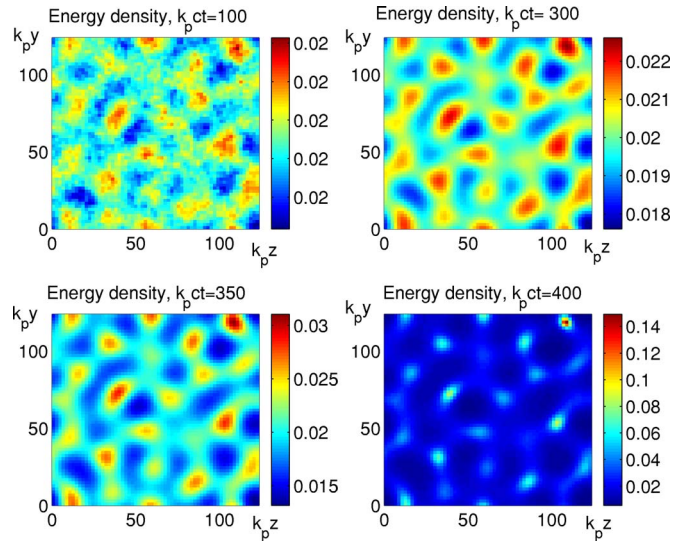
FIG. 12. (Color online) The two-dimensional evolution, as given by Eqs. (70) and (74) with $\beta_z = 0$, of the dimensionless pulse energy density $\lambda^2 \mathcal{E}_0 \epsilon_0 |E_p|^2$ for initially random perturbations on a radiation gas background. The color bars give the dimensionless pulse energy density. Reprinted with permission from Shukla and Eliasson, 2004.

case, as given by Eqs. (70) and (74). Fourier analyzing Eq. (74) according to $\delta \mathcal{E}$ and $|E_p|^2 \propto \exp[i(\mathbf{K} \cdot \mathbf{r} - \Omega t)]$, we obtain

$$\delta \mathcal{E} = \frac{2}{3} \lambda \mathcal{E}_0 W \epsilon_0 |E_p|^2, \tag{79}$$

where $W = (\Omega^2 + c^2 K^2)/(-\Omega^2 + c^2 K^2/3)$, with Ω and $\mathbf{K}$ the frequency and wave vector, respectively, of the Fourier component. Next, following Shukla (1992) [see also Kivshar and Agrawal (2003)], we let $E_p = (E_0 + E_1)\exp(i\delta t)$, where δ is the nonlinear phase shift and $E_0(\gg|E_1|)$ is a real constant. To zeroth order in E_1 we have the nonlinear phase shift $\delta = -\kappa E_0^2$. We let $E_1 = d_1 \exp[i(\mathbf{K} \cdot \mathbf{r} - \Omega t)] + d_2 \exp[-i(\mathbf{K} \cdot \mathbf{r} - \Omega t)]$, with d_1 and d_2 real constants. Linearizing Eq. (70) with respect to E_1, we obtain a coupled system of equations for d_1 and d_2. Eliminating d_1 and d_2, we obtain the dispersion relation (Shukla, Marklund, Tskhakaya, *et al.*, 2004)

$$(\Omega - K_z v_g)^2 = \frac{v_g}{2k_0}(K_\perp^2 - \beta_z K_z^2)$$
$$\times \left[\frac{v_g}{2k_0}(K_\perp^2 - \beta_z K_z^2) - \frac{1}{3}\chi W \right], \tag{80}$$

where $\chi = 4\mu\lambda \mathcal{E}_0 \epsilon_0 E_0^2$. Remembering that W depends on the perturbation frequency and wave vector, we see that the solution to Eq. (80) in terms of Ω is nontrivial.

    Letting $\Omega = K_z v_g + i\gamma_m$ in Eq. (80), $|\gamma_m| \ll K_z v_g$, we obtain the approximate modulational instability growth rate

FIG. 13. (Color online) The normalized growth rate $\gamma/(ck_0)$, as given through the dispersion relation (80), as a function of $K_\perp/k_0$ and K_z/k_0. We note that due to cylindrical symmetry, the area of nonzero growth rate is really a conelike structure. Here $A = \lambda^2 \mathcal{E}_0 \epsilon_0 E_0^2$. Reprinted with permission from Shukla, Marklund, Tskhakaya, et al., 2004. Copyright 2004, American Institute of Physics.
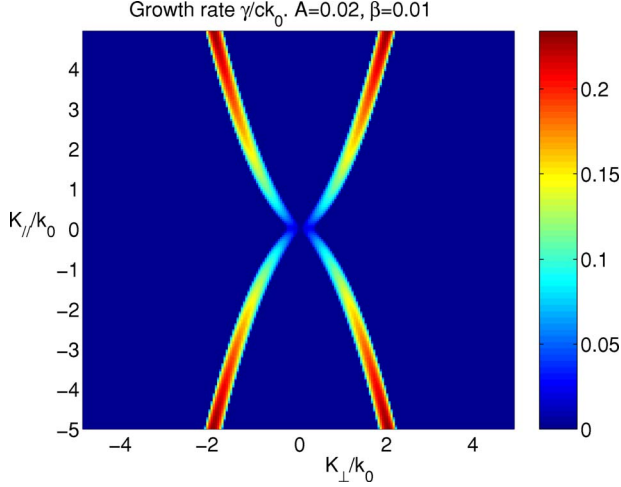
$$\gamma_m \approx \left\{ \frac{v_g}{2k_0}(K_\perp^2 - \beta_z K_z^2) \left[\chi \frac{K_\perp^2 + (1 + v_g^2/c^2)K_z^2}{K_\perp^2 + (1 - 3v_g^2/c^2)K_z^2} \right. \right.$$
$$\left. \left. - \frac{v_g}{2k_0}(K_\perp^2 - \beta_z K_z^2) \right] \right\}^{1/2}. \qquad (81)$$

Thus when $v_g \approx c$, we see that, unlike the standard modulational instability, we have larger growth rate for smaller length scale, with the occurring asymptotically for $K_\perp \sqrt{2} K_z$, where the approximate expression (81) diverges.

If the perturbations are stationary, Eq. (80) yields

$$K_z \approx \pm \frac{1}{v_g} \left\{ \frac{v_g}{2k_0} K_\perp^2 \left[\frac{v_g}{2k_0} K_\perp^2 - \chi \right] \right\}^{1/2} \qquad (82)$$

when $\beta_z K_z^2 \ll K_\perp^2$, and we see that a filamentation instability will occur for $\chi > v_g K_\perp^2/2k_0$.

Solving Eq. (80) for the growth rate, one obtains the instability regions shown in Fig. 13. We note that the results found by Shukla, Marklund, Tskhakaya, et al. (2004) concerning the modulational instability are similar to the ones obtained by Karpman and Washimi (1977), where it was found that the largest growth rates are due to parametric instabilities for wave vectors oblique to the pulse propagation direction. Shukla, Marklund, Tskhakaya, et al. (2004) performed a numerical simulation of the three-dimensional system of Eqs. (70) and (74). In Fig. 14 the collapse of the initially weakly modulated beam $E_p = (\lambda^2 \mathcal{E}_0 \epsilon_0)^{-1/2} A[1 + 0.1 \sin(40\pi k_0 z)] \exp(-r_\perp^2/2a^2)$ can be seen. Using $A = \sqrt{0.02}$ and $a = 10k_0^{-1}$, the beam interact with the initially homogenous radiation gas background. The collapse is seen by the decrease in the beam width $r_\perp = \sqrt{x^2 + y^2}$ and the increase in the beam energy density. In Fig. 15
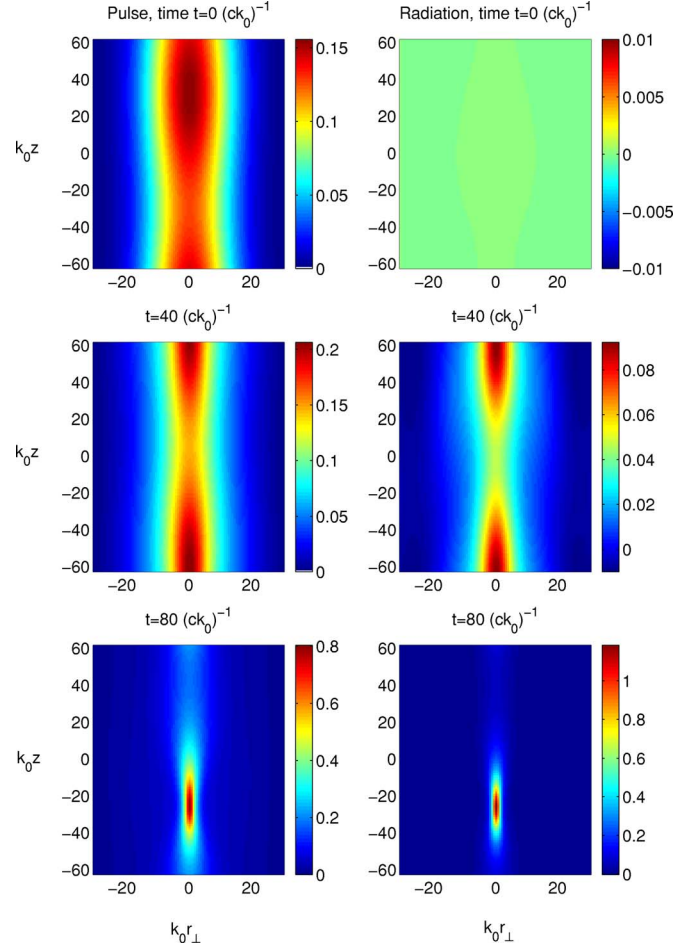
FIG. 14. (Color online) The three-dimensional evolution of a normalized modulated beam energy density $\lambda^2 \mathcal{E}_0 \epsilon_0 |E_p|^2$ (left panels) and the normalized radiation gas energy density $\lambda \, \delta\mathcal{E}$ (right panels). The color gives the intensity. The beam collapses after a finite time, as does the inhomogeneity in the radiation gas. Reprinted with permission from Shukla, Marklund, Tskhakaya, et al., 2004. Copyright 2004, American Institute of Physics.

the evolution of an initially spherical pulse $E_p = (\lambda^2 \mathcal{E}_0 \epsilon_0)^{-1/2} A \exp(-r_\perp/2a^2)$ is seen. As the pulse propagated through the initially homogeneous radiation gas, collapse ensues, as can be seen by the decrease in the pulse width $r = \sqrt{x^2 + y^2 + z^2}$ and the increase in the pulse energy density. The values of A and a are the same as in the beam case. We note that the pulse in the last panel undergoes splitting, and the radiation gas response develops a photon wedge, analogous to a Mach cone, through which energy is radiated.

5. Pulse collapse and photonic wedges

The approximate analytical results in conjunction with the numerical simulations presented above shows collapse, filamentation, and pulse splitting as generic features of the system (70) and (74). On the other hand, both these methods of investigation have shortcomings, and it is therefore of great interest to obtain more analytical predictions valid for a wider range of parameters.
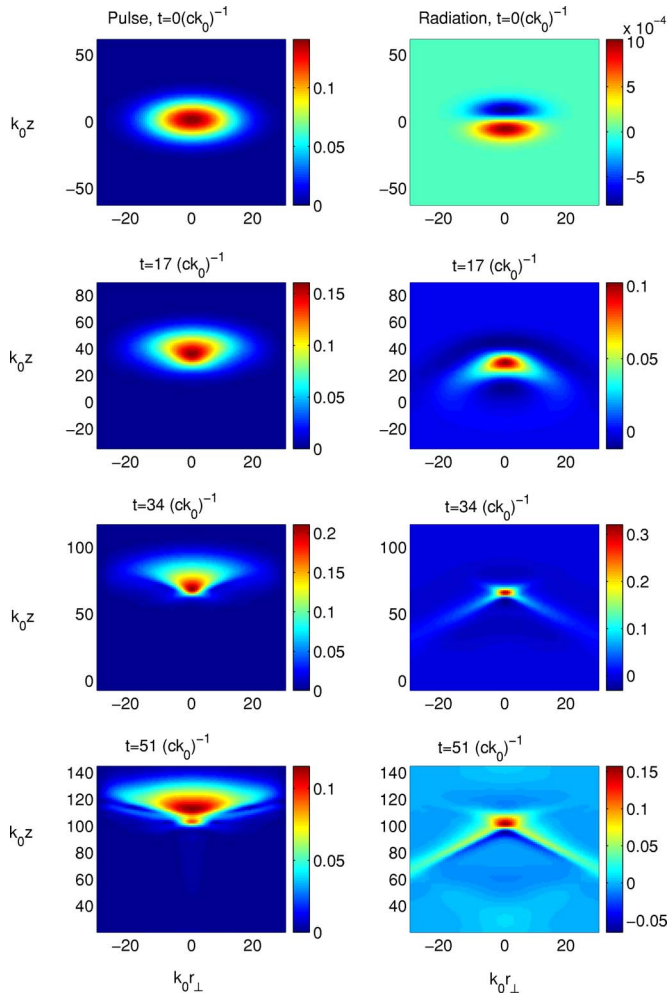
FIG. 15. (Color online) The evolution of a normalized spherical pulse energy density $\lambda^2 \mathcal{E}_0 \epsilon_0 |E_p|^2$ (left panels) and the normalized radiation gas energy density $\lambda \delta \mathcal{E}$ (right panels). The pulse first undergoes compression, and later splitting, while the radiation gas develops a high intensity region, from which photon wedges (similar to a Mach cone) are radiated. Reprinted with permission from Shukla, Marklund, Tskhakaya, *et al.*, 2004. Copyright 2004, American Institute of Physics.

In this section we show that under very general conditions pulse split and collapse are essential features of the photon pulse-acoustic system (70) and (74).

As we have seen, the dynamics of an intense short photon pulse and the radiation background response is described by the system of Eqs. (70) and (74).

Following Shukla, Marklund, Tskhakaya, *et al.* (2004), we renormalize the system of Eqs. (70) and (74), by introducing the new variables $E = (4k_0 \mu \lambda \epsilon_0 \mathcal{E}_0 / v_g)^{1/2} E_p(t, r_\perp, z - v_g t)$, $\tau = v_g t / k_0$, and $\delta \mathcal{E} = (v_g / 2k_0 \mu)(|E|^2 - \mathcal{N})$. It is implied that the wave packet has cylindrical symmetry and moves along the z axis. From Eqs. (70) and (74) we obtain

$$2i\frac{\partial E}{\partial \tau} + \nabla_\perp^2 E - \beta_z \frac{\partial^2}{\partial z^2}E + |E|^2 E + \mathcal{N}E = 0 \qquad (83a)$$

and

$$\left(\frac{\partial^2}{\partial \tau^2} - \frac{k_0^2 c^2}{3v_g^2}\nabla^2\right)\mathcal{N} = \frac{4}{3}\frac{\partial^2}{\partial \tau^2}|E(t,r_\perp,z - v_g t)|^2, \qquad (83b)$$

respectively.

Representing $\delta \mathcal{E}$ in terms of $|E|^2$ and $\mathcal{N}$, the perturbation part of the radiation gas that is concentrated in the region of localization of the wave packet and takes part in its compression has been isolated. The second part of $\delta \mathcal{E}$ corresponds to the interaction of the pulse with the radiation field $\mathcal{N}$. This interaction is described by the last term in Eq. (83a). As seen by Eq. (83b) [or Eq. (74)], the velocity $v_g \approx c$ of the source (the pulse) exceeds the velocity $c/\sqrt{3}$ of the radiation waves, i.e., $v_g > c/\sqrt{3}$, and it is therefore expected that the radiation field n will be localized behind the pulse. Hence it is assumed that the pulse and radiation field are localized in different volumes, and in the region with a possible overlap the relation $\mathcal{N} \ll |E|^2$ is satisfied (see also the end of the next section). This inequality allows us to neglect the last term in Eq. (83a), which means neglecting the back reaction of the radiation on the pulse. In this approximation, the pulse field E drives the radiation field $\mathcal{N}$ through Eq. (83b), while the pulse propagation is unaffected by the radiation field.

From Eq. (83a) we have the conservation of the "field mass" parameter of the pulse

$$N = \int |E|^2 d\mathbf{r}_\perp dz, \qquad (84a)$$

and the Hamiltonian

$$H = \int \mathcal{H} \, d\mathbf{r}_\perp dz, \qquad (84b)$$

where the Hamiltonian density is given by $\mathcal{H} = |\nabla_\perp E|^2 - \beta_z |\partial_z E|^2 - |E|^4/2$.

Some information on the spatiotemporal behavior of the initially localized wave packet can be found by following the evolution of the characteristic widths of the packet in the transversal and longitudinal directions. These widths are defined by

$$R^2(\tau) = \frac{1}{N}\int r_\perp^2 |E|^2 d\mathbf{r}_\perp dz \qquad (85)$$

and

$$Z^2(\tau) = \frac{1}{N}\int z^2 |E|^2 d\mathbf{r}_\perp dz. \qquad (86)$$

Straightforward calculations give the following evolution equations:

$$\frac{\partial^2 R^2}{\partial \tau^2} = \frac{2}{N}\int \left(|\nabla_\perp E|^2 - \frac{1}{2}|E|^4\right)d\mathbf{r}_\perp dz \qquad (87)$$

and

$$\frac{\partial^2 Z^2}{\partial \tau^2} = \frac{2}{N}\beta_z \int \left(\beta_z \left|\frac{\partial E}{\partial z}\right|^2 + \frac{1}{4}|E|^4\right)d\mathbf{r}_\perp dz > 0 \qquad (88)$$

for the widths (85) and (86), respectively.

In the two-dimensional (2D) case, the process of self-compression of the wave packet can be clearly seen (Tskhakaya, 1982; Kuznetsov et al., 1995). A necessary condition for collapse in this case consists in the predominance of the field mass N of the given state over some critical value N_c, i.e., $N > N_c$, where N_c is the field mass calculated for the stationary ground state (Kuznetsov et al., 1995). The ground state is described by the (positive) radially symmetric solution $\Psi = E(r, \tau) \times \exp(-i\lambda\tau)$ of the equation

$$\nabla_\perp^2 \Psi - \lambda\Psi + \Psi^3 = 0, \tag{89}$$

derived from Eq. (83a) and computed with $\lambda = 1$. In the 2D case, the right-hand side of the expression for the mean-square transverse radius (87) is $2H/N$, i.e., a combination of the conserved quantities. Thus integrating Eq. (87) twice, we obtain

$$R^2(\tau) = R^2(0) + C\tau + (H/N)\tau^2, \tag{90}$$

where the constants $R^2(0)$ and C are defined by initial conditions. Hence a sufficient condition for 2D self-focusing, ultimately leading to complete collapse in a finite time, is $H < 0$. Because this is independent of the value of C, there will always exists a finite time t_0 for which the transverse radius vanishes. In the three-dimensional (3D) case and for $\beta_z < 0$ (corresponding to anomalous dispersion) the equality (90) must be replaced by the inequality

$$R^2(\tau) < C_0 + C_1\tau + (H/N)\tau^2, \tag{91}$$

and the sufficient condition for the collapse of the wave packet is again $H < 0$ (Kuznetsov et al., 1995).

Equation (83a) with $\beta_z > 0$ and $\mathcal{N} = 0$ corresponds to the normal dispersion region of the wave packet. In Berge et al. (1996), Berge and Rasmussen (1996), and Berge et al. (1998) the features of the pulse self-focusing, described by the solution to Eq. (83a), have been investigated in detail. Their conclusions can be applied directly to the numerical results presented here concerning the breakup of the wave packet. Berge et al. (1996) showed that the characteristic length $Z^2(\tau)$ of the wave-packet localization along the direction of propagation is bounded from below by a positive constant. The relation (88) indicates an asymptotic longitudinal spreading. Thus a 3D (global) collapse cannot take place in media with normal dispersion, since the necessary conditions for the pulse self-focusing to occur is $\partial R^2/\partial\tau < 0$ and $\partial Z^2/\partial\tau > 0$, which explicitly excludes the 3D case. The self-focusing in the transverse direction is accompanied by a longitudinal spreading and in the following by the splitting of the pulse. This does not, however, immediately exclude partial (local) collapse scenarios.

The process of pulse splitting close to the time of self-focusing $t \to t_0$ has been described by Berge and Rasmussen (1996) and Berge et al. (1998) employing a *quasi-self-similar* analysis. This approach uses, besides the description of the solution of Eq. (83a) (neglecting $\mathcal{N}$), the time-dependent characteristic lengths in the longitudinal $l_z(t)$ and transversal $l_\perp(t)$ directions. Berge and

Rasmussen (1996) and Berge et al. (1998) found that the transverse scale $l_\perp(t)$ exhibits a changing behavior as one passes some critical point $z^*(t)$ on the z axis. Inside the localized region $z < z^*(t)$, the transverse width collapses with the rate $l_\perp(t) \sim (t_0 - t)^{1/2}/(\ln\{\ln[1/(t_0 - t)]\})^{1/2}$, while in the complementary (delocalizing) domain, $z > z^*(t)$, the transverse pulse width spreads out with the rate $l_\perp(t) \sim \sqrt{t \ln\{\ln[1/(t_0 - t)]\}}$. Hence the time derivative of $l_\perp(t)$ changes sign around the point $z^*(t)$. Meanwhile, the self-similar longitudinal scale $l_z(t)$ increases slowly in time. Berge and Rasmussen (1996) and Berge et al. (1998) found that near the self-focusing time $t \to t_0$, $l_z(t) \sim t$, which implies a linear increase of $z^*(t)$ in time such that $z^*(t_0) [\sim \sqrt{\beta_z} l_z(t_0)]$. The presence of the coefficient $\sqrt{\beta_z}$ leads to a decrease in the distance of the critical point $z^*(t_0)$ from the origin for small β_z. The scale $l_\perp(t)$ remains strictly positive at times $t \lesssim t_0$. Consequently, the transversal scale reaches a minimum value at a finite distance $z^*(t_0)$.

Since the wave packet is assumed to be cylindrically symmetric and also symmetric relative to the origin $z = 0$, the total field distribution during self-focusing must exhibit two maxima located at $z = \pm z^*(t_0)$, respectively. The wave packet has therefore been split into two identical smaller cells, symmetrically placed on each side of the origin $z = 0$.

Hence a wave packet, propagating in media with anisotropic dispersion, will be spread out along the direction of the negative dispersion, and split up into smaller cells. These analytic results have been confirmed by numerical solutions (Luther et al., 1994; Berge et al., 1998). The duration Δt of self-focusing, accompanied by the pulse splitting, can be estimated using Eq. (87) as

$$\Delta t \approx \frac{k_0}{v_g} R(0) \sqrt{\frac{N}{H}}. \tag{92}$$

The first part of our numerical solution—where the splitting of the wave packet takes place—coincides with these results. The small coefficient β_z, which determines the negative dispersion, changes the distance (from the origin) along the z axis, at which the field is localized after splitting.

Berge and Rasmussen (1996) and Berge et al. (1998) have shown that this splitting process can be continued (multisplitting process) if newly formed cells possess a transverse energy higher than the self-focusing threshold N_c. In our case, the wave packet only splits into two cells, as the energy localized in each new cell is below the threshold N_c. Furthermore, the wave packet also loses energy to the radiation gas during the splitting process. The formation of these photonic wedges, or the radiation Mach cone, can be analyzed in accordance with the results of Shukla, Marklund, Tskhakaya, et al. (2004), such that, e.g., the energy loss from the pulse can be estimated.

In conjunction with pulse collapse in a radiation gas it should be mentioned that if the field invariant $\mathbf{E}^2 - c^2\mathbf{B}^2 > 0$ pair creation will occur as the pulse intensity

increases, and the loss of energy through photonic wedges will be negligible in comparison to the energy radiated into fermionic degrees of freedom. This will give rise to a rich and complex dynamical interplay between pulse photons, the radiation gas, and the pair plasma (Bulanov *et al.*, 2005). For interactions between a pulse and a pure radiation gas, we have $c|\mathbf{B}| > |\mathbf{E}|$, due to zero dispersion, and pair creation would not occur. However, since we will in practice always have some ionized particles present, pair creation is likely to be the result of pulse collapse due to weak dispersive plasma effects.

6. Strong-field case

Our knowledge of nonlinear refractive properties of the radiation gas gives a means for investigating effects of higher-order nonlinear corrections to the standard first-order Heisenberg-Euler Lagrangian, and to probe the significance of higher-order effects for photonic collapse (Marklund *et al.*, 2003; Marklund, Eliasson, and Shukla, 2004; Shukla and Eliasson, 2004). The dynamics of coherent photons, traveling through an intense radiation gas, may be analyzed as above, following Marklund *et al.* (2003). We obtain a nonlinear Schrödinger equation for the slowly varying pulse envelope E_p according to (Kivshar and Agrawal, 2003)

$$i\left(\frac{\partial}{\partial t} + \mathbf{v}_0 \cdot \boldsymbol{\nabla}\right)E_p + \frac{v_0}{2k_0}\nabla_\perp^2 E_p + \omega_0\frac{n_{nl}(\delta\mathcal{E})}{n_0}E_p = 0, \quad (93)$$

where the subscript 0 denotes the equilibrium background state, $\nabla_\perp^2 = \nabla^2 - (\hat{\mathbf{k}}_0 \cdot \boldsymbol{\nabla})^2$, $\delta\mathcal{E} = \mathcal{E} - \mathcal{E}_0$ is a perturbation, $v_0 = v(\mathcal{E}_0)$, $n_0 = n(\mathcal{E}_0)$, $n_{nl}(\delta\mathcal{E}) = \sum_{m=1}^\infty n_0^{(m)}\delta\mathcal{E}^m/m!$, $n_0^{(m)} = d^m n_0/d\mathcal{E}_0^m$, and the refractive index n is given through Eqs. (37) and (38).

For a dispersion relation $\omega = |\mathbf{k}|c/n(\mathbf{r}, t)$, the motion of a single photon may be described by the Hamiltonian ray equations (71) (Mendonça, 2001). Since $n = n(\mathcal{E})$ and $dn/d\mathcal{E} > 0$ always hold [see Marklund, Shukla, and Eliasson (2005)], a denser region of the radiation gas will exercise an attractive force on the photon (Partovi, 1994), thus creating lensing effects. The single-particle dynamics thus supports that photonic self-compression is an inherent property of the one-loop radiation gas, but we note that as the density of a region increases, the phase velocity approaches a constant value, given by Eq. (41), i.e., $\nabla \ln n \to 0$.

Following Marklund *et al.* (2003), the response of the radiation gas to a plane-wave pulse may be formulated in terms of an acoustic wave equation, generalizing Eq. (74) to the strong-field case, according to (Marklund, Shukla, and Eliasson (2005))

$$\left(\frac{\partial^2}{\partial t^2} - \frac{v_0^2}{3}\nabla^2\right)\delta\mathcal{E} = -\frac{\mathcal{E}_0}{n_0}\left(\frac{\partial^2}{\partial t^2} + v_0^2\nabla^2\right)n_{nl}(|E_p|^2). \quad (94)$$

If the time response of $\delta\mathcal{E}$ is slow, Eq. (94) gives

$$\delta\mathcal{E} \approx \frac{3\mathcal{E}_0 n_0'}{n_0}\left(1 + \frac{n_0''}{2n_0'}|E_p|^2\right)|E_p|^2. \quad (95)$$

Using Eq. (95) and the expression for $n_{nl}(\delta\mathcal{E})$, we can write Eq. (93) as

$$i\left(\frac{\partial}{\partial t} + \mathbf{v}_0 \cdot \boldsymbol{\nabla}\right)E_p + \frac{v_0}{2k_0}\nabla_\perp^2 E_p + \omega_0\left(\frac{3\mathcal{E}_0 n_0'}{n_0}\right)^2$$
$$\times\left(1 + \frac{n_0''}{2n_0'}|E_p|^2\right)|E_p|^2 E_p = 0. \quad (96)$$

When $n_0''|E_p|^2/2n_0' \ll 1$, we have a self-focusing nonlinearity in Eq. (96), but as $|E_p|$ grows the character of the nonlinear coefficient changes. The coefficient is positive when $|E_p|^2 < E_{sat}^2 \equiv |2n_0'/n_0''|$, but since $n_0'' < 0$ for all $\mathcal{E}_0$ (Marklund, Shukla, and Eliasson, 2005), the sign changes as the pulse amplitudes grow above the saturation field strength E_{sat}, making the nonlinearity defocusing and arresting the collapse. The numerical value of this turning point is dependent on the background parameter $\mathcal{E}_0$. For low intensity radiation gases, $n_0'' \approx 0$, and Eq. (96) always displays self-focusing, i.e., field strengths can reach values above the Schwinger field. When $\mathcal{E}_0$ roughly reaches the critical value $\mathcal{E}_{crit}$, the weak-field approximation breaks down, and Eqs. (37) and (42) can be used to derive an expression for E_{sat}. As an example displaying the general character of the intense background case, consider $\mathcal{E}_0 = \mathcal{E}_{crit} \times 10^2$. We find that $E_{sat} \approx 2 \times 10^{17}$ V/cm $> E_{crit}$, i.e., the pulse saturates above the Schwinger critical field. Thus both the weak and moderately strong intensity cases, the latter described here by Eq. (96), display self-compression above the Schwinger critical field.

This analysis can be generalized to take into account the statistical spread in the coherent pulse, giving rise to a damping of instabilities (Marklund, 2004).

7. Other field configurations

Above we have seen that the propagation of an electromagnetic pulse through a radiation field gives rise to instabilities, wave collapse, self-focusing, and pulse splitting. These concepts can be carried over to the case of multiple beams or pulses propagating through a radiation gas, including pulse incoherence. Marklund, Shukla, Brodin, *et al.* (2005) showed that when several pulses are present, they can exchange energy via a background radiation gas and instabilities can occur, even if their propagation is parallel.

Shukla, Marklund, Brodin, *et al.* (2004) considered an incoherent nonthermal high-frequency spectrum of photons. As will be shown, this spectrum can interact with low-frequency acousticlike perturbations. The high-frequency part is treated by means of a wave kinetic description, whereas the low-frequency part is described by an acoustic wave equation with a driver (Marklund *et al.*, 2003) which follows from a radiation fluid description. The high-frequency photons drive low-frequency acoustic perturbations according to (Marklund *et al.*, 2003)

$$\left(\frac{\partial^2}{\partial t^2} - \frac{c^2}{3}\nabla^2\right)\mathcal{E} = -\frac{2\lambda\mathcal{E}_0}{3}\left(\frac{\partial^2}{\partial t^2} + c^2\nabla^2\right)$$

$$\times \int \hbar\,\omega f(\mathbf{k},\mathbf{r},t)d^3k, \qquad (97)$$

where the constant $\mathcal{E}_0$ is the *background* radiation fluid energy density and f is the high-frequency photon distribution function. This hybrid description, where the high-frequency part is treated kinetically, and the low-frequency part is described within a fluid theory, applies when the mean-free path between photon-photon collisions is shorter than the wavelengths of low-frequency perturbations. We note that the specific intensity $I_k = \hbar\omega f/\epsilon_0$ satisfies Eq. (72), and is normalized such that $\langle|E|^2\rangle = \int I_k d^3k$, where E is the high-frequency electric-field strength. These equations resemble the photon-electron system in the paper by Shukla and Stenflo (1998), where the interaction between randomly phased photons and sound waves in an electron-positron plasma has been investigated.

Next, we consider a small low-frequency long-wavelength perturbation of a homogeneous background spectrum, i.e., $f = f_0 + f_1\exp[i(Kz - \Omega t)]$, $|f_1| \ll f_0$ and $\mathcal{E} = \mathcal{E}_1\exp[i(Kz - \Omega t)]$, and linearize our equations. Thus we obtain the nonlinear dispersion relation

$$1 = -\frac{\mu K}{3}\frac{\Omega^2 + K^2c^2}{\Omega^2 - K^2c^2/3}\int\frac{k^2}{\Omega - Kc\hat{\mathbf{k}}\cdot\hat{\mathbf{z}}}\hat{\mathbf{z}}\cdot\frac{\partial f_0}{\partial \mathbf{k}}d^3k, \quad (98)$$

where $\mu = \frac{4}{3}\lambda^2c^2\hbar\mathcal{E}_0$.

(a) For a monoenergetic high-frequency background, we have $f_0 = n_0\delta(\mathbf{k} - \mathbf{k}_0)$. The nonlinear dispersion relation (98) then reduces to

$$(\Omega^2 - K^2c^2/3)(\Omega - Kc\cos\theta_0)^2$$

$$= \frac{\mu n_0 k_0 K}{3}(\Omega^2 + K^2c^2)$$

$$\times[Kc + (2\Omega - 3Kc\cos\theta_0)\cos\theta_0], \qquad (99)$$

where we have introduced $\cos\theta_0 \equiv \hat{\mathbf{k}}_0\cdot\hat{\mathbf{z}}$. This monoenergetic background has a transverse instability when $\theta_0 = \pi/2$, with the growth rate

$$\Gamma = \frac{Kc}{\sqrt{6}}\left[\sqrt{\left(\frac{v_T}{c}\right)^4 + 14\left(\frac{v_T}{c}\right)^2 + 1} - \left(\frac{v_T}{c}\right)^2 - 1\right]^{1/2}, \qquad (100)$$

where $\Gamma \equiv -i\Omega$ and $v_T \equiv (\mu n_0 k_0 c)^{1/2}$ is a characteristic speed of the system. The expression in the square brackets is positive definite.

In fact, when $\mathcal{E}_0\hbar ck_0 n_0/E_{\text{crit}}^4 \ll 1$, a condition which is satisfied due to Eq. (4), we have $v_T \ll c$. Using Eq. (99), we then have two branches. The branch corresponding to $\Omega \approx Kc/\sqrt{3}$ is always stable for small v_T, while for the branch corresponding to $\Omega \approx Kc\cos\theta_0$ we obtain the growth rate
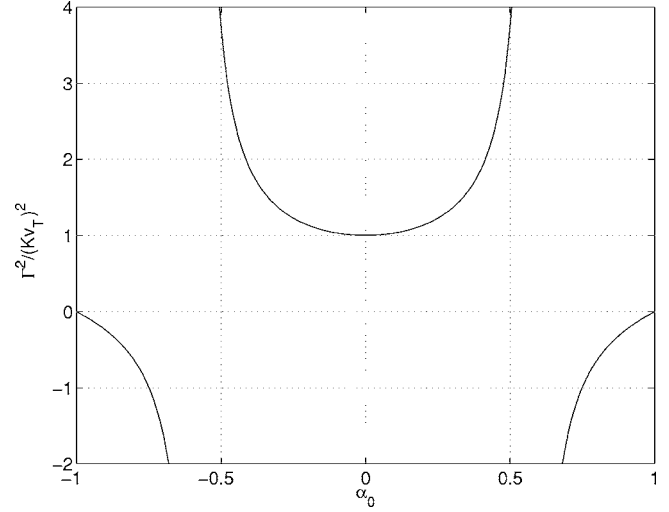
FIG. 16. $(\Gamma/Kv_T)^2$, according to Eq. (101), plotted as a function of $\alpha_0 = \cos\theta_0$ in the monoenergetic case. Reprinted from Shukla, Marklund, Brodin, *et al.*, 2004. Copyright 2004, with permission from Elsevier.

$$\Gamma = Kv_T\sqrt{\frac{1 - \cos\theta_0}{1 - 3\cos\theta_0}}, \qquad (101)$$

which is consistent with Eq. (100) in the limit $\theta_0 \to \pi/2$. In Fig. 16, the behavior of the growth rate (101) is depicted.

(b) High-frequency photons have generally a spread in momentum space. For simplicity, we choose the background intensity distribution as a shifted Gaussian, i.e.,

$$I_{k0} = \frac{\mathcal{I}_0}{\pi^{3/2}k_W^3}\exp\left[-\frac{(\mathbf{k} - \mathbf{k}_0)^2}{k_W^2}\right], \qquad (102)$$

where $\mathcal{I}_0 = \langle|E_0|^2\rangle$ is the (constant) background intensity and k_W is the width of the distribution around $\mathbf{k}_0$. Assuming that the deviation of $\mathbf{k}_0$ from the $\hat{\mathbf{z}}$ axis is small, and that $\delta \equiv k_0/k_W \ll 1$, we can integrate Eq. (98) with Eq. (102), keeping terms linear in δ, to obtain

$$1 \approx -\pi b^2\frac{\eta^2 + 1}{\eta^2 - 1/3}\left[\frac{3\sqrt{\pi}}{2} + 8\delta\eta\cos\theta_0 + \left(\delta\cos\theta_0\right.\right.$$

$$\left.\left. -\frac{3\sqrt{\pi}}{4}\eta - 4\delta\eta\cos\theta_0\right)(2\,\text{arctanh}\,\eta - i\pi)\right], \quad (103)$$

for $0 < \eta < 1$. Here $\eta \equiv \Omega/Kc$ and $b^2 = (4/9\pi^{3/2})\lambda^2\epsilon_0\mathcal{E}_0\mathcal{I}_0\exp(-k_0^2/k_W^2)$. Thus we see that the nonzero width of the distribution complicates the characteristic behavior of the dispersion relation considerably. It is clear that the width will reduce of the growth rate compared to the monoenergetic case.

We may also look at the case when the time dependence is weak, i.e., $\partial^2\mathcal{E}/\partial t^2 \ll c^2\nabla^2\mathcal{E}$, such that Eq. (97) yields $\mathcal{E} = 2\lambda\mathcal{E}_0\int\hbar\omega_k f d^3k$. Upon using this relation, we find that $\nabla\omega = -\mu k\nabla\int k'f'd^3k'$. Hence Eq. (72) becomes

$$\frac{\partial f}{\partial t} + \mathbf{v}_g \cdot \frac{\partial f}{\partial \mathbf{r}} + \mu k \left(\frac{\partial}{\partial \mathbf{r}} \int k' f' d^3 k' \right) \cdot \frac{\partial f}{\partial \mathbf{k}} = 0. \qquad (104)$$

A similar equation may be derived for the specific intensity I_k. Equation (104) describes the evolution of high-frequency photons on a slowly varying background radiation fluid, and it may be used to analyze the long-term behavior of amplitude modulated intense short incoherent laser pulses. The results in this section can be generalized to several partially coherent pulses (Marklund, Shukla, Brodin, *et al.*, 2005).

C. Effects due to plasmas

Plasma channels are closely connected to both the plasma dispersion and propagation of wave modes in waveguides. Shen and Yu (2003) and Shen *et al.* (2003) first suggested the use of plasma cavitation as a means of fostering conditions in which nonlinear quantum vacuum effects, such as photon-photon scattering, could take place. As a high intensity electromagnetic pulse propagates through a plasma, the interaction with the plasma may completely evacuate regions giving conditions similar to the that of Secs. III.A.3 and III.A.4.

Moreover, although in many cases the presence of a plasma will swamp effects due to photon-photon scattering, it can under certain circumstances provide a means for the propagation of nonclassical plasma modes. Due to the nontrivial dispersion of electromagnetic waves in plasmas, there will be a net effect due to photon-photon scattering, such that low-frequency modes will be generated. In general, effects of a nonlinear quantum vacuum is expected to become pronounced for next generation lasers (Bulanov *et al.*, 2000, 2004; Mourou *et al.*, 2006).

Also, for future applications, the combination of photon-photon scattering induced pulse compression in conjunction with pair creation (Nitta *et al.*, 2004) could provide interesting insights both into fundamental properties of the quantum vacuum as well as into the prospects of creating high power electromagnetic sources. The effects of plasmas within the environment of a quantum vacuum therefore deserve further investigations.

1. Plasma cavitation and plasma channels

If the power of the laser pulse propagating through the plasma surpasses the critical value $P_{\text{crit}} = 17(\omega/\omega_p)^2$ GW, where ω is the laser frequency and ω_p is the electron plasma frequency, there may be complete expulsion of plasma particles from the high intensity region (Max *et al.*, 1974), thus forming a waveguide (Shen and Yu, 2003). In such waveguides, the effects of photon-photon scattering could be of importance (Shen *et al.*, 2003).

The nonlinear interactions of plasmas with high intensity lasers is of great current interest [see, e.g., Tajima and Taniuti (1990); Goloviznin and Shep (1999); Shen and Yu (2002); Bulanov *et al.* (2003); Pukhov (2003); Cairns *et al.* (2004); Shukla, Eliasson, and Marklund

(2004); and Mourou *et al.* (2006), for recent reviews]. In the context of doing fundamental physics and mimicking astrophysical events in laboratory environments, the evolution of laser intensities has received a lot of attention. Examples of experimental suggestions are axion detection (as a dark matter candidate) (Bernard, 1999; Bradley *et al.*, 2003; Dupays *et al.*, 2005); pair production [see, e.g., Ringwald (2001a, 2001b, 2003), and Burke *et al.* (1997), Meyerhofer (1997), and Bamber *et al.* (1999) for a discussion of the detection of pair production from real photons]; laboratory calibration of observations, relativistic jets, analog general relativistic event horizon experiments [such as Hawking and Unruh radiation (Hawking, 1974; Unruh, 1976)], and probing quantum spacetime properties (Chen and Tajima, 1999; Chen, 2003). The possibility of reaching extreme power levels with such setups is one of the promising aspects of laser-plasma systems (Bingham, 2003), and also holds the potential of overcoming the laser intensity limit $\sim 10^{25}$ W/cm^2 (Mourou *et al.*, 1998). As the field strength approaches the critical Schwinger field $E_{\text{crit}} \sim 10^{16}$ V/cm (Schwinger, 1951), there is possibility of photon-photon scattering, even within a plasma (Shen *et al.*, 2003), as the ponderomotive force due to the intense laser pulse gives rise to plasma channels (Yu *et al.*, 1982). Under such extreme circumstances, the effects of pair creation will be pronounced. Electron-positron plasmas are also produced by interactions of matter with powerful multiterawatt and petawatt laser pulses (Liang *et al.*, 1998; Gahn *et al.*, 2000). The concept of trident pair production, as described within the framework of perturbation theory, could give a means for creating electron-positron pairs by intense laser pulses in vacuum (Berezhiani *et al.*, 1992). Moreover, the future x-ray free-electron laser systems (Ringwald, 2001a, 2001b, 2003; Patel, 2002) could result in methods for creating pair plasmas in the laboratory (Alkhofer *et al.*, 2001). The possible field strength output could reach $E \approx 0.1 E_{\text{crit}}$ (Alkhofer *et al.*, 2001). Even on an experimental level, pair production due to collisions of electron backscattered photons with the original photon beam has been observed (Burke *et al.*, 1997). Thus there is ample evidence that the investigation of nonlinear interactions of pair plasmas and high intensity electromagnetic fields deserves attention (Kozlov *et al.*, 1979a; Farina and Bulanov, 2001a).

a. Effect of relativistic nonlinearities

Here we follow the results of Shukla *et al.* (2005). The propagation of a circularly polarized intense laser pulse in an unmagnetized plasma is governed by (Yu *et al.*, 1982) $(\partial_t^2 - c^2 \nabla^2)\mathbf{A} + (\omega_p^2 N/\gamma)\mathbf{A} = 0$, where $\mathbf{A}$ is the vector potential of the laser pulse, $\omega_p = (n_0 e^2/\epsilon_0 m_e)^{1/2}$ is the unperturbed electron plasma frequency, $\gamma = \sqrt{1 + e^2|\mathbf{A}|^2/m^2 c^2}$ is the relativistic gamma factor including the electron mass variation in intense laser fields, and $N = n_e/n_0$ is the ratio of the electron number density to the background plasma number density n_0.
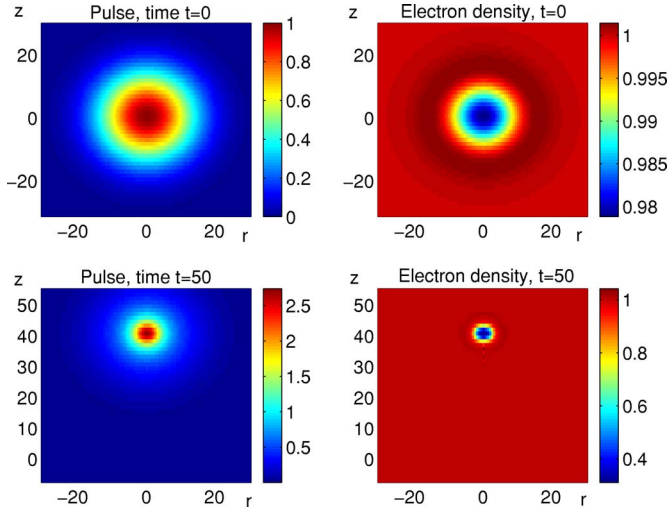
FIG. 17. (Color online) The variation of I, as given by Eq. (106), and N vs r (the radial coordinate) and z for an initial laser pulse which initially has a Gaussian shape. We observe pulse compression and formation of a light bullet. Reprinted with permission from Shukla et al., 2005.

At intensities beyond 10^{18} W/cm^2, the electron quiver speed $v_{osc} = 6 \times 10^{-10} c \lambda \sqrt{I}$ exceeds the speed of light, and hence nonlinear effects in plasmas cannot be ignored. Here I is the intensity in W/cm^2 and λ is the laser wavelength in microns. Thus the relativistic ponderomotive force (Yu et al., 1982; Shukla et al., 1986) $\mathbf{F} = -m_e c^2 \nabla \gamma$ of intense laser pulses will separate charges and thereby would create a huge ambipolar electric potential ϕ in the plasma. At equilibrium, the balance between the relativistic ponderomotive force and a slow electric force $e \nabla \phi$ will yield $\phi = (m_e c^2/e)(\gamma - 1)$, which when substituted into Poisson's equation gives $N = 1 + \lambda_e^2 \nabla^2 \gamma$. Here $\lambda_e = c/\omega_p$ is the electron skin depth, and ions are assumed to be immobile. The electron density will be locally evacuated by the relativistic ponderomotive force of ultraintense nonuniform laser fields. The laser pulse localization and compression would then occur due to nonlinearities associated with relativistic laser ponderomotive force created electron density evacuation and relativistic electron mass increase in the laser fields. This phenomena can be studied by means of the equation

$$\frac{\partial^2 \mathcal{A}}{\partial t^2} - \nabla^2 \mathcal{A} + \frac{\mathcal{A}}{\sqrt{1 + |\mathcal{A}|^2}}\left(1 + \nabla^2 \sqrt{1 + |\mathcal{A}|^2}\right) = 0, \quad (105)$$

where $\mathcal{A} = e\mathbf{A}/m_e c$, and the time and space variables are in units of ω_p^{-1} and λ_e, respectively. For the propagation of a modulated laser pulse along the z axis, we obtain from Eq. (105) after invoking the slowing varying envelope approximation,

$$2i\omega\left(\frac{\partial I}{\partial t} + v_g \frac{\partial I}{\partial z}\right) + \nabla^2 I + I - \frac{I}{P}(1 + \nabla^2 P) = 0, \quad (106)$$

where we have set $\mathcal{A} = (1/2)I(r,z,t)(\hat{\mathbf{x}} + i\hat{\mathbf{y}})\exp(-i\omega t + ikz) + \text{c.c.}$, and denoted $P = (1 + I^2)^{1/2}$. Here the normal-

ized laser frequency and normalized laser group velocity are denoted by $\omega = (1 + k^2)^{1/2}$ and $v_g = k/\omega$, respectively. In the one-dimensional case [viz., set $\nabla^2 = \partial^2/\partial z^2$ in Eq. (106)], we have the localization of intense electromagnetic waves in the form of a large-amplitude one-dimensional bright soliton (Yu et al., 1982). We have numerically solved Eq. (106) in order to study the evolution of a cylindrically symmetric modulated laser pulse. The results are displayed in Fig. 17.

Initially, the pulse is assumed to have a Gaussian shape, $I = I_0 \exp[-(z^2 + r^2)/200]$, and we used the normalized wave number $k = 2$ and initial pulse amplitude $I_0 = 1$. We notice that the compression of the pulse envelope (left panels), which is correlated with the excavation of the normalized electron density (right panels). Our numerical results reveal that self-compression of the pulse occurs more rapidly when one accounts for the relativistic light ponderomotive force induced electron density depletion, contrary to the constant density case (viz., $N = 1$). Physically, the enhanced compression and self-focusing of an intense laser pulse occur due to the localization of light in a self-created electron density cavity.

The fact that evacuation of the plasma takes place as the light intensification due to self-compression occurs means that the situation discussed in Shen et al. (2003), where the quantum electrodynamical effect of photon-photon scattering at high intensities takes place, could be realized in the next generation laser-plasma systems. Moreover, as intensities in the evacuated region increase, the concept of vacuum catastrophic collapse, at which the pulse due to quantum vacuum nonlinearities self-compresses, may ensue (Marklund, Eliasson, and Shukla, 2004). The intensities that can be reached at this stage, in principle, surpass the Schwinger field, but then the process of pair creation has to be investigated and removed, since this would otherwise quickly dissipate the electromagnetic energy into fermionic degrees of freedom. The problem of self-consistent analysis of pair production in a plasma environment has been approached by Bulanov et al. (2005) where a model for incorporating a particle source term was given [see also Eq. (136)].

b. Self-interaction in electron-positron plasmas

Consider the propagation of intense light in an electron-positron plasma. By averaging the inertialess equations of motion for electrons and positrons over one electromagnetic wave period, the expression for electron and positron number densities n_e and n_p, respectively, in the presence of relativistic ponderomotive force (Shukla et al., 1986) of an arbitrary large amplitude laser pulse takes the form

$$n_{e,p} = n_0 \exp\left[-\frac{m_e c^2}{k_B T_e}(\gamma - 1) - \frac{q_{e,p}}{k_B T_{e,p}}\phi\right], \quad (107)$$

where $q_e = -e$ and $q_p = e$ are the electron and positron charges, k_B is Boltzmann's constant, T_e (T_p) is the electron (positron) temperature, and $\gamma = \sqrt{1 + e^2|\mathbf{A}|^2/m_e^2 c^2}$ for

circularly polarized light. The ambipolar potential ϕ associated with the plasma slow motion is found from Poisson's equation

$$\nabla^2\phi = \frac{e}{\epsilon_0}(n_e - n_p). \qquad (108)$$

From particle momentum conservation equations, the electron and positron velocities are given by $\mathbf{v}_{e,p} = -q_{e,p}\mathbf{A}/m_e\gamma_{e,p}$, where $\gamma_{e,p} = (1-v_{e,p}^2/c^2)^{-1/2} \equiv \gamma$.

The dynamics of the intense light is obtained from Maxwell's equations and reads

$$\left(\frac{\partial^2}{\partial t^2} - c^2\nabla^2\right)\mathbf{A} + \frac{\omega_p^2}{\gamma n_0}(n_e + n_p)\mathbf{A} = 0, \qquad (109)$$

where $\mathbf{A}$ is the vector potential.

For a circularly polarized electromagnetic wave $\mathbf{A} = (1/2)\tilde{A}(\mathbf{r},t)(\hat{\mathbf{x}}+i\hat{\mathbf{y}})\exp(i\mathbf{k}\cdot\mathbf{r}-i\omega_0 t)$, using the scalings $n_{e,p}=n_0 N_{e,p}$, $t=\tau\omega_0/\omega_p^2$, $\mathbf{r}=c(\boldsymbol{\xi}-\mathbf{u}_g\tau)/\omega_p$, $\mathbf{u}_g=(\omega_0/\omega_p)\mathbf{v}_g/c$, $\tilde{A}=(m_ec/e)\mathcal{A}$, and $\phi=(m_ec^2/e)\Phi$, Eqs. (108) and (109) can be written in the dimensionless form as

$$i\frac{\partial\mathcal{A}}{\partial\tau} + \frac{1}{2}\nabla^2\mathcal{A} + \left(1 - \frac{N_e+N_p}{2\sqrt{1+|a|^2}}\right)\mathcal{A} = 0, \qquad (110)$$

and $\nabla^2\Phi = N_e - N_p$, respectively, where $N_e = \exp[\beta_e(1-\sqrt{1+|\mathcal{A}|^2}+\Phi)]$, $N_p = \exp[\beta_p(1-\sqrt{1+|\mathcal{A}|^2}-\Phi)]$, $\beta_{e,p} = c^2/v_{Te,p}^2$, and $v_{Te,p}=(k_BT_{e,p}/m_e)^{1/2}$. Here the dispersion relation $\omega_0^2=c^2k^2+\omega_p^2(n_{e0}+n_{p0})/n_0$ has been used, and $\mathbf{v}_g=(c^2/\omega_0)\mathbf{k}$ is the group velocity. In the quasineutral limit $N_e=N_p$, we have $\Phi=(1-\sqrt{1+|\mathcal{A}|^2})(\beta_p-\beta_e)/(\beta_p+\beta_e)$. Equation (110) then becomes

$$i\frac{\partial\mathcal{A}}{\partial\tau} + \frac{1}{2}\nabla^2\mathcal{A} + \left[1 - \frac{\exp[\beta(1-\sqrt{1+|\mathcal{A}|^2})]}{\sqrt{1+|\mathcal{A}|^2}}\right]\mathcal{A} = 0, \qquad (111)$$

where $\beta=2\beta_e\beta_p/(\beta_e+\beta_p)$ is the temperature parameter.

The dispersion relation for the modulational and filamentational instabilities for an arbitrary large amplitude electromagnetic pump can be derived from Eq. (111) following standard techniques (Shukla *et al.*, 1987, 1988). From the ansatz $\mathcal{A}=(a_0+a_1)\exp(i\delta\tau)$, where a_0 is real, $a_0\gg|a_1|$ and δ is a constant nonlinear frequency shift, the lowest-order solution gives $\delta=1-\exp[\beta(1-\sqrt{1+a_0^2})]/\sqrt{1+a_0^2}$. Linearizing Eq. (111) with respect to a_1, with the ansatz $a_1=(X+iY)\exp(i\mathbf{K}\cdot\boldsymbol{\xi}-i\Omega\tau)$, where X and Y are real constants and $\Omega(\mathbf{K})$ is the frequency (wave vector) of the low-frequency (in comparison with the light frequency) modulations, the nonlinear dispersion relation reads

$$\Omega^2 = \frac{K^4}{4} - \frac{K^2}{2}\frac{a_0^2(1+\beta\sqrt{1+a_0^2})}{(1+a_0^2)^{3/2}}e^{\beta(1-\sqrt{1+a_0^2})}, \qquad (112)$$

which gives the modulational instability growth rate $\Gamma = -i\Omega$ according to

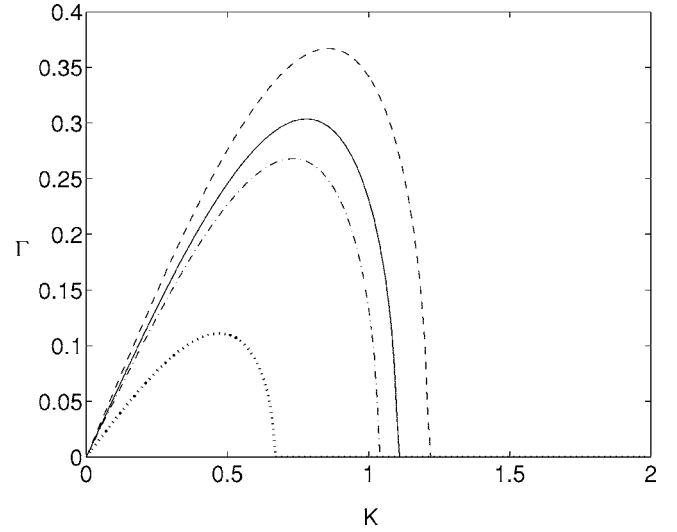FIG. 18. The modulational instability growth rate Γ as given by Eq. (113) vs the wave number K, for $\beta=200$ and $a_0=0.1$ (dashed lines), $\beta=100$ and $a_0=0.1$ (solid line), $\beta=100$ and $a_0=0.2$ (dash-dotted lines), and for $\beta=100$ and $a_0=0.05$ (dotted line). Reprinted from Shukla, Marklund, and Eliasson, 2004. Copyright 2004, with permission from Elsevier.

$$\Gamma = \frac{K}{\sqrt{2}}\left[\frac{a_0^2(1+\beta\sqrt{1+a_0^2})}{(1+a_0^2)^{3/2}}e^{\beta(1-\sqrt{1+a_0^2})} - \frac{K^2}{2}\right]^{1/2}. \qquad (113)$$

The growth rate increases with larger β values (i.e., for lower temperature), while for the intensity field we do not necessarily obtain higher growth rates for higher intensities; see Fig. 18. This is attributed to an interplay between the relativistic particle mass variation and relativistic light ponderomotive driven density responses. From Eq. (113) one observes a decrease in the growth rate for large enough β. However, this result should be interpreted with caution since for large-amplitude fields in a low-temperature plasma electron inertia effects will become important and may dominate over thermal effects. Then, in this case the assumption that electrons (and positrons) obey a modified Boltzmann distribution may no longer be valid.

Since $N_e=N_p=\exp[\beta(1-\sqrt{1+|\mathcal{A}|^2})]$, the increase of the pulse intensity will cause an almost complete expulsion of electrons and positrons from that region; see Figs. 19 and 20. Simulations show the evolution of an initially weakly modulated beam

$$\mathcal{A} = 10^{-3}[1 + 0.02\sin(z/8) + 0.02\cos(z/4)$$
$$+ 0.02\cos(3z/8)]\exp(-r^2/32),$$

where $r^2=x^2+y^2$, while the electron perturbation is zero initially. Thus, as can be seen in Figs. 19 and 20, the modulated beam self-compresses and breaks up into localized filaments. This gives rise to electron and positron holes, and as the pulse intensity grows the conditions for pure elastic photon-photon scattering improve within these holes.
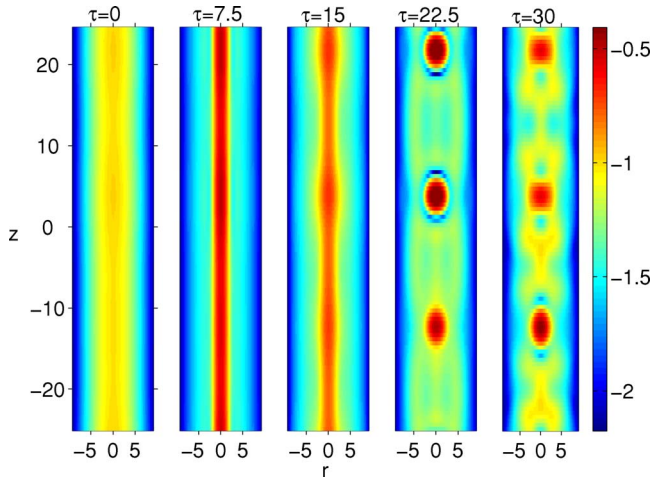
FIG. 19. (Color online) The light amplitude $\mathcal{A}$ in $\log_{10}$ scale at five different times τ [see Eq. (111)]. The horizontal axis represents the distribution along the radial (r) coordinate, and the axial (z) distribution is on the vertical axis. Reprinted from Shukla, Marklund, and Eliasson, 2004. Copyright 2004, with permission from Elsevier.
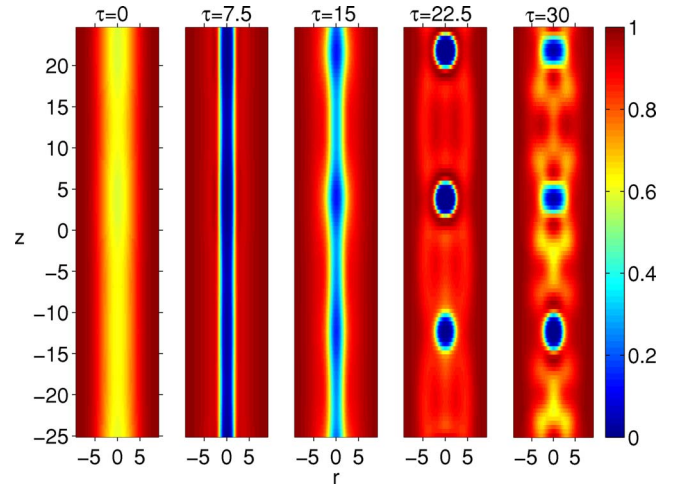
FIG. 20. (Color online) The normalized electron number density $N_e = \exp[\beta(1 - \sqrt{1 + |\mathcal{A}|^2})]$ as a function of r and z at five different times τ [$\mathcal{A}$ is given by Eq. (111)]. Note the efficient expulsion of plasma particles in the later panels, and their correlation to the intensity peaks in Fig. 19. Reprinted from Shukla, Marklund, and Eliasson, 2004. Copyright 2004, with permission from Elsevier.

c. Thin-foil amplification

As noted in the previous two sections, trapping and amplification of laser pulses can take place given the right plasma environment. This could be an important tool for stepping up available electromagnetic intensities, and could therefore be important for investigations into photon-photon scattering. Here we will describe a method which could yield high intensity pulses.

Laser-foil interactions have been used as a method for proton acceleration on tabletop scales (Zepf *et al.*, 2003; Silva *et al.*, 2004; McKenna *et al.*, 2005). By letting a high intensity laser pulse impinge normally on a thin metal foil the foil material is ionized, creating a plasma in which protons are accelerated up to MeV energies. The exact mechanism(s) behind the proton acceleration is still not completely clear although there exists a number of plausible suggestions [see Zepf *et al.* (2003), for a discussion]. It was suggested by Shen and Meyer-ter-Vehn (2001a) that this could be used to create confined high density relativistic electron plasmas. Letting two counterpropagating laser beams illuminate a thin foil normally, a spatially confined high density plasma could be created, and be used for, e.g., harmonic generation, pair production, and γ photon generation (Shen and Meyer-ter-Vehn, 2001b).

Building on the work of Shen and Meyer-ter-Vehn (2001a), Shen and Yu (2002) suggested to let two oppositely directed laser beams interact via two closely placed thin foils. As above, when the high intensity lasers impinges normally on thin foils, the foil material will be ionized and a plasma will be produced. Shen and Yu (2002) showed that this may lead to electromagnetic trapping.

Shen and Yu (2002) started with the trapping of a circularly polarized electromagnetic pulse propagating in the z direction in a positive electron density profile, us-

ing the stationary equations of Shen and Meyer-ter-Vehn (2001a, 2001b),

$$M = (\gamma^2 - 1)c\theta'/\omega, \tag{114a}$$

$$W = \tfrac{1}{2}(\gamma^2 - 1)^{-1}[(c\gamma'/\omega)^2 + M^2] + \tfrac{1}{2}\gamma(\gamma - 2N_i), \tag{114b}$$

where M and W are two constants of motion, $\gamma = \sqrt{1 + e^2|A|^2/m_e^2c^2}$ is the relativistic gamma factor, ω is the laser frequency, A is the vector potential $\propto \exp[i\omega t + i\theta(z)]$, $N_i = n_i/n_c$, n_i is the constant ion density, $n_c = 1.1 \times 10^{21} (\lambda/\mu\text{m})^2 \text{ cm}^{-3}$ is the critical electron density, λ is the laser wavelength, and the prime denotes differentiation with respect to z. It is possible to find solitary solutions of Eq. (114) representing trapped electromagnetic pulses between parallel high-density plasma regions (Esirkepov *et al.*, 1998; Kim *et al.*, 2000). These analytical soliton solutions suggest the possibility to trap laser light between foils. Shen and Yu (2002) performed particle-in-cell simulations of the system (114). Using the foil spacing $\Delta = 0.46\lambda$ they showed that such configurations would yield a 100-fold amplification of initial laser pulse intensities, over a trapping time of 26 laser cycles, which is in the fs range for μm lasers.

In multidimensional environments, true analytical soliton solutions are not known, but it is a well-established fact, due to approximate and numerical investigations (Kivshar and Agrawal, 2003), that solitary-like solutions exists in dimensions $\geqslant 2$. However, these solutions are unstable, and will suffer either attenuation or self-compression, depending on intensity and pulse width (Desaix *et al.*, 1991) (see Fig. 9). Thus in a two-dimensional thin-foil environment, light intensification could take place. The production of high-intensity pulses

by these thin-foil amplification also has the valuable property of being realizable in a relatively small scale setting.

d. Laser plasmas and relativistic flying parabolic mirrors

As we have seen above, the propagation of intense electromagnetic pulses in plasmas yields interesting nonlinear dynamics, and effects such as pulse self-compression can occur. These nonlinear effects act as a very promising tool for, e.g., producing intense ion beams (Esirkepov *et al.*, 1999, 2004; Bulanov *et al.*, 2004), which is of importance in laboratory astrophysics (Chen, 2003). With regards to the nonlinear quantum vacuum, an interesting proposal has been put forward by Bulanov *et al.* (2003). The self-compression of laser pulses, towards intensities close to the Schwinger limit, can take place by using relativistic flying parabolic mirrors.

Bulanov *et al.* (2003) consider a plasma wakefield in the wave-breaking regime. They let a short intense laser pulse create a wakefield in a plasma, such that the wakefield phase velocity equals the laser pulse group velocity (which is close to c) in an underdense plasma (Tajima and Dawson, 1979).[6] Due to nonlinearity, the resulting wakefield will experience wave steepening entering the wave-breaking regime, together with a local electron density spike approaching infinity. With such a setup, a sufficiently weak counterpropagating laser pulse will be partially reflected from the electron density maximum. The relativistic dependence of the Langmuir "mirror" on the driving laser pulse intensity will cause bending of the surfaces of constant phase, thus creating a parabolic plasma mirror (Bulanov and Sakharov, 1991). This curvature of the plasma mirror will focus the counterpropagating (weak) pulse to a spot size $\lambda/4\gamma^2$ along the mirror paraboloid axis in the laboratory frame, where λ is the wavelength of the source of the reflected pulse and γ is the relativistic gamma factor of the wakefield. Similarly, the focal spot width is $\lambda/2\gamma$ in the transverse direction. With this, Bulanov *et al.* (2003) showed that the intensity gain will be roughly $64(D/\lambda)^2\gamma^3$, where D is the width of the pulse effectively reflected by the mirror. The focal spot intensity of the reflected pulse can then be estimated to

$$I_{\text{focal}} \approx 8\left(\frac{\omega_d}{\omega}\right)^2\left(\frac{D}{\lambda}\right)^2\gamma^3 I, \tag{115}$$

where ω_d is the frequency of the pulse driving the Langmuir wave, ω is the frequency of the source of the reflected pulse, and I is the intensity of the source of the reflected pulse. Bulanov *et al.* (2003) gave the following example of light intensification through Eq. (115). A 1-μm pulse generates the Langmuir mirror in a plasma

---

[6]We note that the formation of subcycle intense solitary waves could penetrate into a highly overdense plasma (Shen *et al.*, 2004), transferring energy between low- and high-density regions of the plasma, which could be of importance in, e.g., laser fusion.
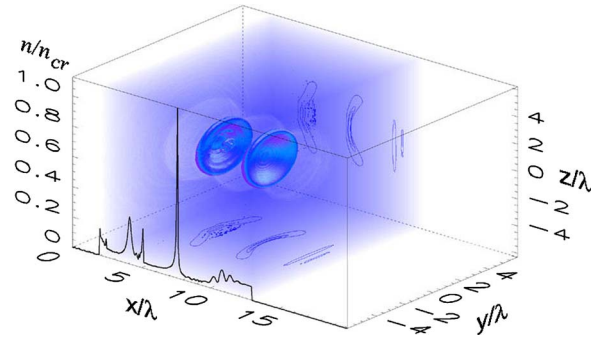
FIG. 21. (Color online) Typical electron density profile in the wakefield, where isosurfaces represent densities $n=0.15n_{\text{crit}}$, and n_{crit} denotes the density at which the plasma goes from underdense to overdense. Reprinted with permission from Bulanov *et al.*, 2003.

where $n_e \sim 10^{17}$ cm^{-3}. The estimate $\gamma \approx \omega_d/\omega_p$ then gives $\gamma \sim 100$. The pulse to be reflected is assumed to have $I \sim 10^{17}$ W/cm^2, and $D=400$ μm. Then $I_{\text{focal}} \sim 10^{29}$ W/cm^2, to be compared with the critical intensity $I_c = c\epsilon_0 E_{\text{crit}}^2 \approx 3 \times 10^{29}$ W/cm^2. The estimated focal intensity thus seems to reach the Schwinger limit. However, with the given value on I it is likely that the backreaction on the Langmuir wave has to be taken into account thus altering the estimate.

Bulanov *et al.* (2003) also presented numerical results using a fully relativistic code, see Figs. 21 and 22. Using a three-dimensional particle-in-cell code, an intense laser pulse drives the Langmuir wave along the x axis, while the counterpropagating source pulse for the reflected wave has an intensity $\sim 10^{15}$ W/cm^2 in the μm wavelength range. The value of the of the source pulse intensity is chosen in order to avoid degradation of the
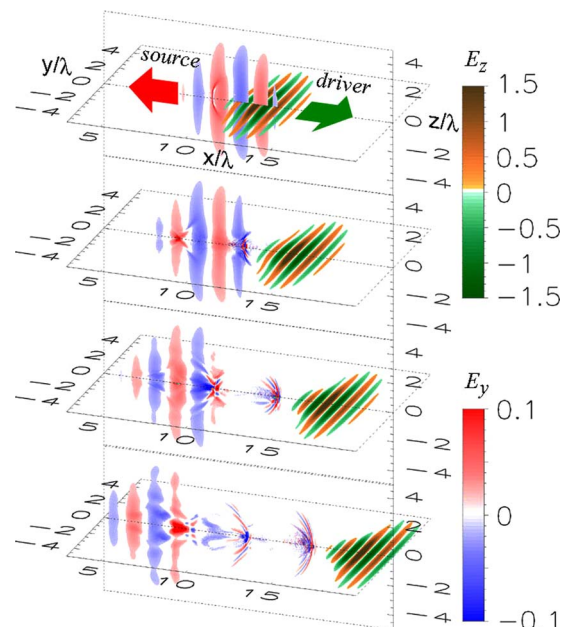
FIG. 22. (Color online) The electric-field components at different times. Reprinted with permission from Bulanov *et al.*, 2003.

Langmuir mirror. Figure 21 shows the electron density profile of the Langmuir wave. Using a Langmuir laser driver with an intensity of 4×10^{18} W/cm^2 and μm wavelength, the plasma waves move with a phase velocity $0.87c$, and the gamma factor is 2. The density profile is shown along the x axis, and a steep gradient can be seen. Figure 22 shows the electric-field components of the source pulse and its reflection ($y=0$ plane) and the Langmuir driver ($z=0$ plane). The focusing of the reflected can be seen. The intensity increase in the focal spot is 256 times the source intensity, i.e., I_{focal} $\sim 10^{17} - 10^{18}$ W/cm^2 for a μm source laser. This is similar to the intensification obtained for the thin foil setup in Sec. III.C.1.c.

e. Electromagnetic wave localization

The nonlinear interaction of high-intensity ultrashort electromagnetic waves with hot plasmas is of primary interest for the fast ignitor concept of inertial confinement fusion and for the development of high power sources of hard EM radiation, as well as for laser-plasma particle and photon accelerators, and compact astrophysical objects containing intense electromagnetic bursts. Recent progress in the development of superstrong electromagnetic pulses with intensities I $\sim 10^{21} - 10^{23}$ W/cm^2 has also made it possible to create relativistic plasmas in the laboratory by a number of experimental techniques. At the focus of an ultraintense short electromagnetic pulse, electrons can acquire velocities close to the speed of light, opening the possibility of simulating in laboratory conditions, by using dimensionless simulation parameters, phenomena that belong to the astrophysical realm. In the past, several authors presented theoretical (Kozlov *et al.*, 1979b; Kaw *et al.*, 1992; Esirkepov *et al.*, 1998; Farina and Bulanov, 2001b) and particle-in-cell simulation (Bulanov *et al.*, 1999; Naumova *et al.*, 2001) studies of intense electromagnetic envelope solitons in a cold plasma, where the slow plasma response to the EM waves is modeled by the electron continuity and relativistic momentum equations, supplemented by Poisson's equation. Assuming beamlike particle distribution functions, relativistic electromagnetic solitons in a warm quasineutral electron-ion plasma have been investigated (Lontano *et al.*, 2003). Experimental observations (Borghesi *et al.*, 2002) show bubblelike structures in proton images of laser-produced plasmas, which are interpreted as remnants of electromagnetic envelope solitons.

Shukla and Eliasson (2005) presented a fully relativistic nonlinear theory and computer simulations for nonlinearly coupled intense localized circularly polarized EM waves and relativistic electron hole (REH) structures (Eliasson and Shukla, 2006) in a relativistically hot electron plasma, by adopting the Maxwell-Poisson-relativistic Vlasov system that accounts for relativistic electron mass increase in electromagnetic fields and relativistic radiation ponderomotive force (Shukla *et al.*, 1986; Bingham *et al.*, 2004), in addition to trapped electrons which support the driven REHs. Such a scenario

of coupled intense EM waves and REHs is absent in any fluid treatment (Kozlov *et al.*, 1979b; Kaw *et al.*, 1992; Esirkepov *et al.*, 1998; Farina and Bulanov, 2001b) of relativistic electromagnetic solitons in a plasma. Electromagnetic wave localization is a topic of significant interest in photonics (Mendonça, 2001), as well as in compact astrophysical objects, e.g., gamma-ray bursts (Piran, 2004).

The electromagnetic wave equation accounting for the relativistic electron mass increase and electron density modification due to the radiation relativistic ponderomotive force (Mendonça, 2001) $F = -m_e c^2 \partial \gamma / \partial z$, where $\gamma = (1 + p_z^2/m_e^2 c^2 + e^2 |\mathbf{A}|^2/m_e^2 c^2)^{1/2}$ is the relativistic gamma factor, are included. Here p_z is the z component of the electron momentum and $\mathbf{A}$ is the perpendicular (to $\hat{\mathbf{z}}$, where $\hat{\mathbf{z}}$ is the unit vector along the z axis) component of the vector potential of the circularly polarized EM waves. The dynamics of nonlinearly coupled EM waves and REHs is governed by

$$\frac{\partial^2 \mathbf{A}}{\partial t^2} - \frac{1}{\alpha^2}\frac{\partial^2 \mathbf{A}}{\partial z^2} + \int_{-\infty}^{\infty} \frac{f}{\gamma} dp_z \mathbf{A} = 0, \qquad (116)$$

$$\frac{\partial f}{\partial t} + \frac{p_z}{\gamma}\frac{\partial f}{\partial z} + \frac{\partial(\phi - \gamma/\alpha^2)}{\partial z}\frac{\partial f}{\partial p_z} = 0, \qquad (117)$$

and

$$\frac{\partial^2 \phi}{\partial z^2} = \int_{-\infty}^{\infty} f dp_z - 1, \qquad (118)$$

where $\mathbf{A}$ is normalized by $m_e c/e$, ϕ by $k_B T_e/e$, p_z by $m_e V_{Te}$, and z by r_D. Here $\gamma = (1 + \alpha^2 p_z^2 + |\mathbf{A}|^2)$, $V_{Te} = (k_B T_e/m_e)^2$, $\alpha = V_{Te}/c$, and $r_D = V_{Te}/\omega_p$. In Eq. (116), we used the Coulomb gauge $\nabla \cdot \mathbf{A} = 0$ and excluded the longitudinal (z) component $\partial^2 \phi / \partial t \partial z = j_z$, where j_z is the parallel current density, by noticing that this component is equivalent to Poisson's equation (118) (Shukla and Eliasson, 2005).

Shukla and Eliasson have discussed stationary as well as time-dependent solutions of Eqs. (116)–(118) in the form of REH which traps localized electromagnetic wave envelopes. Typical profiles for the amplitude of the localized EM vector potential W and potential and density of the REH, as well as the local electron plasma frequency squared (Ω^2) including the relativistic electron mass increase, are depicted in Fig. 23. We observe that for large electromagnetic fields the REH potential becomes larger and the REH wider, admitting larger eigenvalues λ that are associated with the nonlinear frequency shift. This is due to the relativistic ponderomotive force of localized EM waves pushing electrons away from the center of the REH, leading to an increase of the electrostatic potential and a widening of the REH. We see that the depletion of the electron density in the REH is only minimal, while the local electron plasma frequency Ω is reduced owing to the increased mass of electrons accelerated by the REH potential; the maximum potential $\phi_{\text{max}} \approx 15$ in Fig. 23 corresponds in physi-
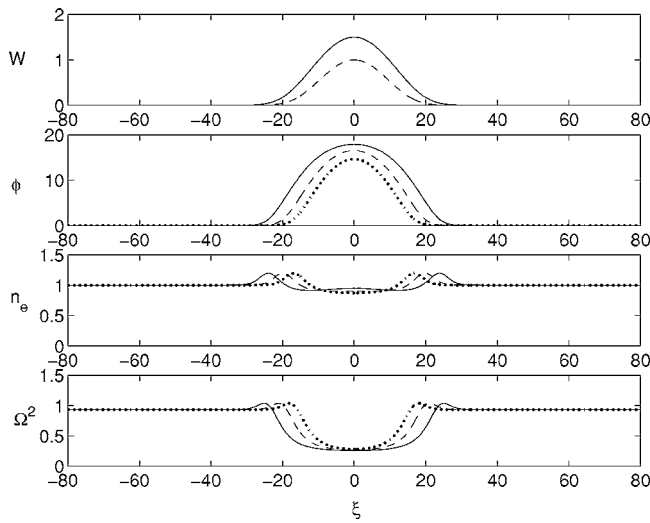
FIG. 23. Large-amplitude trapped EM wave envelope (upper panel), the potential (second panel), the electron number density (third panel), and the square of the local electron plasma frequency (lower panel) for large-amplitude EMW waves with a maximum amplitude of $W_{max}=1.5$ (solid lines) and $W_{max}=1.0$ (dashed lines), and as a comparison a REH with small-amplitude EM waves which have $W_{max} \ll 1$ (dotted lines). The parameters are as follows: normalized speed $v_0=0.7$, $\alpha=0.4$, and trapping parameter $\beta=-0.5$, corresponding to a vortex distribution presented by Bujarbarua and Schamel (1981) and Schamel (2000) involving an equilibrium Synge-Jüttner distribution function (de Groot *et al.*, 1980). The selected value of β is related to the maximum REH potential according to a specific relation similar to one in Bujarbarua and Schamel (1981) and Schamel (2000). Reprinted with permission from Shukla and Eliasson, 2005.

cal units to a potential $\alpha^2 \phi_{max} \times 0.5 \times 10^6 \approx 1.2 \times 10^6$ V, accelerating electrons to gamma factors of ≈ 6.

In order to study the dynamics of interacting solitary structures composed of localized REHs loaded with trapped EM waves, Shukla and Eliasson (2005) numerically solved the time-dependent, relativistic Vlasov equation (117) together with the nonlinear Schrödinger equation, that is deduced from Eq. (116) in the slowly varying envelope approximation. The results are displayed in Figs. 24 and 25. As an initial condition to the simulations, Shukla and Eliasson used solutions to the quasistationary equations described above, where the left REH initially has speed $v_0=0.7$ (normalized by c) and is loaded with EM waves with $W_{max}=1.5$, while the right REH has speed $v_0=-0.3$, and is loaded with EM waves with $W_{max}=2.5$. Furthermore, Shukla and Eliasson (2005) used $k_0=v_g=0$ in the initial condition for A and in the solution of the nonlinear Schrödinger equation (Shukla and Eliasson, 2005). Figure 24 displays the phase-space distribution of electrons and the electromagnetic field amplitude at different times. We see that the REHs loaded with trapped EM waves collide, merge, and then split into two REHs, while there are two strongly peaked EM wave envelopes at $z \approx 30$ and $z \approx 70$ remaining after the splitting of the REH. A popu-
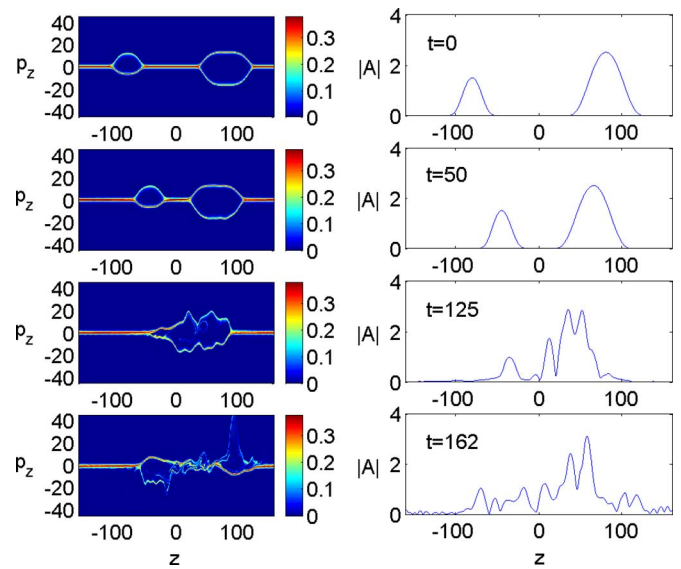
FIG. 24. (Color online) Phase-space plots of the electron distribution function (left panels) and the modulus of the electromagnetic field (right panels) for $t=0$, $t=50$, $t=125$, and $t=162$. Reprinted with permission from Shukla and Eliasson, 2005.

lation of electrons has also been accelerated to large energies, seen at $z=100$ in the lower left panel of Fig. 24. The time development of the EM wave amplitudes, REH potential, the squared local plasma frequency, and the electron number density is shown in Fig. 25. Collision and splitting of the REHs can be observed, as well as creation of the two localized EM envelopes at $z \approx 70$; clearly visible in the left two panels at $t>150$.
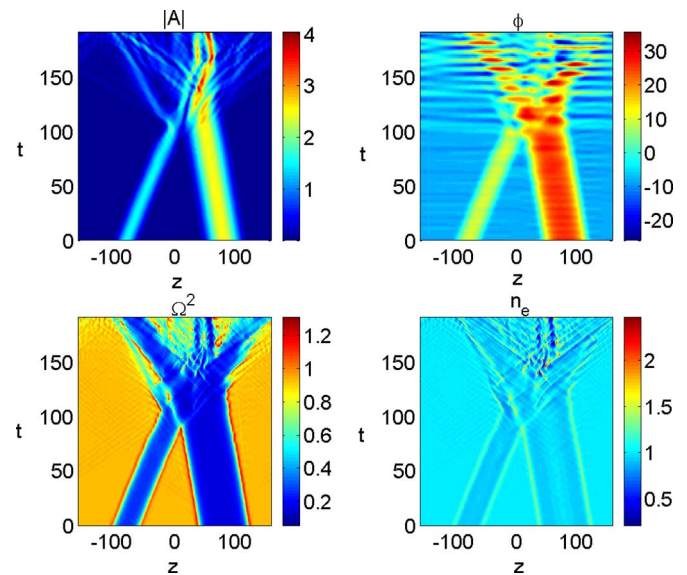
FIG. 25. (Color online) The electromagnetic field (upper left panel), potential (upper right panel), squared local plasma frequency (lower left panel), and electron density (lower right panel) for two colliding REHs. Reprinted with permission from Shukla and Eliasson, 2005.

2. Photon-photon scattering within plasmas

a. Charged particle effects and Cherenkov radiation

As presented by Dremin (2002) and Marklund, Brodin, *et al.* (2005), similar to a charged particle moving in a isotropic dielectric, a charged particle can suffer Cherenkov losses when propagating through a intense gas of photons. The main difference compared to the case of a regular medium is the frequency spectrum of the emitted radiation. Since the natural cutoff in the quantum vacuum is given by the Compton frequency, γ rays may be emitted by such a particle.

In 1934, Cherenkov observed the type of radiation now bearing his name (Čerenkov, 1934). His experimental result was explained by Tamm and Frank (1937). In an isotropic dielectric medium, a charged particle in rectilinear motion satisfying the so-called Cherenkov condition, i.e., its velocity exceeds the (parallel) phase speed in the medium in which it moves, will radiate (Chefranov, 2004). The radiation shock front, called the Cherenkov cone, is analogous to the Mach cone formed as objects move with supersonic speeds through air. In quantum-mechanical terms, the Cherenkov condition corresponds to energy and momentum conservation. Cherenkov radiation has technological uses, e.g., in determining particle velocities.

The dispersion relation for electromagnetic waves in an isotropic and homogeneous photon gas with refractive index n is $\omega=kc/n$, where $n^2=1+\delta$ and $\delta=4\lambda\mathcal{E}/3$ (Bialynicka-Birula and Bialynicki-Birula, 1970; Marklund *et al.*, 2003) [see Eq. (29)]. Thus the refractive index in this case is always larger than 1, and a particle may therefore have a speed u exceeding the phase velocity in the medium. The Cherenkov condition $u\geqslant c/n$ for emission of radiation can thus be satisfied. This condition can also be expressed in terms of the relativistic gamma factor $\gamma=(1-u^2/c^2)^{-1/2}$, namely, $\delta\gamma^2\geqslant1$. We will here assume that a particle with charge Ze, satisfying the Cherenkov condition, moves through an equilibrium radiation gas. The energy loss at the frequency ω per unit length of the path of the charged particle is then

$$\frac{dU_\omega}{ds}d\omega=\frac{Z^2\alpha}{c}\frac{(\delta\gamma^2-1)}{(\gamma^2-1)}\hbar\omega d\omega,\tag{119}$$

and the number of quanta N emitted per unit length along the particles path is

$$\frac{dN}{ds}d\omega=\frac{Z^2\alpha}{c}\frac{(\delta\gamma^2-1)}{(\gamma^2-1)}d\omega.\tag{120}$$

Since δ is normally much less than 1, we need a large gamma factor to satisfy the Cherenkov condition. Subsequently, for $\delta\gamma^2=1$, we have

$$U=N\hbar\omega_e \quad \text{and} \quad N=Z^2L\alpha\delta/\lambda_e,\tag{121}$$

respectively, where we have used the Compton frequency as a cutoff. Here L is the distance traveled by the charge.

At the present time, the cosmic microwave background has an energy density of the order $\mathcal{E}$ $\sim10^{-15}$ J/m^3, i.e., $\delta\sim10^{-42}$, i.e., the gamma factor has to be $\gamma\geqslant10^{21}$ for the Cherenkov condition to be satisfied. Thus Cherenkov radiation is not likely to occur in today's radiation background. In fact, it is well known that cosmic rays contain nonthermal hadrons, of which some are protons, that can reach gamma factors 10^{11}, but larger values are improbable due to the GZK cutoff (Greisen, 1966; Zatsepin and Kuzmin, 1966). As a comparison, we consider the situation at the time of matter-radiation decoupling. Since $\mathcal{E}_{emitted}=\mathcal{E}_{received}(T/2.7)^4$, where the temperature T is given in K, we have $\mathcal{E}$ $\sim10^{-2}$ J/m^3 at the time of decoupling ($T\approx8000$ K), implying $\delta\sim10^{-28}$. Thus the limiting value on the gamma factor for the Cherenkov condition to be satisfied is γ $\geqslant10^{14}$–10^{15}, still out of reach for high-energy cosmic rays. However, as we demonstrate below, the situation changes drastically for earlier processes at even higher T. In particular, we will focus on the era with $10^9\leqslant T\leqslant10^{11}$ K when the required γ factors range from $\gamma\sim10^4$ to $\gamma>3$.

The effect presented above is naturally compared with inverse Compton scattering. Setting $Z=1$, the cross section for this scattering is $\sigma\approx\pi r_e^2m_e^2/M^2\gamma$, where r_e is the classical electron radius and M is the charged particle mass. We thus obtain a collision frequency $\nu=c\mathcal{N}\sigma$, where $\mathcal{N}$ is the number density of the photons. Comparing this frequency with the frequency ν_{ch} $=(\gamma Mc)^{-1}dU/dt$, we note that fast particles are mainly scattered due to the Cherenkov effect when $\nu<\nu_{ch}$, i.e.,

$$1<\frac{\delta}{\alpha\pi(m_e/M)\mathcal{N}\lambda_e^3}=\frac{M}{m_e}\frac{T}{T_{ch}}.\tag{122}$$

Here T is the temperature of the photon gas, $\mathcal{N}$ $=[30\zeta(3)a/k_B\pi^4]T^3$, $\mathcal{E}=aT^4$, k_B is the Boltzmann constant, $a=\pi^2k_B^4/15\hbar^3c^3\approx7.6\times10^{-16}$ J/m^3 K^4, and $T_{ch}=[2025\zeta(3)/44\pi^3\alpha]m_ec^2/k_B\approx10^{12}$ K using the polarization averaged effective action charge $\bar\lambda=(8\kappa+14\kappa)/2=11\kappa$. Thus for a single fast proton to be scattered mainly due to the Cherenkov effect, we need $T>T_{ch}\times10^{-3}\sim10^9$ K, well within the valid limit of photon-photon scattering theory. We note that at radiation gas temperatures around 10^{12} K the quantum vacuum becomes truly nonlinear, and higher-order QED effects must be taken into account.

For the early Universe considered above, a moderately relativistic plasma is also present, which means that collective charged particle interactions can play a role. We take these plasma effects into account by introducing the plasma frequency ω_p. The photon dispersion relation is $\omega^2\approx k^2c^2(1-\delta)+\omega_p^2$. Thus the Cherenkov condition is satisfied for charged particles with relativistic factors $\gamma\geqslant1/\sqrt{\delta-\omega_p^2/k^2c^2}$. For temperatures where the Cherenkov radiation starts to dominate over inverse Compton scattering, $T\sim10^9$–10^{10} K, we have $\omega_p\sim10^{15-16}$ rad/s, and thus Cherenkov radiation is emitted in a broad band starting in the UV range, $\omega\sim10^{17}$ rad/s, and continuing up to the Compton frequency $\sim8\times10^{20}$ rad/s.

The Cherenkov radiation emitted during the era when $T \sim 10^9$ K will be redshifted due to the cosmological expansion. Thus the present value of the cutoff frequency will be approximately 2×10^{12} rad/s, i.e., in the short-wavelength range of the microwave spectrum. However, we do not expect direct detection of this radiation in the present Universe, since the process is only expected to be of importance before the time of radiation decoupling. Still, there are possible important observational implications due to the Cherenkov mechanism presented here. As shown by the inequality (122), the effect will be more pronounced for massive particles with a given gamma factor, and protons are therefore expected to be more constrained than electrons by the QED Cherenkov emission. In particular, Eq. (122) puts stronger limits than Compton scattering for suprathermal protons observed today to be relics of the early Universe. In fact, it seems rather unlikely, given the inequality (122), that such protons could survive during the $T = 10^9$–10^{10} K era.

b. Unmagnetized plasmas

Pair production and pair plasmas play an important role in the dynamics of environments surrounding pulsars [see, e.g., Beskin *et al.* (1993); Arendt and Eilek (2002); Asseo (2003)]. Charged particles will attain relativistic energies close to the pulsar magnetic poles and radiate γ-ray photons. This, together with the superstrong magnetic field present around these objects (Beskin *et al.*, 1993), is believed to produce a pair plasma (Tsai and Erber, 1975). Thus nonlinear QED effects are already known to be an important ingredient for pulsar physics. Since the pair plasma gives rise to radio-wave emissions, and because of the large energy scales involved, pulsar atmospheres are likely to host other QED effects as well, such as vacuum nonlinearities in the form of photon-photon scattering.

As presented by Stenflo *et al.* (2005), for circularly polarized electromagnetic waves propagating in a cold multicomponent plasma rather than in vacuum, the wave operator on the left-hand sides of Eqs. (9) and (10) is replaced by

$$\Box \rightarrow \frac{1}{c^2}\frac{\partial^2}{\partial t^2} - \nabla^2 + \frac{\omega_p^2}{c^2} \rightarrow \frac{-\omega^2 + \sum\limits_{j} \omega_{pj}^2/\gamma_j}{c^2} + k^2, \quad (123)$$

where the sum is over particle species j, and we have assumed that the EM fields vary as $\exp(ikz - i\omega t)$, the relativistic factor of each particle species is $\gamma_j = (1 + q_j^2 E_0^2/m_j^2 c^2 \omega^2)^{1/2}$, where E_0 denotes the absolute value of the electric-field amplitude (Stenflo, 1976; Stenflo and Tsintsadze, 1979). Due to the symmetry of circularly polarized EM waves, most plasma nonlinearities cancel, and the above substitution holds for arbitrary wave amplitudes. Here $\omega_{pj} = (n_{0j}q_j^2/\epsilon_0 m_j)^{1/2}$ is the plasma frequency of particle species j and n_{0j} denotes the particle density in the laboratory frame.

Next, we investigate the regime $\omega^2 \ll k^2 c^2$. From Faraday's law and the above inequality we note that the

dominating QED contribution to Eq. (10) comes from the term proportional to $B^2\mathbf{B}$. Combining Eqs. (10) and (12), noting that $B^2 = B_0^2 = k^2 E_0^2/\omega^2$ is constant for circularly polarized EM waves, and using $\omega^2 \ll k^2 c^2$, i.e., $\mathbf{M} \approx 4\kappa\epsilon_0^2 c^4 B^2\mathbf{B}$ and $|\mathbf{M}| \gg \omega|\mathbf{P}|/k$, we obtain from Eq. (10) the nonlinear dispersion relation

$$\omega^2 = \frac{2\alpha}{45\pi}\left(\frac{E_0}{E_{\text{crit}}}\right)^2 \frac{k^4 c^4}{\sum\limits_{j} \omega_{pj}^2/\gamma_j + k^2 c^2}. \quad (124)$$

This low-frequency mode makes the particle motion ultrarelativistic even for rather modest wave amplitudes. For electrons and positrons in ultrarelativistic motion ($\gamma_j \gg 1$) with equal densities n_0 and elementary charge $\pm e$, we thus use the approximation $\Sigma_j \omega_{pj}^2/\gamma_j \approx 2en_0 c\omega/\epsilon_0 E_0 = 2\omega_p^2(\omega/\omega_e)E_{\text{crit}}/E_0$ [see Eqs. (1) and (4)], where $\omega_p = (e^2 n_0/\epsilon_0 m_e)^{1/2}$. The dispersion relation (124) then reduces to

$$\omega^3 = \frac{\alpha}{45\pi}\left(\frac{\omega_e}{\omega_p}\right)\left(\frac{E_0}{E_{\text{crit}}}\right)^3 \frac{k^4 c^4}{\omega_p + (E_0/E_{\text{crit}})(kc\omega_e/2\omega\omega_p)kc}. \quad (125)$$

We note that the ratio ω_e/ω_p is much larger than unity for virtually all plasmas, i.e., for electron densities up to $\sim 10^{38}$ m^{-3}. In some applications, such as in pulsar astrophysics, it is convenient to reexpress the dispersion relation in terms of the relativistic gamma factor using $E_0/E_{\text{crit}} \approx (\omega/\omega_e)\gamma$. Thus we obtain

$$\lambda = \gamma\lambda_e\left(\frac{4\alpha}{45\pi}\right)^{1/2}\left[1 + \sqrt{1 + \frac{16\alpha}{45\pi}\left(\frac{\omega_p}{\omega_e}\right)^2\gamma}\right]^{-1/2} \quad (126)$$

from Eq. (125) for the wavelength $\lambda = 2\pi/k$.

c. Magnetized plasmas

Following Marklund, Shukla, Stenflo, *et al.* (2005) [see also Marklund *et al.* (2004a)], for a circularly polarized wave $\mathbf{E}_0 = E_0(\hat{\mathbf{x}} \pm i\hat{\mathbf{y}})\exp(ikz - i\omega t)$ propagating along a constant magnetic field $\mathbf{B}_0 = B_0\hat{\mathbf{z}}$, the electromagnetic invariants satisfy

$$F_{cd}F^{cd} = -2E_0^2\left(1 - \frac{k^2 c^2}{\omega^2}\right) + 2c^2 B_0^2 \quad \text{and} \quad F_{cd}\hat{F}^{cd} = 0. \quad (127)$$

Thus Eq. (43) can be written as

$$\Box A^a = -4\epsilon_0\kappa\left[E_0^2\left(1 - \frac{k^2 c^2}{\omega^2}\right) - c^2 B_0^2\right]\Box A^a - \mu_0 j^a \quad (128)$$

in the Lorentz gauge, and $\Box = \partial_a\partial^a$. For circularly polarized electromagnetic waves propagating in a magnetized cold multicomponent plasma, the four-current can be "absorbed" in the wave operator on the left-hand side by the replacement (as in the previous section) $\Box \rightarrow -D(\omega, k)$, where D is the plasma dispersion function, given by [see, e.g., Stenflo (1976); Stenflo and Tsintsadze (1979)]

$$D(\omega,k) = k^2 c^2 - \omega^2 + \sum_j \frac{\omega \omega_{pj}^2}{\omega \gamma_j \pm \omega_{cj}}. \tag{129}$$

Here the sum is over the plasma particle species j, $\omega_{cj} = q_j B_0 / m_j$ and $\omega_{pj} = (n_{0j} q_j^2 / \epsilon_0 m_j)^{1/2}$ is the gyrofrequency and plasma frequency, respectively, and $\gamma_j = (1 + \nu_j^2)^{1/2}$ is the gamma factor of species j, with ν_j satisfying

$$\nu_j^2 = \left(\frac{e E_0}{c m_j}\right)^2 \frac{1 + \nu_j^2}{[\omega(1 + \nu_j^2)^{1/2} \pm \omega_{cj}]^2}. \tag{130}$$

Here n_{0j} denotes particle density in the laboratory frame and m_j particle rest mass.

The dispersion relation, obtained from Eq. (128), reads

$$D = \frac{4\alpha}{45\pi}(\omega^2 - k^2 c^2) \left[\left(\frac{E_0}{E_{\text{crit}}}\right)^2 \frac{\omega^2 - k^2 c^2}{\omega^2} - \left(\frac{c B_0}{E_{\text{crit}}}\right)^2 \right]. \tag{131}$$

We note that as the plasma density goes to zero, the effect due to photon-photon scattering, as given by the right-hand side of Eq. (131), vanishes since then $\omega^2 - k^2 c^2 = 0$.

Next, we focus on low-frequency ($\omega \ll kc$) mode propagation in an ultrarelativistic electron-positron plasma ($\gamma_e \gg 1$), where two species have the same number density n_0. Then, Eq. (131) gives

$$\frac{k^2 c^2}{\omega^2} \approx \frac{4\alpha}{45\pi} \left[\left(\frac{E_0}{E_{\text{crit}}}\right)^2 \frac{k^2 c^2}{\omega^2} + \left(\frac{c B_0}{E_{\text{crit}}}\right)^2 \right] \frac{k^2 c^2}{\omega^2}$$
$$\mp \frac{\omega_p^2}{\omega \omega_e} \frac{E_{\text{crit}}}{E_0}. \tag{132}$$

For background magnetic-field strengths B_0 in the pulsar range $\sim 10^6 - 10^{10}$ T, $cB_0 \ll E_{\text{crit}}$, and we therefore drop the term proportional to B_0^2 in Eq. (132). Next, using the normalized quantities $\Omega = \omega \omega_e / \omega_p^2$, $K = (4\alpha/45\pi)^{-1/2} kc \omega_e / \omega_p^2$, and $\tilde{E} = (4\alpha/45\pi) E_0 / E_{\text{crit}}$, the dispersion relation (132) reads

$$\Omega^2 = \tilde{E}^2 K^2 \mp \frac{\Omega^3}{\tilde{E} K^2}. \tag{133}$$

The dispersion relation (133) describes three different modes, two with + polarization and one with − polarization. We note that for $K \ll 1$, the dispersion relation (133) agrees with that of Stenflo and Tsintsadze (1979), whereas in the opposite limit $K \gg 1$, the QED term in Eq. (133) dominates. For the given density, the latter regime applies, except for extremely long wavelengths ($> 10^8$ m), and thus we note that QED effects are highly relevant for the propagation of these modes in the pulsar environment. For small K there is only one mode, but two new modes appear for $K \gtrsim 2.6$. Thus for large K, applicable in the pulsar environment, there are three low-frequency modes ($\omega \ll kc$) that depend on nonlinear QED effects for their existence.

The effects of the quantum vacuum on electromagnetic wave dispersion also allows for nonlinear effects, such as wave steepening, shock front formation, and soliton propagation (Marklund, Tskhakaya, and Shukla, 2005).

d. Magnetohydrodynamic plasmas

When analyzing low-frequency magnetized plasma phenomena, magnetohydrodynamics (MHD) gives an accurate and computationally economical description. Specifically, a simple plasma model is obtained if the characteristic MHD time scale is much longer than both the plasma oscillation and plasma particle collision time scales, and the characteristic MHD length scale is much longer than the plasma Debye length and gyroradius. These assumptions make it possible to describe a two-component plasma in terms of a one-fluid description. The one-fluid description means a tremendous computational simplification, especially for complicated geometries. Moreover, if the mean fluid velocity, the mean particle velocity, and the Alfvén speed are much smaller than the speed of light in vacuum, the description becomes nonrelativistic and simplifies further.

Heyl and Hernquist (1999) considered the propagation of MHD modes, including the effects of photon-photon scattering and an axion field. Following Thompson and Blaes (1998), Heyl and Hernquist start with the Lagrangian [see Eq. (13)]

$$\mathcal{L} = \mathcal{L}_{\text{QED}} + \tfrac{1}{2} \alpha \epsilon_0 \theta \mathcal{G} = \mathcal{L}_0 + \mathcal{L}_c + \tfrac{1}{2} \alpha \epsilon_0 \theta \mathcal{G}, \tag{134}$$

where the field invariant $\mathcal{G}$ is defined by Eq. (7) and θ is the axion field, that acts as a Lagrange multiplier for the MHD condition $\mathcal{G} = 0$. The modified Maxwell's equations can be derived from Eq. (134). They become [cf. Eq. (15)]

$$\partial_a F^{ab} = -4 \left(\frac{\partial \mathcal{L}_{\text{QED}}}{\partial \mathcal{F}}\right)^{-1} \left[\hat{F}^{cb} \partial_c \left(2\alpha \epsilon_0 \theta + 8\mathcal{G} \frac{\partial \mathcal{L}_c}{\partial \mathcal{G}^2} \right) \right.$$
$$\left. + 4 F^{cb} \partial_c \left(\frac{\partial \mathcal{L}_c}{\partial \mathcal{F}} \right) \right]. \tag{135}$$

Given a background magnetic field, these equations allow for both fast and Alfvén modes. The fast modes will suffer the same type of shock-wave formation as presented by Heyl and Hernquist (1997b), in the absence of the MHD effects. A single Alfvén mode will not experience the effects of photon-photon scattering due to the absence of self-interactions. This is not true for the case of counterpropagating Alfvén modes for which photon-photon scattering introduces higher-order corrections to their propagation.

IV. APPLICATIONS

A. Measuring photon-photon scattering

Classically, electromagnetic waves only interact indirectly, via scattering, by passing through a suitable medium such as a nonlinear optical fiber (Hasegawa, 1975;
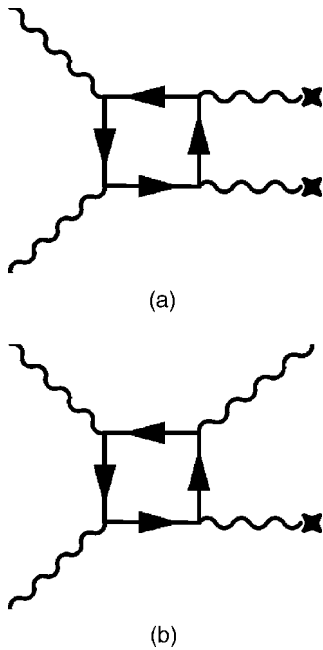
(a)

(b)

FIG. 26. Feynman box diagrams for (a) Delbrück scattering and (b) photon splitting, respectively. Here each cross denotes external field legs, e.g., an atomic Coulomb field or a strong background magnetic field.

Kivshar and Agrawal, 2003). To some extent, this is still true in QED. One may view the quantum vacuum as a medium through which photons scatter off virtual charged particles, predominantly electron-positron pairs, producing nonlinear effects similar to the ones found in nonlinear optics. However, since nonlinear effects enter the effective Lagrangian through Lorentz invariants, a plane wave will not self-interact, and more sophisticated techniques are needed in order to excite the nonlinear quantum vacuum. In this section, such means will be reviewed with the aim of establishing methods for direct detection of low-energy elastic real photon-photon scattering.

The concept of elastic photon-photon scattering is theoretically well established. Furthermore, the scattering of virtual photons is routinely observed in particle accelerator environments, and is thus well confirmed in experiments. Moreover, inelastic photon-photon scattering is also experimentally well confirmed, but this is not the case for elastic photon-photon scattering [although experiments have been made where it in principle would have been possible to make modification such that a direct measurement of elastic photon-photon scattering could have been made (Bamber et al., 1999)]. Thus as a fundamental test of QED and its predictions about the properties of the quantum vacuum, an experiment on the latter type of scattering may be considered an important issue.

Closely related to photon-photon scattering is Delbrück scattering (Delbrück, 1933) and photon splitting (Adler et al., 1970; Adler, 1971; Chistyakov et al., 1998); see Fig. 26 (cf. Fig. 4 for a comparison with photon-photon scattering). Delbrück scattering is the elastic
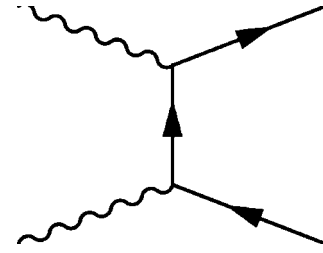

FIG. 27. Feynman diagram for the pair-creation process.

scattering of photons in a Coloumb field, e.g., an atomic nucleus, mediated by virtual electron-positron pairs, while photon splitting is the down-conversion of a photon into two photons of lower frequency through an external field, e.g., a strong magnetic field. These processes contain external fields mediating the interaction between photons, making the cross section larger than for pure photon-photon scattering. In fact, using high-Z atomic targets, Delbrück scattering for high-energy photons has been detected (Jarlskog et al., 1973), and photon splitting, although not detected in a laboratory environment, is assumed to be a prominent component of many astrophysical environments, such as magnetars and soft γ-ray repeaters (Adler and Shubert, 1996; Baring and Harding, 1997, 2001; Harding et al., 1997). In fact, the splitting of photons in the atomic Coulomb field has been reported by Akhmadaliev et al. (2002), where good agreement with the calculated exact Coulomb field cross section was obtained.

The effects of photon scattering also manifest themself in the anomalous magnetic moments of the electron and muon (Calmet et al., 1977; Bailey et al., 1979; Berestetskii et al., 1982; Rodionov, 2004). Even so, the detection of direct light-by-light scattering of real photons remains elusive, even though considerable efforts have been made in this area. The possibility to detect low-energy photon-photon scattering would open up for new tests of QED, since fermion loop diagrams could give gauge-invariant tests of the fermion propagator, as well as discerning between QED and other theories predicting or postulating photon properties. Thus photon-photon scattering can both produce interesting effects, as described, as well as produce important tests for fundamental physical theories.

1. Pair production in external fields

The case of inelastic photon-photon scattering deserves some attention in this context. Here the aim is, to some extent, antimatter production on a large scale (see Fig. 27). There are a number of ways, both experimentally confirmed as well as schemes suggested on numerical or theoretical grounds, to produce and store (Oshima et al., 2004) positronium and antimatter, e.g., laser generated relativistic superthermal electrons interacting with high-Z materials (Liang et al., 1998), the trident process in conjunction with ultraintense short laser pulses in plasmas (Berezhiani et al., 1992), pair production by circularly polarized waves in plasmas (Bulanov,

2004), laser thin foil interactions (Shen and Meyer-ter-Vehn, 2001b; Shen and Yu, 2002), using Bose-Einstein condensation traps (Surko *et al.*, 1989; Greaves *et al.*, 1994) [see Surko and Greaves (2004) for an overview] and using fullerenes (Oohara and Hatakeyama, 2003). The formation of antiplasmas and long lifetime trapping of antimatter is currently studied, and could shed light on the fundamental laws of nature, e.g., giving new *CPT* and Lorentz invariance tests (Bluhm *et al.*, 1999; Bluhm, 2004), or producing an annihilation laser (Mills, 2002). Since electron-positron pairs also constitute a unique type of plasma, prominent in, e.g., the pulsar magnetosphere, the formation of large collections of pairs in the laboratory will further enable the study of astrophysical conditions (Greaves and Surko, 1997), which we so far have only been able to observe over astronomical distances, and without control over the physical parameter range. Antimatter production in most laboratory applications rely on the plasma being cold. However, as laser powers approach the Schwinger critical regime, we will see an increased interest in using these for producing high-temperature pair plasmas as well, and for exciting the quantum vacuum.

After the laser was introduced, it was realized that future laser systems could be tools for fundamental physics research, and the pair creation process was reconsidered by Reiss (1962), Nikishov and Ritus (1964a, 1964b, 1965, 1967), and Narozhny *et al.* (1965). Thus the mechanism behind the production of electron-positron pairs from electromagnetic fields and photons is well known, and was first directly observed by Burke *et al.* (1997) at the SLAC facility. Since this observation, schemes making use of the next generation laser systems have therefore been the focus of research efforts using immense laser intensities for producing, not necessarily cold, pair plasmas in the laboratory. Indeed, as reported by Gahn *et al.* (2000), femtosecond tabletop lasers can indirectly create positrons due to electron acceleration in plasma channels.

Since the pair production from the nonlinear quantum vacuum formally depends crucially on the invariant $|\mathbf{E}|^2 - c^2 |\mathbf{B}|^2$ being positive (Schwinger, 1951), schemes with strong electric fields have been also attracted interest (Sauter, 1931; Schwinger, 1951; Brezin and Itzykson, 1970; Narozhny and Nikishov, 1970; Popov, 1971, 1972, 1973, 1974; Popov and Marinov, 1973; Mostepanenko and Frolov, 1974; Marinov and Popov, 1977; Casher *et al.*, 1979; Grib *et al.*, 1988; Kluger *et al.*, 1991; Ringwald, 2001a) (by the same argument, strong static magnetic fields do not excite the quantum vacuum, unless perturbed). The pair-production rate per unit volume at the one-loop level is given by (Schwinger, 1951)

$$w = \frac{\omega_e^4}{(2\pi c)^3} \left(\frac{|\mathbf{E}|}{E_{\text{crit}}} \right)^2 \sum_{n=1}^{\infty} \frac{1}{n^2} \exp\left(-n\pi \frac{E_{\text{crit}}}{|\mathbf{E}|} \right) \qquad (136)$$

for a uniform electric field $\mathbf{E}$. Here the sum is over real poles in the imaginary part of the integral (13). Thus the pair-creation rate is vanishingly small in most circumstances. The electron-nucleus electric field (although not uniform) requires a nucleus charge of the order α^{-1} for vacuum breakdown, and such nuclei are unlikely to exist in any other state than a transient one (Reinhardt and Greiner, 1977; Greiner *et al.*, 1985; Milonni, 1994). However, the situation may be different for laser fields, where ultrashort high intensity fields are available. Brezin and Itzykson (1970) derived the pair-creation rate for varying fields and generalized the pair-creation rate (136). In the low-frequency limit (i.e., $\omega \ll \omega_e$, where ω_e is the Compton frequency), their expression coincides with Eq. (136), taking into account only the first term in the sum. Thus Eq. (136) can be used, with good accuracy, to predict the pair-production efficiency of different processes, even if the fields are alternating.

In above cases, derivations of the pair-creation rate rely on the assumption of an electric field dominating over the magnetic field. In plasmas, the phase velocity v can exceed the velocity of light. This was used by Bulanov (2004) to analyze pair production in the field of a circularly polarized electromagnetic wave in an underdense plasma. Since for a circularly polarized wave $c|\mathbf{B}| = (kc/\omega)|\mathbf{E}| = (c/v)|\mathbf{E}|$, we see that $|\mathbf{E}|^2 - c^2|\mathbf{B}|^2 > 0$. Thus the condition for pair creation according to Schwinger (1951) is satisfied, and positrons are therefore predicted to be produced in a laser-plasma environment. Moreover, Avetisyan *et al.* (1991) solved the Dirac equation perturbatively to find the production of electron-positron pairs by inelastic multiphoton scattering in a plasma. They found the probability distribution for transverse electromagnetic perturbations in the plasma, and used this (Avetissian *et al.*, 2002) to investigate pair production due to nonlinear photon-photon scattering from oppositely directed laser beams. Analytical results for the number of particles created on short interaction time scales were found. Fried *et al.* (2001) investigated the possibility for pair production via crossing laser beams, and concluded that laser intensities have to reach 10^{29} W/m^2 before this could be used as a means for electron-positron generation.

Pair production may possibly also be achieved without the intervention of a plasma or other dispersive media. According to Narozhny *et al.* (2004a, 2004b), focused and/or counterpropagating laser pulses can interact via the nonlinear quantum vacuum as to produce real electron-positron pairs. The prediction of Narozhny *et al.* (2004b) is that pair creation for colliding pulses is expected for intensities of the order 10^{26} W/cm^2, which is two orders of magnitude lower than for single pulse generation. Moreover, Narozhny *et al.* (2004a) claim that the effect of pair creation puts an upper theoretical limit on laser focusing, since the electromagnetic energy will be dissipated into fermionic degrees of freedom for high intensities.

As intense fields create electron-positron pairs, the particle density increases. If intense photon beams can be sustained for long enough times, this will create a pair plasma. In this case, plasma effects on the electromagnetic field need to be taken into account. The backreaction of pair creation on the electromagnetic field was considered by Kluger *et al.* (1991) in $1+1$ dimensions.

Starting from a semiclassical approximation, a kinetic model taking pair production into account using an emissive term in the electron equation of motion was presented. From a numerical analysis of the governing equations it was found that high enough field intensities will induce plasma oscillations. Due to the realization that the right conditions for pair creation by lasers could soon be at our disposal, the problem of backreaction and the dynamics of the interaction of the electron-positron plasma on photons has produced an increasing number of publications over the years. Prozorkevich *et al.* (2000), Alkhofer *et al.* (2001), and Roberts *et al.* (2002) have similarly developed self-consistent schemes where a collisionless plasma is coupled to the time-dependent electric field, via Maxwell's equations and the pair-creation source term. In their application to the x-ray free-electron laser, they arrived at plasma behavior reminiscent of a modulational instability, and suggested necessary and sufficient conditions to generate a pair plasma using the x-ray free-electron laser. Collisions in plasmas created due to intense electromagnetic fields may also be taken into account using a quantum kinetic description with a pair-creation source term (Bloch *et al.*, 1999, 2000).

A somewhat different scheme using intense lasers was suggested by Liang *et al.* (1998). Letting two intense laser pulses impinge on the surface of a thin foil made of a suitable material, e.g., gold, plasma formation takes place. The jitter energy for a large fraction [∼50% (Wilks *et al.*, 1992)] of produced plasma electrons is suggested to exceed the pair-creation threshold $2m_ec^2$. Thus in this scheme pair creation is a result of the thermal plasma, instead of direct laser interaction with the quantum vacuum. Similarly, Helander and Ward (2003) suggested that runaway electrons in tokamak plasmas could have the same effect. Since electrons with sufficient energy experience a decreasing plasma friction force as the energy increases, such particles will in effect be accelerated to very high energies until direct collisions with plasma particles occur. The typical runaway electron energy is $\gtrsim 3m_ec^2$, and these collisions could therefore trigger positron production, as electrons lose their energy via brehmsstrahlung in the Coulomb field, the so-called Bethe-Heitler process. The number of positrons in a facility such as JET was estimated to ∼10^{13}–10^{14}, a very large number compared to other laboratory positron production methods.

The predicted pair-production rates normally assume spatially uniform electromagnetic fields, which is often in good agreement with experimental parameters. Recently, however, oriented crystals have become an important tool in studying effects of quantum electrodynamics in strong fields, such as spin effects in electron energy loss and crystal assisted pair production [see Kirsebom *et al.* (2001), and references therein]. In these experiments, the fields may not be considered uniform, and the models described above can therefore only partially account for observed effects. Nitta *et al.* (2004) remedied this shortcoming by using the trial trajectory method (Khokonov and Nitta, 2002), based on the
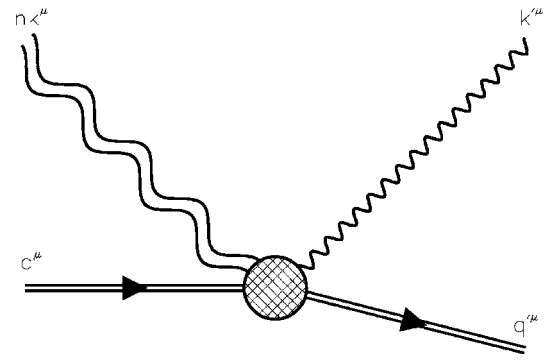

FIG. 28. Nonlinear Compton scattering, as given in Eq. (137). Reprinted with permission from Bamber *et al.*, 1999.

method developed by Baĭer and Katkov (1968). Previous attempts to analyze experimental results were based on numerical schemes, but Nitta *et al.* (2004) found an analytical expression for the pair-creation rate in an inhomogeneous field, in good agreement with the observed pair-creation rate. Furthermore, the inhomogeneous case also displayed pair creation for low-amplitude fields, where the uniform field treatment effectively gives a zero pair-creation rate. This result could be of interest in the case of strongly magnetized stars, which have a characteristic dipole behavior.

Since waves in vacuum are described in terms of their behavior along the null coordinates $u=z-ct$ and $v=z+ct$, it is of interest to generalize the Schwinger results of pair creation to the case of fields depending on u and/or v. This was done by Tomaras *et al.* (2000), and later generalized by Avan *et al.* (2003) to a more complicated coordinate dependence. Furthermore, the momentum spectrum of produced pairs was derived for arbitrary time-dependent gauge fields by Dietrich (2003), via the exact solution of the equation of motion for the Dirac Green's function.

2. Laser-induced pair creation

The production of antimatter is of great importance for a variety of experimental tests of fundamental issues in physics, e.g., Lorentz invariance tests, as well as being of interest in its own right. Moreover, there can also be a test of the nonlinear properties of QED, since high-energy photons may create matter and antimatter out of the quantum vacuum. This process is well established as a model for pair production in the vicinity of neutron stars, and corresponds to the imaginary part of the full Heisenberg-Euler Lagrangian, and can thus be interpreted as energy being dissipated from bosonic to fermionic degrees of freedom.

The implications of pair creation was understood very early on in the history of QED, but the direct creation of electron-positron plasmas from photons has long escaped experimental efforts. Thus an important piece in our view of the quantum vacuum had long eluded the attempts of detection. However, with rapid advances in laser intensity, the prospects for performing a successful experiment in pair creation using laser sources took a

turn for the better. As described below, inelastic photon-photon scattering, where two real photons gives rise to a real electron-positron pair, has now been experimentally confirmed (Burke *et al.*, 1997; Bamber *et al.*, 1999), and holds the promise of further elucidating our picture of the nonlinear quantum vacuum [see also Meyerhofer (1997)].

In nonlinear Compton scattering, multiphoton absorption by an electron results in the emission of a single high-energy photon according to (see Fig. 28)

$$e + n\omega \rightarrow e' + \gamma. \tag{137}$$

The effect (137) was first measured by Bula *et al.* (1996) using a GeV electron beam and a terawatt laser source, obtained by chirped-pulse amplification. In the experiment up to four laser photons interacted with a single electron. High-energy photons produced by nonlinear Compton scattering can be used in the laser-assisted production of a pair plasma. The usage of laser-produced photons for the electron-positron pair production was suggested long before lasers reached the necessary intensities (Reiss, 1962; Nikishov and Ritus, 1964a, 1964b, 1965, 1967; Narozhny *et al.*, 1965) (the direct production of pairs by photons requires $\hbar\omega \gtrsim 2m_e c^2$ in the center-of-mass system). By recolliding high-frequency photons with original laser photons, according to the Breit-Wheeler[7] process (Bethe and Heitler, 1934; Breit and Wheeler, 1934)

$$\gamma + n\omega \rightarrow e^+ e^-, \tag{138}$$

the production of electron-positron pairs can be achieved in a laboratory environment. This can be compared to the trident process

$$e^- + n\omega \rightarrow e' e^+ e^-. \tag{139}$$

While the multiphoton process (138) requires $n \geqslant 4$ with experimental values used by Burke *et al.* (1997), the trident process requires $n \geqslant 5$ with the same experimental data. The two-step process (137) and (138) was first used by Burke *et al.* (1997) in the laser production of electron-positron pairs.

Bula *et al.* (1996) reported on the observation of nonlinear Compton scattering (137), where scattered electrons were detected using a 46.6-GeV electron beam in conjunction with a 1054- and 527-nm laser with focal intensity $\sim 10^{18}$ W/cm^2. This process can also be understood in terms of a plane-wave interaction with an electron. For a weak electromagnetic field with amplitude E, the maximum speed attained by an electron (initially at rest) due to the passing of a plane wave is

$$v_{\max} = \frac{eE}{m_e \omega}, \tag{140}$$

where m_e is the rest mass of the electron and ω is the frequency of the plane wave. As the field strength in-

creases, higher-order radiation effects becomes important as $v_{\max} \rightarrow c$, which in terms of light quanta can be interpreted as multiphoton absorption by the electron, with the release of a single distinguishable light quanta as a result, i.e., the process (137). In this sense, nonlinear Compton scattering becomes important as the parameter

$$\eta = \frac{v_{\max}}{c} = \frac{eE}{m_e c\omega} = \frac{e|A_b A^b|^{1/2}}{m_e c^2} \tag{141}$$

approaches unity. Here the four-vector potential A^b satisfies the Lorentz gauge.

For an electron with initial energy $\mathcal{E}_0$, the absorption of n photons of the frequency ω at an angle θ between the electron and laser beam, results in the minimum electron energy

$$\mathcal{E}_{\min} = \frac{\mathcal{E}_0}{1 + ns/m_{\text{eff}}^2 c^4}, \tag{142}$$

where $s = 2\mathcal{E}_0\omega(1 + \cos\theta)$ is the scattering parameter and $m_{\text{eff}} = m(1 + \eta^2)^{1/2}$ is the effective mass. With the experimental parameters used by Bula *et al.* (1996), the intensity parameter becomes $\eta \approx 0.6$. Linear Compton scattering ($\eta \ll 1$, $n = 1$) would then result in $\mathcal{E}_{\min} \approx 25.6$ GeV at $\theta = 17°$. Since the spectrum of multiphoton Compton scattered electrons extends below 25.6 GeV, it was possible to identify nonlinear effects (Bula *et al.*, 1996).

In the same way, as the intensity parameter η approaching unity signifies the onset of the nonlinear Compton effect, the parameter (Burke *et al.*, 1997; Bamber *et al.*, 1999)

$$\Upsilon = \frac{|F_{ab}p^b|}{m_e c^2 E_{\text{crit}}} \tag{143}$$

characterizes the strength of the vacuum polarization, as it contains information on the photon frequency as well as the background field strength, the two important parameters for vacuum breakdown. Here F_{ab} is the Maxwell tensor of the background electromagnetic field and p_a is the four-momentum of the probe photon. As Υ approaches unity, the pair-production rate according to the process (138) becomes significant (Nikishov and Ritus, 1964a, 1964b, 1965, 1967; Narozhny *et al.*, 1965; Burke *et al.*, 1997). For the case of single-particle ($n = 1$) Breit-Wheeler scattering, laser wavelengths of 527 nm would require single-photon energies of 111 GeV in order for significant pair production to occur, while for the multiphoton Breit-Wheeler process photons of the same wavelength colliding with backscattered photons with energies 29 GeV give $\Upsilon \approx 0.5\eta$ (Burke *et al.*, 1997). Thus for large enough η, the pair-production rate would yield a well-defined energy spectrum (Fig. 29) with a detectable level of electrons and positrons (see Figs. 30 and 31).

Burke *et al.* (1997) presented the first results of a successful measurement along the lines presented above. The signal consisted of ~100 positrons above the back-

---

[7]Breit and Wheeler (1934) considered single-photon scattering $\omega_1 + \omega_2 \rightarrow e^+ e^-$ thus somewhat different from the multiphoton process discussed here.
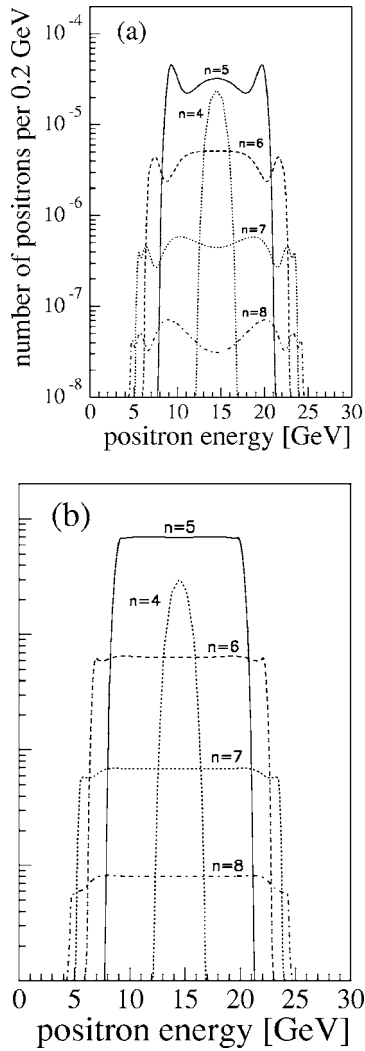
FIG. 29. Calculated positron energy spectra for a 30-GeV photon interacting with a 527-nm laser beam. (a) The polarization is parallel while in (b) the polarization is perpendicular. *n* gives the number of photons involved in the interaction. Reprinted with permission from Bamber *et al.*, 1999.

ground value using a 46.6-GeV electron beam and a 527-nm Nd:glass laser with focal intensity $\sim 10^{18}$ W/cm^2 (Meyerhofer, 1997).

3. Other mechanisms for pair production

Narozhny *et al.* (2004a) considered pair production in an electromagnetic field created by two counterpropagating laser pulses, and showed that pair production can be experimentally observed when the intensity of each beam is similar to 10^{26} W/cm^2, three orders of magnitude lower than that of a single pulse. However, the cross section for the Schwinger process at optical frequencies (or below) is so small at any laser intensity that this effect is insignificant (Mittleman, 1987).

Production of pairs is also possible in the Coulomb field of a nucleus via virtual photons ("tridents"), which is a dominant energy-loss mechanism at high energies. In a trident Bahba process high-energy electrons, with
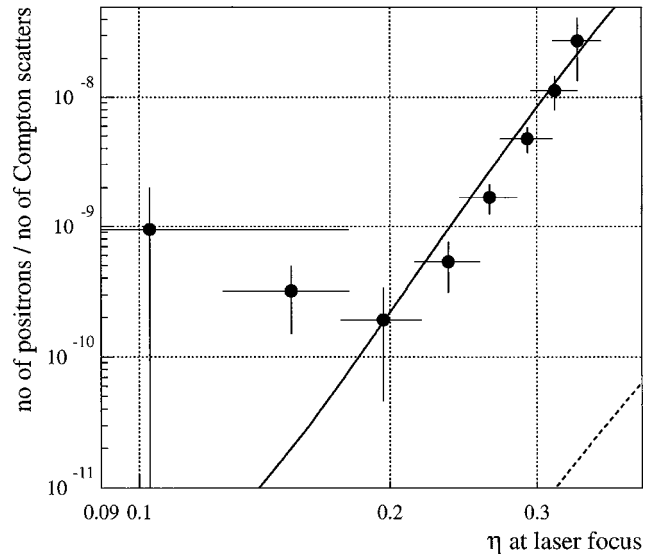
FIG. 30. Positron production rate per Compton scatterer as a function of the intensity parameter η, as given by Eq. (141). The solid line is the numerical estimate from the two-step process (137) and (138), while the dashed line represents the trident process (139). The measurements performed by Burke *et al.*, 1997 are given by the dots in the plot. Reprinted with permission from Burke, 1997.

kinetic energies exceeding the pair-production threshold $2m_e c^2$, can produce electron-positron pairs by scattering in the Coulomb potential of the nucleus. In the past, some authors (Bunkin and Kasakov, 1970; Scharer *et al.*, 1973) had presented a preliminary discussion about pair production by relativistic electrons accelerated by intense laser, while others (Berezhiani *et al.*, 1992) presented a detailed investigation of pair production due to scattering of high-energy electrons produced in strong wakefields driven by intense short laser pulses. This was

FIG. 31. Pair-production rate, as compared with the multiphoton Breit-Wheeler process (138) and trident process (139), as a function of Υ given by Eq. (143). Reprinted with permission from Bamber *et al.*, 1999.

found to be an efficient mechanism for a "pair factory." Recently, Berezhiani *et al.* (2005) carried out computer simulations of laser plasma dynamics in overdense plasmas and showed that an intensive product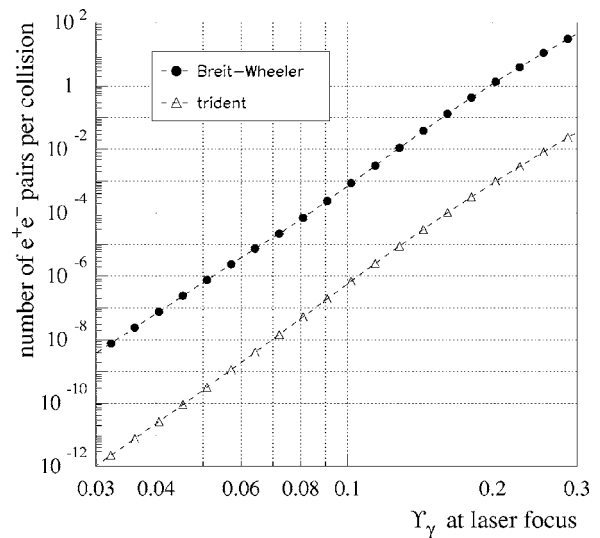ion of pairs by the drive motion of plasma electron takes place due to the trident process. Furthermore, Bulanov *et al.* (2005) have shown that electromagnetic waves could be damped due to electron-positron pair production [see also Mikheev and Chistyakov (2001), for a discussion on the process in a strong magnetic field].

4. Laser experiments on photon-photon scattering

The evolution of laser intensity is truly astounding (Perry and Mourou, 1994; Mourou *et al.*, 1998, 2006; Tajima and Mourou, 2002) (see Fig. 1), and with the event of the x-ray free-electron laser a new domain in experimental physics will open up. There have been an interesting set of both suggested and performed experiments using lasers of previous and current intensities. Note that one of the major obstacles in these investigations has been residual gas components in the vacuum environment. However, depending on the problem of study, the means for inhibiting the residual gas to have a detrimental effect on the measurement varies. In high-intensity laser experiments on elastic photon-photon scattering, the electron expulsion at the leading edge of the laser pulses will in fact make the generation of background radiation weaker (at a vacuum of 10^{-9} torr), and particle effects would therefore have a negligible effect in these experiments (Lundström *et al.*, 2006). This is contrast to a weak-field experiment, such as cavity environments, where the effects due to a residual gas may be significant. However, it is possible to design the mode interaction such as to produce a unique signature of photon-photon interaction, thus making it possible, in principle, to detect scattering by the proper filtering techniques (Eriksson *et al.*, 2004).

a. Vacuum birefringence

The concept of vacuum birefringence is well known and has been theoretically explored in many publications (Klein and Nigam, 1964a, 1964b; Erber, 1966; Adler, 1971; Adler and Shubert, 1996; Heyl and Hernquist, 1997a). The birefringence of the vacuum manifests itself as the difference in the refractive index between the propagating ordinary and extraordinary modes (Rikken and Rizzo, 2000). Thus although a very difficult high precision experiment, this difference may in principle become measurable in strong enough background magnetic (or electric) fields. This idea has been exploited in the Polarizzazione del Vuoto con LASer (PVLAS) Collaboration setup (Bakalov *et al.*, 1994; Melissinos, 2002), for which the difference (Bakalov *et al.*, 1998)

$$\Delta n = n - n_\perp = 3\kappa\epsilon_0 c^2 |\mathbf{B}_0|^2 \approx 4 \times 10^{-24} |\mathbf{B}_0|^2 \qquad (144)$$

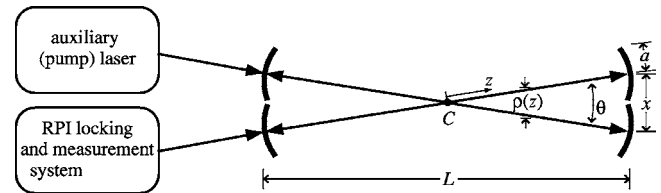is to be measured. Here $|\mathbf{B}_0|$ is given in T.

FIG. 32. The interferometric setup for detection of vacuum birefringence. The figure reference in the above setup is Fig. 1 in Luiten and Petersen, 2004b. Reprinted with permission from Luiten and Petersen, 2004b.

A linearly polarized laser beam is sent through the static field $\mathbf{B}_0$, with $\mathbf{E} \cdot \mathbf{B}_0 = |\mathbf{E}||\mathbf{B}_0| \cos \theta$. Due to the birefringence of the magnetized vacuum, as given by Δn, the beam will attain an ellipticity

$$\Psi = \frac{\pi L}{\lambda} \Delta n \sin(2\theta) \qquad (145)$$

over a propagation distance L, where λ is the wavelength of radiation. The change in ellipticity is proposed as a measurement of the birefringence of vacuum. Bakalov *et al.* (1998) also presented a detailed discussion of noise sources as well as a rather detailed description of the actual experimental setup. Current superconducting magnets can reach field strengths up to $5-25$ T, and could in principle yield detectable changes in the polarization state of a laser beam traversing it. Unfortunately, strong magnetic fields generate forces within the detection equipment which may interfere with the ellipsometric measurement. Moreover, magnetic fields cannot be shielded in any efficient way, and this is therefore a problem that is likely to persist (Cameron *et al.*, 1993).

Another approach towards measuring vacuum birefringence is using laser interferometry. This technique can reach astonishing accuracy and sensitivity, and is currently the most promising method of choice in gravitational wave detection (Saulson, 1994). Using laser interferometry for detecting light-by-light scattering through vacuum birefringence rests on the same principle as described above, but replacing the strong magnetic field by ultrashort laser pulses (Partovi, 1993; Boer and van Holten, 2002; Luiten and Petersen, 2004b). Since laser beams, i.e., laser light with typical pulse length much larger than its wavelength, has a very low-energy density compared to the strongest laboratory magnetic fields, one has instead to resort to ultrashort highly focused laser pulses. Such configurations could indeed result in magnetic-field components of the order 10^5 T, orders of magnitude larger than quasistationary magnetic fields produced by superconducting coils (Lee and Fairbanks, 2002). Due to the degree of pulse focusing, interaction of the strong field with the detector can be almost eliminated. On the other hand, the ultrashort time and length scales require a very high resolution in the detection. An experimental suggestion along these lines was put forward by Luiten and Petersen (2004a, 2004b), using a high precision birefringence measuring technique (Hall *et al.*, 2000). Luiten and Petersen (2004b) argue that this

technique may be used to construct a tabletop detector of vacuum polarization using current state-of-the-art optical techniques. The setup consists of two concentric resonant cavities with an interaction cross section. One of the cavities acts as the vacuum polarizer, while the other cavity supplies test photons for which the ellipticity is to be detected (see Fig. 32). Depending on the Fabry-Perot resonator reflectivity, the integration time was estimated. With a reflectivity $R=99.97\%$ the necessary operation time of the device would be 2.6 years, $R=99.994\%$ yields 1.7 days, and $R=99.997\%$ gives 2.5 h, using a 20-W, 200-fs laser and a resonator of length 3 m.

Jeah-Sheng et al. (2004) have built and tested a 3.5-m Fabry-Perot inteferometer with a precision ellipsometer for QED tests and axion search, along the lines of the vacuum birefringence test presented above. Note that the results presented by Jeah-Sheng et al. (2004) are for a prototype detector, and, although promising, a measurement of the vacuum polarization has not been performed [see also Sheng-Jui et al. (2003)]. Moreover, the PVLAS Collaboration has recently claimed (Zavattini et al., 2006) to have measured the dichroism of a magnetized vacuum, an effect possible due to interaction between light pseudoscalars and photons.

b. Harmonic generation

Ding and Kaplan (1989) suggested that the nonlinear vacuum could be given measurable properties by the possible harmonic generation of radiation in an external field. The work attracted lots of attention, and some questions as to whether the result was correct or not was raised (Ding and Kaplan, 1990; Ford and Steel, 1990; Raizen and Rosenstein, 1990). While some of the critiques were flawed, the main problem in the work of Ding and Kaplan was the assumption of a constant background field (Ford and Steel, 1990). It is well known that a homogeneous and time-independent background field cannot transfer momentum to photons, and such a field is therefore not capable of driving a frequency upshift as suggested by Ding and Kaplan [see McKenna and Platzman (1963)]. However, Ding and Kaplan (1992) showed that a spatially inhomogeneous background field could indeed result in higher harmonics. This idea was further developed by Kaplan and Ding (2000), where Maxwell's equations were analyzed with a weakly varying background magnetic field.

Using the slowly varying amplitude approximation (Hasegawa, 1975), Kaplan and Ding (2000) showed that the envelope of the electromagnetic field satisfies the second harmonic generation equation

$$4ik\frac{\partial \mathbf{a}}{\partial t} + \nabla_\perp^2 \mathbf{a} = -2ik\kappa\mathbf{F}, \tag{146}$$

where

$$\mathbf{F} = \frac{1}{\kappa}\left(\frac{\partial \mathbf{D}^{(2)}}{\partial t} + \nabla \times \mathbf{H}^{(2)}\right)\exp(2ikz - 2i\omega t) \tag{147}$$

is the second harmonic generation background source term. Here $\mathbf{D}^{(2)}$ and $\mathbf{H}^{(2)}$ are derived from the Heisenberg-Euler Lagrangian (5) from nonlinear field combinations giving rise to terms proportional to $\exp(2i\omega t)$. Kaplan and Ding (2000) use Eq. (146) to study the evolution of 2D Gaussian beams propagating in an external nonconstant magnetic field, giving the estimated output power. Moreover, a discussion of more complicated background magnetic-field geometries, e.g., the magnetic quadrupole case, was given. Considering μm lasers with focal intensities $\sim 10^{22}$ W/cm^2 generating a pulse propagating through the background magnetic field strengths 10^3 T [which in the paper by Kaplan and Ding (2000) is suggested to be produced by explosive mechanisms], a rough estimate gives a production of 85 photons/day by second harmonic generation. However, in this estimate temporal effects, which may be of importance in the next generation ultrashort intense lasers, have been omitted, and could yield alterations in their estimates.

c. Four-wave interactions

In the second harmonic generation presented above, the interaction of photons is mediated by a background magnetic field. However, crossing electromagnetic waves would similarly interact and yield new modes of different frequencies. One of the more prominent modes in such a mechanism is given by the four-wave interaction mediated mode satisfying the resonance condition between frequencies and wave vectors (i.e., photon energy and momentum conservation) (Rozanov, 1993). It is therefore not a surprise, given the evolution of laser powers and frequencies, that the search for photon-photon scattering using resonant four-wave interactions has caught the attention of researchers in this area. This approach has also come furthest in the experimental attempts to detect elastic scattering among photons (Bernard, 1998, 1999, 2000; Moulin and Bernard, 1999; Bernard et al., 2000).

Moulin et al. (1996) presented experiments on light-by-light scattering performed in the optical regime. With this, they managed to put new experimental upper limits on the photon-photon scattering cross section. Unfortunately, no scattering was detected, but stimulated the continued research along the lines of four-wave interactions as an experimental tool for probing the quantum vacuum. Using the resonance conditions[8] $\omega_4=\omega_1+\omega_2-\omega_3$ and $\mathbf{k}_4=\mathbf{k}_1+\mathbf{k}_2-\mathbf{k}_3$, one may, in general, derive a set of wave interaction equations for slowly varying amplitudes a_i, $i=1,\ldots,4$, of the form (Weiland and Wilhelmsson, 1977)

$$\frac{da_i}{dt} = Ca_j a_k a_l^*, \tag{148}$$

given any type of media through which the waves may interact. Here the coupling constants C depend on the

---

[8]The interaction between modes of different frequencies gives rise to several new modes, but resonance conditions and time averaging, mimicking the act of detection over certain time scales, yield the desired equations.

interaction in question, as well as on the physical parameters of the system around which the waves are modulated. In the case of a nonlinear quantum vacuum, the coupling constant will depend on κ of the Lagrangian (5).

The coupling constants may be interpreted in terms of the nonlinear susceptibility of the vacuum. Moulin and Bernard (1999) considered the interaction of three crossing waves, characterized by their respective electric-field vectors $\mathbf{E}_i$, producing a fourth wave E_4. Starting from Maxwell's equations with the usual weak-field limit Heisenberg-Euler third-order nonlinear corrections [see the Lagrangian (5)], they derive

$$i\left(\frac{\partial}{\partial t} + c\frac{\partial}{\partial z}\right)E_4 + \frac{c^2}{2\omega_4}\nabla_\perp^2 E_4 = -\frac{\omega_4}{2}\chi^{(3)}E_1E_2E_3^* \quad (149)$$

for the driven wave amplitude E_4, where the overall harmonic time dependence $\exp(-i\omega t)$ has been factored out. Here $\chi^{(3)}$ is the third-order nonlinear susceptibility given by

$$\chi^{(3)} = \frac{\alpha}{45\pi}\frac{K}{E_{\text{crit}}^2} \approx 3\times 10^{-41} K \text{ m}^2/\text{V}^2, \quad (150)$$

where K is a dimensionless form factor of order unity. The value of K depends on the polarization and propagation directions of the pump modes, and reaches a maximum of $K=14$ for degenerate four-wave mixing (Moulin and Bernard, 1999). Moulin and Bernard (1999) furthermore discuss the influence of a nonperfect vacuum, where the susceptibility of the gas will introduce a threshold, in terms of a critical gas pressure, for the nonlinear QED effect to be detected. Bernard (2000) and Bernard et al. (2000) recently presented experiments on four-wave mixing in vacuum, improving previous attempts by nine orders of magnitude, although no direct detection of photon-photon scattering was achieved. Experiments along the same lines as described for four-wave mixing above can also be used for a large number of other, non-QED, test, such as axion[9] search (Bernard, 1999; Bradley et al., 2003; Dupays et al., 2005). Thus progress of low-energy QED experiments could also prove to be useful for, e.g., dark matter searches.

There are more recent proposals for detection of photon-photon scattering using four-wave interactions. Lundström et al. (2006) have done more detailed calculations concerning experimental constraints, in particular for the Astra Gemini laser (operational in 2007) at the Rutherford Appleton Laboratory (CCLRC, 2005), as well as nonperfect vacuum problems, etc., and concluded that it will be feasible to detect elastic scattering among photons if using a high-repetition-rate, high-intensity laser system.

---

[9]Axions are bosons which were introduced in order to explain the absence of CP symmetry breaking in QCD (Peccei and Quinn, 1977; Weinberg, 1978; Wilczek, 1978), and the axion is still to be detected.

5. Cavity experiments

As mentioned in Sec. III.A.4, the effects of photon-photon scattering on cavity EM fields is to produce new wave modes. The new modes excited in the cavity will (approximately) satisfy the cavity dispersion relation. Thus by varying the cavity cross section the pump modes may be filtered out, leaving the new modes for detection. The treatment of cavity mode interaction in the quantum vacuum was described by Brodin et al. (2001, 2002) and Eriksson et al. (2004).

If no damping or dissipation is present, Eqs. (69) yield a linear growth of the vector potential amplitude A_3 of mode 3. In order to gain an understanding of the saturation level, we make the following modification to Eq. (69). Let $d/dt \rightarrow d/dt - (\omega_3/2\pi Q)$, where Q is the cavity quality factor. A steady-state amplitude

$$A_3 = \frac{i\pi QK_{\text{cyl}}}{4}\frac{\alpha}{90\pi}\frac{\omega_3^2 A_1^2}{E_{\text{crit}}^2}A_2^* \quad (151)$$

is thus obtained. Here ω_3 is the frequency of the mode generated by the third-order QED nonlinearities. The number of excited photons in the cavity mode can be described by $N \approx (\epsilon_0 \int |E_3|^2\, d^3r)/\hbar\omega_3$. Using the saturation value (151) for the vector potential of mode 3, the number of photons generated by the nonlinear interaction of two cavity modes is given by

$$N_{\text{QED}} = \frac{\epsilon_0\alpha^2 VQ^2\omega_3^5 K_{\text{cyl}}^2 J_0^2(\beta_3)|A_1|^4|A_2|^2}{129\,600\,\hbar\,E_{\text{crit}}^4}, \quad (152)$$

where the coupling constant K_{cyl} can be found in Eriksson et al. (2004), $V = \pi a^2 z_0$, a is the cylindrical cavity radius, z_0 is the cavity length, and β_3 is a zero for the Bessel function J_1 corresponding the generated mode satisfying the resonance condition (61). We note that the number of generated photons depends on a large number of parameters, and one thus needs to specify the cavity geometry, etc., in order to obtain an estimate of the magnitude of the effects. Eriksson et al. (2004) choose the following wave mode numbers: $(\ell_1, \ell_2, \ell_3) = (3, 15, 21)$ (fulfilling $\ell_3 = 2\ell_1 + \ell_2$), $\beta_2 = \beta_3 = 3.83$, corresponding to the first zero of J_1, and $\beta_1 = 7.01$ corresponding to the second zero. This gives $z_0/a = 9.53$ through the frequency matching condition (61) and determines the frequency relations to $\omega_3/\omega_2 = 1.26$ and $\omega_3/\omega_1 = 1.12$. Substituting these values gives $K_{\text{cyl}} = 3.39$ [see Eriksson et al. (2004)]. The remaining key parameters are the quality factor and pump field strength. Liepe (2000) has shown that it is possible to reach intense cavity surface fields, of the order $|A_1|, |A_2| \sim 0.01 - 0.03$ V s/m, with quality factors as high as $Q = 4\times 10^{10}$ at temperatures of 1 K. Thus in this case Eq. (152) gives

$$N_{\text{QED}} \approx 18. \quad (153)$$

For a cavity wall temperature of 0.5 K, the number of thermal photons is $N_{\text{thermal}} = 1/[\exp(\hbar\omega_3/k_B T) - 1] \approx 7$, which is thus lower than N_{QED}. In order to reach further accuracy in the measurement, a cavity filtering system

can be set up so that pump modes may be reduced or eliminated. It can furthermore be shown that the nonlinearities of the cavity walls will not generate modes swamping QED photons (Eriksson *et al.*, 2004).

B. Laser-plasma systems and the x-ray free-electron laser

The x-ray free-electron laser (XFEL) promises new and exciting applications for a coherent electromagnetic source. Applications range from probing astrophysical conditions in the laboratory to new possibilities to do molecular biology. Could the XFEL also provide insight into quantum electrodynamical nonlinearities, such as photon-photon scattering? If affirmative, this would enhance our understanding of the quantum vacuum, as well as providing new prospects of testing fundamental properties of physical laws, such a Lorentz invariance and symmetry breaking. Indeed, it has been stated that the facilities at DESY and SLAC would be able to produce electron-positron pairs directly from the vacuum (Ringwald, 2001a, 2001b, 2003), due to the estimated focal intensities at these sources. If this scenario is demonstrated, it is likely that effects of elastic photon-photon scattering would come into play at an even earlier stage. Due to the possible effects of scattering amongst photons, such as photonic self-compression and collapse, it is therefore of interest to include such effects into the analytical and numerical models used in predicting the behavior of these systems. Furthermore, the creation of a pair plasma in the laboratory could be affected by new low-frequency modes from nonlinear quantum vacuum effects, thus altering the properties of energy transfer within such plasmas, as well as providing indirect tests for QED. XFEL also gives the opportunity to do laboratory astrophysics in a new parameter regime, making the quantum vacuum more accessible.

However, it is not necessary to enter the new regime of XFEL in order to facilitate tests of QED and Lorentz invariance, as well as doing laboratory astrophysics. Effects such as Unruh radiation (Unruh, 1976) and the related Hawking effect (Hawking, 1974) can hopefully be investigated using the next generation laser-plasma systems (Bingham, 2003), such as the high-repetition-rate Astra Gemini laser (to be operational in 2007) (CCLRC, 2005). In such regimes it will also be of interest to investigate QED effects, such as photon-photon scattering. As seen in the previous sections, the introduction of plasma dispersion allows for new electromagnetic wave modes in both unmagnetized and magnetized plasmas (Marklund *et al.*, 2004a; Marklund, Shukla, Stenflo, *et al.*, 2005), when nonlinear quantum vacuum effects are included. For example, at the laboratory level, current high laser powers are able to accelerate particles to highly relativistic speeds. Furthermore, pulse self-compression in laser-plasma systems may play an important role in attaining power levels well above current laser limits [see, e.g., Bulanov *et al.* (2003); Shorokhov *et al.* (2003)]. As intensities approach the Schwinger limit in future laser-plasma setups, effects of pair-creation and photon-photon scattering have to be taken into account

(Bulanov *et al.*, 2003; Bulanov, 2004). Laser-plasma systems can have electron densities of the order 10^{26} m^{-3}, and laser intensities can be close to 10^{23}–10^{25} W/cm^2 (Mourou *et al.*, 1998; Bingham, 2003). Moreover, as stated by Bulanov *et al.* (2003), laser self-focusing in plasmas could come close to E_{crit}, from which pair creation is likely to follow. In fact, it has been estimated that the National Ignition Facility would be able to produce pairs by direct irradiation of a deuterium pellet (Lee *et al.*, 1995). On the other hand, the creation of laboratory electron-positron plasmas is already a feasible task (Surko *et al.*, 1989; Greaves *et al.*, 1994), as is the usage of these plasmas for making pair plasma experiments (Greaves and Surko, 1995). Thus the possibility to study laser-plasma interactions in pair plasmas could be a reality in the nearby future. Currently available positron densities in laboratories are well below those of regular laser-plasma systems, but according to Lee *et al.* (1995) there is a possibility of reaching densities of the order of 10^{27} m^{-3}. Using $n_0 \sim 10^{26}$ m^{-3} and a field intensity 10^{16} V/m [due to laser self-compression (Bulanov *et al.*, 2003)] at the wavelength 0.3×10^{-6} m, we find from Eq. (125) that $\omega \approx 7.8 \times 10^5$ rad/s, i.e., the frequency is in the low-frequency band, as an example of QED effects in laboratory plasmas.

In combination with plasma particle expulsion due to electromagnetic wave trapping, the possibility of catastrophic collapse due to photon-photon collisions arises (Bulanov *et al.*, 2003; Marklund, Eliasson, and Shula, 2004). This scenario it highly interesting, since it would make three-dimensional ultraintense solitonic structures possible in vacuum bounded by a plasma or wave-guide structure a truly exciting prospect. This may even prove a valuable tool for intense pulse storage, if a successful cavity nonlinear QED experiment is performed.

C. Astrophysical importance

The implications of the QED vacuum are well known within astrophysics, and the pair plasma in pulsar surroundings is partly dependent on mechanisms which has no classical counterpart (Asseo, 2003). Furthermore, photon splitting (Adler *et al.*, 1970; Bialynicka-Birula and Bialynicki-Birula, 1970; Adler, 1971) supports the notion that strongly magnetized objects, such as neutron stars and magnetars, could be used as probes of nonlinear QED effects.

However, most effects discussed within astrophysical applications concerning QED deals with single-photon effects, and thus do not take collective effects into account. It is well known from plasma physics that collective effects alter the charged particle behavior in nontrivial and important ways. In fact, it would not be possible to understand most plasma effects without resorting to a collective description. The analogy between the quantum and a plasma system has been stated before (Dittrich and Gies, 2000), and is both useful and imaginative. Thus, in line with this, it is likely that collective quantum vacuum effects could yield crucial information about astrophysical systems, where extreme en-

ergy levels are reached. Even kinetic effects, such as Landau damping, could play a role in the dynamics of photons in the vicinity of strongly magnetized objects. This could prove a new realm of photon kinetics, and applications to astrophysical sources, such as magnetar quakes (Kondratyev, 2002), are of interest for future research directions.

Especially strong magnetic field effects due to the quantum vacuum is of great interest in astrophysical applications. Since Earth-based magnetic field strengths are very limited, and are likely to remain so for the foreseeable future, magnetars and similar objects offers a unique perspective on the quantum vacuum (Erber, 1966; Baring and Harding, 2001). Pulsar magnetospheres exhibit extreme field strengths in a highly energetic pair plasma. Ordinary neutron stars have surface magnetic field strengths of the order of 10^6–10^9 T, while magnetars can reach 10^{10}–10^{11} T (Kouveliotou et $al.$, 1998), coming close to, or even surpassing, energy densities $\epsilon_0 E_{\mathrm{crit}}^2$ corresponding to the Schwinger limit. Such strong fields will make the vacuum fully nonlinear, due to the excitation of virtual pairs. Photon splitting can therefore play a significant role in these extreme systems (Harding, 1991; Baring and Harding, 2001).

The pair plasma creation in pulsar environments itself rests on nonlinear QED vacuum effects. The emission of short-wavelength photons due to the acceleration of plasma particles close to the polar caps results in a production of electrons and positrons as photons propagate through the pulsar intense magnetic field (Beskin et $al.$, 1993). The precise density of the pair plasma created in this fashion is difficult the estimate, and the answer is model dependent. However, given the Goldreich-Julian density $n_{\mathrm{GJ}}=7\times10^{15}(0.1\ \mathrm{s}/P)(B/10^8\ \mathrm{T})\ \mathrm{m}^{-3}$, where P is the pulsar period and B is the pulsar magnetic field, the pair plasma density is expected to satisfy $n_0=Mn_{\mathrm{GJ}}$, M being the multiplicity (Beskin et $al.$, 1993; Luo et $al.$, 2002). The multiplicity is determined by the model through which the pair plasma is assumed to be created, but a moderate estimate is $M=10$ (Luo et $al.$, 2002). Thus with these prerequisites the density in a hot dense pair plasma is of the order $10^{18}\ \mathrm{m}^{-3}$, and the pair plasma experiences a relativistic factor $\sim10^2$–10^3 (Asseo, 2003). We may use these estimates to obtain estimates for particular QED processes in plasmas. For example, inserting the above values in Eq. (126) we obtain $\lambda\sim10^{-12}$–10^{-11} m. On the other hand, the primary beam will have $n_0\sim n_{\mathrm{GJ}}$ and $\gamma\sim10^6$–10^7 (Asseo, 2003), from which Eq. (126) yields $\lambda\sim10^{-8}$–10^{-7} m. Thus in this case we obtain short-wavelength effects.

The field of laboratory astrophysics ties the experimental domain of laser-plasma systems to areas of research where we so far have been restricted to observations (HEDLA, 2005). Interesting studies, such as shock front formation relevant to supernova explosions, could in principle be achieved in facilities such as NIF. However, the scales of the astrophysical event and laboratory setup differ by orders of magnitude. Thus it is reasonable to ask if it is possible to apply laboratory findings to

astrophysical events. Ryutov et $al.$ (2000) consider the prospects of investigating MHD phenomena of relevance for supernova hydrodynamics. From self-similarity in the governing system of equations and boundary conditions, as well as from dimensionless variables (such as the magnetic Reynolds number Re_M) they argued that laboratory results could be translated to astrophysical settings (however, Re_M in the laboratory cannot reach the extreme values of supernova ejecta but can reach values much larger than 1). Similarly, Budil et $al.$ (2000) discussed the applicability of petawatt lasers to radiative-hydrodynamics relevant to, e.g., supernova remnant evolution. The testbed experimental results presented by Budil et $al.$ (2000) indicated that the results could be useful in calibrate models of radiation hydrodynamics in supernova remnants [see also Shigemori et $al.$ (2000)]. Thus the use of high-intensity lasers for probing astrophysical phenomena, in particular as tool for testing and calibrating simulations of certain events, has undergone rapid development over the last decade. For testing QED effects within astrophysical systems the relevant dimensionless parameters are the frequency compared to the Compton frequency, the field strength over the Schwinger critical field strength (1), as well as the sign of the relativistic invariant $c^2\mathbf{B}^2-\mathbf{E}^2$. As can be seen by the second of these requirements, laboratory experiments of today will at most be weakly nonlinear, whereas the effects in astrophysical systems, such as magnetars, can be strongly nonlinear. However, the combined effect of laser-plasma dynamics and vacuum nonlinearities would yield unique signatures, and could be probes of more exotic phenomena in astrophysical plasmas. One such example in the testing of the Unruh effect (Unruh, 1976; Chen and Tajima, 1999) as a means of understanding the Hakwing effect (Hawking, 1974).

V. CONCLUSION AND OUTLOOK

The possibility of simulating astrophysical events in a laboratory environment has, during the last decade, progressed (Chen, 2003; Remington, 2005). Apart from astrophysical tests, laser-plasma systems also provide an opportunity to test certain aspects of fundamental physics, e.g., the properties of the quantum vacuum, via strong fields. Strong (~10–100 MV/m) coherent electromagnetic fields can nowadays be produced in superconducting cavities (Graber, 1993), and fields within plasmas can come close to the Schwinger limit (1). Moreover, QED effects are part of many astrophysical phenomena, such as pair cascading, and thus laboratory astrophysics has a natural connection to investigations of the quantum vacuum.

Here we have reviewed implications of QED corrections to classical electrodynamics and the propagation of electromagnetic waves and pulses. In particular, QED corrections on photon-plasma interactions were described. Modifications introduced by the nonlinear quantum vacuum were considered for, e.g., coherent and incoherent pulse propagation. Analytical, perturbative, and numerical ways of analyzing the governing equa-

tions were presented. Moreover, properties of nonlinear collective effects were presented, such as three-dimensional pulses collapse and the formation of light bullets.

The application of the results can be seen both in an astrophysical context as well as in a laboratory setting. For example, in magnetar environments (Kouveliotou *et al.*, 1998) photon splitting (Adler, 1971) is important and it is believed to give a plausible explanation for the radio silence of magnetars (Harding, 1991). On the other hand, collective effects, such as the ones presented here, could give valuable insight of QED phenomena in astrophysical environments. In the laboratory, the formation of ultrahigh-intensity pulse trains, due to self-compression and pulse splitting, is a truly exciting prospect. The fact that such configurations are within laboratory reach, using the next generation laser-plasma facilities, makes the predicted effects and their connection to astrophysical events even more interesting and may open up new possibilities for basic and applied research in the future.

ACKNOWLEDGMENTS

REFERENCES

Adler, S. L., 1971, Ann. Phys. (N.Y.) **67**, 599.

Adler, S. L., J. N. Bahcall, C. G. Callan, and M. N. Rosenbluth, 1970, Phys. Rev. Lett. **25**, 1061.

Adler, S. L., and C. Shubert, 1996, Phys. Rev. Lett. **77**, 1695.

Agrawal, G., 2001, *Nonlinear Fiber Optics* (Academic, New York).

Akhmadaliev, Sh. Zh., *et al.*, 2002, Phys. Rev. Lett. **89**, 061802.

Alexandrov, E. B., A. A. Anselm, and A. N. Moskalev, 1985, Zh. Eksp. Teor. Fiz. **89**, 1181 [Sov. Phys. JETP **62**, 680 (1985)].

Alkhofer, R., *et al.*, 2001, Phys. Rev. Lett. **87**, 193902.

Anderson, D., F. Cattani, and M. Lisak, 1999, Phys. Scr. **T82**, 32.

Anderson, D., *et al.*, 1999, Phys. Lett. A **258**, 244.

Arendt, P. N., Jr., and J. A. Eilek, 2002, Astrophys. J. **581**, 451.

Asseo, E., 2003, Plasma Phys. Controlled Fusion **45**, 853.

Avan, J., H. M. Fried, and Y. Gabellini, 2003, Phys. Rev. D **67**, 016003.

Avetisyan, G. K., A. K. Avetisyan, and Kh. V. Serdrakyan, 1991, Zh. Eksp. Teor. Fiz. **99**, 50 [Zh. Eksp. Teor. Fiz. **72**, 26 (1991)].

Avetissian, H. K., *et al.*, 2002, Phys. Rev. E **66**, 016502.

Bahk, S.-W., *et al.*, 2004, Opt. Lett. **29**, 2837.

Baĭer,V. N., and V. M. Katkov, 1968, Zh. Eksp. Teor. Fiz. **55**, 1542 [Sov. Phys. JETP **26**, 854 (1968)].

Baier, V. N., A. I. Milstein, and R. Z. Shaisultanov, 1996, Phys. Rev. Lett. **77**, 1691.

Bailey, J., *et al.*, 1979, Nucl. Phys. B **150**, 1.

Bakalov, D., *et al.*, 1994, Nucl. Phys. B **35**, 180.

Bakalov, D., *et al.*, 1998, Quantum Semiclassic. Opt. **10**, 239.

Bamber, C., *et al.*, 1999, Phys. Rev. D **60**, 092004.

Baring, M. G., and A. K. Harding, 1997, Astrophys. J. **482**, 372.

Baring, M. G., and A. K. Harding, 2001, Astrophys. J. **547**, 929.

Barton, G., 1990, Phys. Lett. B **237**, 559.

Barton, G., and K. Scharnhorst, 1993, J. Phys. A **26**, 2037.

Berestetskii, V. B., E. M. Lifshitz, and L. P. Pitaevskii, 1982, *Quantum Electrodynamics* (Pergamon, Oxford).

Berezhiani, V. I., D. P. Garochava, S. V. Mikhladze, K. I. Sigua, N. L. Tsintsadze, S. M. Mahajan, Y. Kishimoto, and K. Nishikawa, 2005, Phys. Plasmas **12**, 062308.

Berezhiani, V. I., D. D. Tskhakaya, and P. K. Shukla, 1992, Phys. Rev. A **46**, 6608.

Berge, L., E. A. Kuznetsov, and J. J. Rasmussen, 1996, Phys. Rev. E **53**, R1340.

Berge, L., and J. J. Rasmussen, 1996, Phys. Plasmas **3**, 324.

Berge, L., J. J. Rasmussen, and M. R. Schmidt, 1998, Phys. Scr. **T75**, 18.

Bernard, D., 1998, in *Frontier Tests of QED and Physics of the Vacuum*, edited by E. Zavattini, D. Bakalov, and C. Rizzo (Heron, Sofia, Hungary).

Bernard, D., 1999, Nucl. Phys. B (Proc. Suppl.) **72**, 201.

Bernard, D., 2000, Nucl. Phys. B (Proc. Suppl.) **82**, 439.

Bernard, D., *et al.*, 2000, Eur. Phys. J. D **10**, 141.

Beskin, V. I., A. V. Gurevich, and Ya. N. Istomin, 1993, *Physics of the Pulsar Magnetosphere* (Cambridge University Press, Cambridge).

Bethe, H. A., and W. Heitler, 1934, Proc. R. Soc. London, Ser. A **146**, 83.

Bialynicka-Birula, Z., and I. Bialynicki-Birula, 1970, Phys. Rev. D **2**, 2341.

Bingham, R., 2003, Nature (London) **424**, 258.

Bingham, R., J. T. Mendonça, and P. K. Shukla, 2004, Plasma Phys. Controlled Fusion **46**, R1.

Bloch, J. C. R., C. D. Roberts, and S. M. Schmidt, 2000, Phys. Rev. D **61**, 117502.

Bloch, J. C. R., *et al.*, 1999, Phys. Rev. D **60**, 116011.

Bloembergen, N., 1996, *Nonlinear Optics* (World Scientific, Singapore).

Bluhm, R., 2004, Nucl. Instrum. Methods Phys. Res. B **221**, 6.

Bluhm, R., V. A. Kostelecký, and N. Russel, 1999, Phys. Rev. Lett. **82**, 2254.

Boer, D., and J.-W. van Holten, 2002, e-print hep-ph/0204207.

Bordag, M., U. Mohideen, and V. M. Mostepanenko, 2001, Phys. Rep. **353**, 1.

Borghesi, M., *et al.*, 2002, Phys. Rev. Lett. **88**, 135002.

Bradley, R., *et al.*, 2003, Rev. Mod. Phys. **75**, 777.

Breit, G., and J. A. Wheeler, 1934, Phys. Rev. **46**, 1087.

Bressi, G., G. Carugno, R. Onofrio, and G. Ruoso, 2002, Phys. Rev. Lett. **88**, 041804.

Brezin, E., and C. Itzykson, 1970, Phys. Rev. D **2**, 1191.

Brodin, G., M. Marklund, and L. Stenflo, 2001, Phys. Rev. Lett. **87**, 171801.

Brodin, G., M. Marklund, and L. Stenflo, 2002, Phys. Scr. **T98**, 127.

Brodin, G., L. Stenflo, D. Anderson, M. Lisak, M. Marklund, and P. Johannisson, 2003, Phys. Lett. A **306**, 206.

Budil, K. S., *et al.*, 2000, Astrophys. J., Suppl. Ser. **127**, 261.

Bujarbarua, S., and H. Schamel, 1981, J. Plasma Phys. **25**, 515.

Bula, C., *et al.*, 1996, Phys. Rev. Lett. **76**, 3116.

Bulanov, S. S., 2004, Phys. Rev. E **69**, 036408.

Bulanov, S. S., A. M. Fedotev, and F. Pegoraro, 2005, Phys. Rev. E **71**, 016404.

Bulanov, S. V., T. Esirkepov, and T. Tajima, 2003, Phys. Rev. Lett. **91**, 085001; **91**, 085001(E) (2003).

Bulanov, S. V., and A. S. Sakharov, 1991, JETP Lett. **54**, 203.

Bulanov, S. V., *et al.*, 1999, Phys. Rev. Lett. **82**, 3440.

Bulanov, S. V., *et al.*, 2000, JETP Lett. **71**, 407.

Bulanov, S. V., *et al.*, 2004, Plasma Phys. Rep. **30**, 196.

Bunkin, F. V., and A. E. Kazakov, 1970, Dokl. Akad. Nauk SSSR **93**, 1274 [Sov. Phys. Dokl. **15**, 758 (1971).

Burke, D. L., *et al.*, 1997, Phys. Rev. Lett. **79**, 1626.

Cairns, R. A., A. Reitsma, and R. Bingham, 2004, Phys. Plasmas **11**, 766.

Calmet, J., *et al.*, 1977, Rev. Mod. Phys. **49**, 21.

Cameron, R., *et al.*, 1993, Phys. Rev. D **47**, 3707.

Casher, A., H. Neuberger, and S. Nussinov, 1979, Phys. Rev. D **20**, 179.

Casimir, H. B. G., 1948, Proc. K. Ned. Akad. Wet. **52**, 793.

Casimir, H. B. G., and D. Polder, 1948, Phys. Rev. **73**, 360.

Čerenkov, P. A., 1934, Dokl. Akad. Nauk SSSR **2**, 451.

Chefranov, S. G., 2004, Phys. Rev. Lett. **93**, 254801.

Chen, P., and T. Tajima, 1999, Phys. Rev. Lett. **83**, 256.

Chen, P., 2003, Phys. Rev. Lett. **13**, 3.

Chernev, P., and V. Petrov, 1992, Opt. Lett. **17**, 172.

Chistyakov, M. V., A. V. Kuznetsov, N. V. Mikheev, 1998, Phys. Lett. B **434**, 67.

Colladay, D., and V. A. Kostelecký, 1998, Phys. Rev. D **58**, 116002.

Curtis, M. F., 1982, Rev. Mod. Phys. **54**, 1.

de Groot, S. R., W. A. van Leeuwen, and C. G. van Weert, 1980, *Relativistic Kinetic Theory: Principles and Applications* (North-Holland, Amsterdam).

Delbrück, M., 1933, Z. Phys. **84**, 144.

De Lorenci, V. A., R. Klippert, M. Novello, and J. M. Salim, 2000, Phys. Lett. B **482**, 134.

Desaix, M., D. Anderson, and M. Lisak, 1991, J. Opt. Soc. Am. B **8**, 2082.

DESY X-Ray Free Electron Laser, 2005, http://xfel.desy.de/

Dewar, R. L., 1974, Phys. Rev. A **10**, 2017.

Dicus, D. A., C. Kao, and W. W. Repko, 1998, Phys. Rev. D **57**, 2443.

Dietrich, D. D., 2003, Phys. Rev. D **68**, 105005.

Ding, Y. J., and A. E. Kaplan, 1989, Phys. Rev. Lett. **63**, 2725.

Ding, Y. J., and A. E. Kaplan, 1990, Phys. Rev. Lett. **65**, 2746.

Ding, Y. J., and A. E. Kaplan, 1992, J. Nonlinear Opt. Phys. Mater. **1**, 51.

Dittrich, W., 1979, Phys. Rev. D **19**, 2385.

Dittrich, W., and H. Gies, 1998, Phys. Rev. D **58**, 025004.

Dittrich, W., and H. Gies, 2000, *Probing the Quantum Vacuum* (Springer-Verlag, Berlin).

Dremin, I. M., 2002, JETP Lett. **75**, 167.

Duncan, R. C., 2002, e-print astro-ph/0002442.

Dunne, G. V., 2004, in *From Fields to Strings: Circumnavigating Theoretical Physics*, edited by M. Shifman, A. Vainshtein, and J. Weather (World Scientific, Singapore, in press).

Dupays, A., C. Rizzo, M. Roncadelli, and G. F. Bignami, 2005, Phys. Rev. Lett. **95**, 211302.

Eliasson, B., and P. K. Shukla, 2006, Phys. Rep. **422**, 225.

Eliezer, S., 2002, *The Interaction of High-Power Lasers with Plasmas* (IOP, Bristol).

Elmfors, P., and B.-S. Skagerstam, 1995, Phys. Lett. B **348**, 141; **348**, 141(E) (1995).

Erber, T., 1966, Rev. Mod. Phys. **38**, 626.

Eriksson, D., G. Brodin, M. Marklund, and L. Stenflo, 2004, Phys. Rev. A **70**, 013808.

Esirkepov, T., *et al.*, 2004, Phys. Rev. Lett. **92**, 175003.

Esirkepov, T. Zh., *et al.*, 1998, Pis'ma Zh. Eksp. Teor. Fiz. **68**, 33 [JETP Lett. **68**, 36 (1998)].

Esirkepov, T. Zh., *et al.*, 1999, Pis'ma Zh. Eksp. Teor. Fiz. **70**, 80 [JETP Lett. **70**, 82 (1999)].

Farina, D., and S. V. Bulanov, 2001a, Phys. Rev. E **64**, 066401.

Farina, D., and S. V. Bulanov, 2001b, Phys. Rev. Lett. **86**, 5289.

Ford, G. W., and D. G. Steel, 1990, Phys. Rev. Lett. **65**, 2745.

Fradkin, E. S., D. M. Gitman, and Sh. M. Shvartsman, 1991, *Quantum Electrodynamics with Unstable Vacuum* (Springer-Verlag, Berlin).

Fried, H. M., Y. Gabellini, B. H. J. McKellar, and J. Avan, 2001, Phys. Rev. D **63**, 125001.

Gaeta, A. L., 2003, Science **301**, 54.

Gahn, C., *et al.*, 2000, Appl. Phys. Lett. **77**, 2662.

Gies, H., 1999a, Phys. Rev. D **60**, 105002.

Gies, H., 1999b, Phys. Rev. D **60**, 105033.

Gies, H., 2000, Phys. Rev. D **61**, 085021.

Goloviznin, V. V., and T. J. Schep, 1999, Pis'ma Zh. Eksp. Teor. Fiz. **70**, 445 [JETP Lett. **70**, 450 (1999)].

Graber, J., 1993, Ph.D. dissertation (Cornell University); see also http://w4.lns.cornell.edu/public/CESR/SRF/BasicSRF/SRFBas1.html

Greaves, R. G., and C. M. Surko, 1995, Phys. Rev. Lett. **75**, 3846.

Greaves, R. G., and C. M. Surko, 1997, Phys. Plasmas **4**, 1528.

Greaves, R. G., M. D. Tinkle, and C. M. Surko, 1994, Phys. Plasmas **1**, 1439.

Greiner, W., B. Müller, and J. Rafelski, 1985, *Quantum Electrodynamics of Strong Fields* (Springer, Berlin).

Greisen, K., 1966, Phys. Rev. Lett. **16**, 748.

Grib, A. A., S. G. Mamaev, and V. M. Mostepanenko, 1988, *Vacuum Effects in Strong Fields* (Atomizdat, Moscow).

Hall, J. L., J. Ye, and L.-S. Ma, 2000, Phys. Rev. A **62**, 013815.

Harber, D. M., J. M. Obrecht, J. M. McGuirk, and E. A. Cornell, 2005, Phys. Rev. A **72**, 033610.

Harding, A. K., 1991, Science **251**, 1033.

Harding, A. K., M. G. Baring, and P. L. Gonthier, 1997, Astrophys. J. **476**, 246.

Hasegawa, A., 1975, *Plasma Instabilities and Nonlinear Effects* (Springer-Verlag, Berlin).

Hawking, S. W., 1974, Nature (London) **248**, 30.

Hayata, K., and M. Koshiba, 1993, Phys. Rev. E **48**, 2312.

HEDLA-2004, 2005, *Proceedings of the 5th International Conference on High Energy Density Laboratory Astrophysics (Tuscon, Arizona, March 2004)*, Astrophys. Space Sci. 298, Issue 1–2.

Heisenberg, W., and H. Euler, 1936, Z. Phys. **98**, 714.

Helander, P., and D. J. Ward, 2003, Phys. Rev. Lett. **90**, 135004.

Heyl, J. S., and L. Hernquist, 1997a, J. Phys. A **30**, 6485.

Heyl, J. S., and L. Hernquist, 1997b, Phys. Rev. D **55**, 2449.

Heyl, J. S., and L. Hernquist, 1999, Phys. Rev. D **59**, 045005.

Heyl, J. S., and N. J. Shaviv, 2002, Phys. Rev. D **66**, 023002.

Heyl, J. S., N. J. Shaviv, and D. Lloyd, 2003, Mon. Not. R. Astron. Soc. **342**, 134.

Iacopini, E., and E. Zavattini, 1979, Phys. Lett. **85B**, 151.

Institute for Laser Engineering, Osaka University, 2005, http://www.ile.osakau.ac.jp/

Jackiw, R., and V. A. Kostelecký, 1999, Phys. Rev. Lett. **82**, 3572.

Jarlskog, G., *et al.*, 1973, Phys. Rev. D **8**, 3813.

Jeah-Sheng, W., N. Wei-Tou, and C. Sheng-Jui, 2004, Class. Quantum Grav. **21**, S1259.

Kaplan, A. E., and Y. J. Ding, 2000, Phys. Rev. A **62**, 043805.

Karpman, V. I., 1971, Plasma Phys. **13**, 477.

Karpman, V. I., 1998, Phys. Plasmas **5**, 932.

Karpman, V. I., and H. Washimi, 1977, J. Plasma Phys. **18**, 173.

Kaw, P. K., *et al.*, 1992, Phys. Rev. Lett. **68**, 3172.

Khokonov, M. Kh., and H. Nitta, 2002, Phys. Rev. Lett. **89**, 094801.

Kim, A., *et al.*, 2000, JETP Lett. **72**, 241.

Kirsebom, K., *et al.*, 2001, Phys. Rev. Lett. **87**, 054801.

Kivshar, Y. S., and G. P. Agrawal, 2003, *Optical Solitons* (Academic, San Diego).

Klein, J. J., and B. P. Nigam, 1964a, Phys. Rev. **136**, B1279.

Klein, J. J., and B. P. Nigam, 1964b, Phys. Rev. **136**, B1540.

Kluger, Y., *et al.*, 1991, Phys. Rev. Lett. **67**, 2427.

Kondratyev, V. N., 2002, Phys. Rev. Lett. **88**, 221101.

Kouveliotou, C., *et al.*, 1998, Nature (London) **393**, 235.

Kozlov, V. A., *et al.*, 1979, Zh. Eksp. Teor. Fiz. **76**, 148 [Sov. Phys. JETP **49**, 75 (1979)].

Kuznetsov, E. A., J. J. Rasmussen, K. Rypdal, and S. K. Turitsyn, 1995, Physica D **87**, 273.

Lamoreaux, S. K., 1997, Phys. Rev. Lett. **78**, 5; **81**, 5475(E) (1998).

Latorre, J. I., P. Pascual, and R. Tarrach, 1995, Nucl. Phys. B **437**, 60.

Lee, R. W., *et al.*, 1995, *Science on High-Energy Lasers* (Lawrence Livermore National Laboratory, Livermore).

Lee, S. A., and W. M. Fairbanks, 2002, in *Laser Physics at the Limits*, edited by H. Figger, D. Meschede, and C. Zimmermann (Springer-Verlag, Berlin).

Liang, E. P., S. C. Wilks, and M. Tabak, 1998, Phys. Rev. Lett. **81**, 4887.

Liepe, M., e-print physics/0009098.

Lipa, J. A., J. A. Nissen, S. Wang, D. A. Stricker, and D. Avaloff, 2003, Phys. Rev. Lett. **90**, 060403.

Lodenqual, J., *et al.*, 1974, Astrophys. J. **190**, 141.

Lontano, M., *et al.*, 2003, Phys. Plasmas **10**, 639.

Luiten, A. N., and J. C. Petersen, 2004a, Phys. Lett. A **330**, 429.

Luiten, A. N., and J. C. Petersen, 2004b, Phys. Rev. A **70**, 033801.

Lundström, E., *et al.*, 2006, Phys. Rev. Lett. **96**, 083602.

Luo, Q., *et al.*, 2002, Phys. Rev. E **66**, 026405.

Luther, G. G., A. C. Newell, and J. V. Moloney, 1994, Physica D **74**, 59.

Mamaev, S. G., V. M. Mostepanenko, and M. I. Eĭdes, 1981, Sov. J. Nucl. Phys. **33**, 569.

Marinov, M. S., and V. S. Popov, 1977, Fortschr. Phys. **25**, 373.

Marklund, M., 2004, Phys. Scr. **T113**, 59.

Marklund, M., G. Brodin, and L. Stenflo, 2003, Phys. Rev. Lett. **91**, 163601.

Marklund, M., G. Brodin, L. Stenflo, and P. K. Shukla, 2005, New J. Phys. **7**, 70.

Marklund, M., B. Eliasson, and P. K. Shukla, 2004, JETP Lett. **79**, 262.

Marklund, M., P. K. Shukla, G. Brodin, and L. Stenflo, 2004a, *Proceedings of the 12th International Congress on Plasma Physics, Nice, France, 2004*, 03–0100; e-Proceedings available at http://hal.ccsd.cnrs.fr/ccsd-00003094/en

Marklund, M., P. K. Shukla, G. Brodin, and L. Stenflo, 2004b, New J. Phys. **6**, 172.

Marklund, M., P. K. Shukla, G. Brodin, and L. Stenflo, 2005, J. Plasma Phys. **71**, 527.

Marklund, M., P. K. Shukla, and B. Eliasson, 2005, Europhys. Lett. **71**, 327.

Marklund, M., P. K. Shukla, L. Stenflo, G. Brodin, and M. Servin, 2005, Plasma Phys. Controlled Fusion **47**, L25.

Marklund, M., D. D. Tskhakaya, and P. K. Shukla, 2005, Europhys. Lett. **72**, 950.

Max, C. E., J. Arons, and J. B. Langdon, 1974, Phys. Rev. Lett. **33**, 209.

McKenna, J. M., and P. M. Platzman, 1963, Phys. Rev. **129**, 2354.

McKenna, P., *et al.*, 2005, Phys. Rev. Lett. **94**, 084801.

Melissinos, A. C., 2002, e-print hep-ph/0205169.

Mendonça, J. T., 2001, *Theory of Photon Acceleration* (IOP, Bristol).

Mentzel, M., D. Berg, and G. Wunner, 1994, Phys. Rev. D **50**, 1125.

Meyerhofer, D. D., 1997, IEEE J. Quantum Electron. **33**, 1935.

Mikheev, N. V., and N. V. Chistyakov, 2001, JETP Lett. **73**, 642.

Mills, A. P., Jr., 2002, Nucl. Instrum. Methods Phys. Res. B **192**, 107.

Milonni, P. W., 1994, *The Quantum Vacuum* (Academic, San Diego).

Mittleman, M. H., 1987, Phys. Rev. A **35**, 4624.

Mostepanenko, V. M., and V. M. Frolov, 1974, Sov. J. Nucl. Phys. **19**, 451.

Mostepanenko, V. M., and N. N. Trunov, 1997, *The Casimir Effect and its Applications* (Oxford Science Publications, Oxford).

Moulin, F., and D. Bernard, 1999, Opt. Commun. **164**, 137.

Moulin, F., D. Bernard, and F. Amiranoff, 1996, Z. Phys. C **72**, 607.

Mourou, G. A., C. P. J. Barty, and M. D. Perry, 1998, Phys. Today **51** (1), 22.

Mourou, G. A., T. Tajima, and S. V. Bulanov, 2006, Rev. Mod. Phys. **78**, 309.

Narozhny, N. B., and A. I. Nikishov, 1970, Sov. J. Nucl. Phys. **11**, 596.

Narozhny, N. B., *et al.*, 1965, Sov. Phys. JETP **20**, 622.

Narozhny, N. B., *et al.*, 2004a, Phys. Lett. A **330**, 1.

Narozhny, N. B., *et al.*, 2004b, Zh. Eksp. Teor. Fiz. **80**, 434 [JETP Lett. **80**, 382 (2004)].

Naumova, N. M., *et al.*, 2001, Phys. Rev. Lett. **87**, 185004.

Nibbelink, S. G., and M. Pospelov, 2005, Phys. Rev. Lett. **94**, 081601.

Nikishov, A. I., and V. I. Ritus, 1964a, Sov. Phys. JETP **19**, 529.

Nikishov, A. I., and V. I. Ritus, 1964b, Sov. Phys. JETP **19**, 1191.

Nikishov, A. I., and V. I. Ritus, 1965, Sov. Phys. JETP **20**, 757.

Nikishov, A. I., and V. I. Ritus, 1967, Sov. Phys. JETP **25**, 1135.

Nitta, H., M. Kh. Khokonov, Y. Nagata, and S. Onuki, 2004, Phys. Rev. Lett. **93**, 180407.

Novello, M., *et al.*, 2001, Phys. Rev. D **63**, 103516.

OMEGA EP Laser Facility, University of Rochester, 2005, http://omegaep.lle.rochester.edu/

Oohara, W., and R. Hatakeyama, 2003, Phys. Rev. Lett. **91**, 205005.

Oshima, N., *et al.*, 2004, Phys. Rev. Lett. **93**, 195001.

Partovi, M. H., 1993, e-print hep-ph/9308293.

Partovi, M. H., 1994, Phys. Rev. D **50**, 1118.

Patel, N., 2002, Nature (London) **415**, 110.

Peacock, J. A., 1998, *Cosmological Physics* (Cambridge University Press, Cambridge).

Peccei, R. D., and H. R. Quinn, 1977, Phys. Rev. Lett. **38**, 1440.

Perry, M. D., and G. Mourou, 1994, Science **264**, 917.

Piran, T., 2004, Rev. Mod. Phys. **76**, 1143.

Popov, V. S., 1971, Zh. Eksp. Teor. Fiz. Pis'ma Red. **13**, 261 [JETP Lett. **13**, 185 (1971)].

Popov, V. S., 1972, Zh. Eksp. Teor. Fiz. Pis'ma Red. **13**, 261 [Sov. Phys. JETP **35**, 659 (1972)].

Popov, V. S., 1973, Zh. Eksp. Teor. Fiz. Pis'ma Red. **18**, 53 [JETP Lett. **18**, 29 (1973)].

Popov, V. S., 1974, Yad. Fiz. **19**, 155 [Sov. J. Nucl. Phys. **19**, 81 (1974)].

Popov, V. S., and M. S. Marinov, 1973, Sov. J. Nucl. Phys. **16**, 449.

Prozorkevich, A. V., *et al.*, 2000, e-print nucl-th/0012039.

Pukhov, A., 2003, Rep. Prog. Phys. **66**, 47.

Raizen, M. G., and B. Rosenstein, 1990, Phys. Rev. Lett. **65**, 2744.

Reinhardt, J., and W. Greiner, 1977, Rep. Prog. Phys. **40**, 219.

Reiss, H. R., 1962, J. Math. Phys. **3**, 59.

Relativistic Heavy Ion Collider, 2005, Brookhaven National Laboratory, http://www.bnl.gov/rhic/

Remington, B. A., 2005, Plasma Phys. Controlled Fusion **47**, A191.

Rikken, G. L. J. A., and C. Rizzo, 2000, Phys. Rev. A **63**, 012107.

Rikken, G. L. J. A., and C. Rizzo, 2003, Phys. Rev. A **67**, 015801.

Ringwald, A., 2001a, Phys. Lett. B **510**, 107.

Ringwald, A., 2001b, e-print hep-ph/0112254.

Ringwald, A., 2003, e-print hep-ph/0304139.

Ritus, V. I., 1976, Sov. Phys. JETP **42**, 774.

Roberts, C. D., S. M. Schmidt, and D. V. Vinnik, 2002, Phys. Rev. Lett. **89**, 153901.

Rodionov, V. N., 2004, JETP **98**, 395.

Rothenberg, J. E., 1992, Opt. Lett. **17**, 583.

Rozanov, N. N., 1993, Zh. Eksp. Teor. Fiz. **103**, 1996 [JETP **76**, 991 (1993)].

Rozanov, N. N., 1998, Zh. Eksp. Teor. Fiz. **113**, 513 [JETP **86**, 284 (1998)].

Rutherford Appleton Laboratory Central Laser Facility, 2005, http://www.clf.rl.ac.uk/

Ryutov, D. D., R. P. Drake, and B. A. Remington, 2000, Astrophys. J., Suppl. Ser. **127**, 465.

Saulson, P. R., 1994, *Fundamentals of Interferometric Gravitational Wave Detectors* (World Scientific, Singapore).

Sauter, F., 1931, Z. Phys. **69**, 742.

Scharer, J. W., J. Garrison, J. Wong, and J. E. Swain, 1973, Phys. Rev. A **8**, 1582.

Scharnhorst, K., 1990, Phys. Lett. B **236**, 354.

Scharnhorst, K., 1998, Ann. Phys. **7**, 700.

Schamel, H., 2000, Phys. Plasmas **7**, 4831.

Schwinger, J., 1951, Phys. Rev. **82**, 664.

Scott, A., 2003, *Nonlinear Science* (Oxford University Press, Oxford).

Shaviv, N. J., J. S. Heyl, and Y. Lithwick, 1999, Mon. Not. R. Astron. Soc. **306**, 333.

Shen, B., and J. Meyer-ter-Vehn, 2001a, Phys. Plasmas **8**, 1003.

Shen, B., and J. Meyer-ter-Vehn, 2001b, Phys. Rev. E **65**, 016405.

Shen, B., and M. Y. Yu, 2002, Phys. Rev. Lett. **89**, 275004.

Shen, B., and M. Y. Yu, 2003, Phys. Rev. E **68**, 026501.

Shen, B., M. Y. Yu, and R. Li, 2004, Phys. Rev. E **70**, 036403(R).

Shen, B., M. Y. Yu, and X. Wang, 2003, Phys. Plasmas **10**, 4570.

Sheng-Jui, C., *et al.*, 2003, e-print hep-ex/0308071.

Shigemori, K., *et al.*, 2000, Astrophys. J. Lett. **533**, L159.

Shorokhov, O., P. Pukhov, and I. Kostyukov, 2003, Phys. Rev. Lett. **91**, 265002.

Shukla, P. K., 1992, Phys. Scr. **45**, 618.

Shukla, P. K., R. Bharuthram, and N. L. Tsintsadze, 1987, Phys. Rev. A **35**, R4889.

Shukla, P. K., R. Bharuthram, and N. L. Tsintsadze, 1988, Phys. Scr. **38**, 578.

Shukla, P. K., and B. Eliasson, 2004, Phys. Rev. Lett. **92**, 073601.

Shukla, P. K., and B. Eliasson, 2005, Phys. Rev. Lett. **94**, 065002.

Shukla, P. K., B. Eliasson, and M. Marklund, 2004, Opt. Commun. **235**, 373.

Shukla, P. K., B. Eliasson, and M. Marklund, 2005, J. Plasma Phys. **71**, 213.

Shukla, P. K., M. Marklund, G. Brodin, and L. Stenflo, 2004, Phys. Lett. A **330**, 131.

Shukla, P. K., M. Marklund, and B. Eliasson, 2004, Phys. Lett. A **324**, 193.

Shukla, P. K., M. Marklund, D. D. Tskhakaya, and B. Eliasson, 2004, Phys. Plasmas **11**, 3767.

Shukla, P. K., N. N. Rao, M. Y. Yu, and N. L. Tsintsadze, 1986, Phys. Rep. **138**, 1.

Shukla, P. K., and L. Stenflo, 1998, Phys. Plasmas **5**, 1554.

Silva, L. O., *et al.*, 2004, Phys. Rev. Lett. **92**, 015002.

SLAC Linac Coherent Light Source, 2005, http://www-ssrl.slac.stanford.edu/lcls/

Soljačić, M., and M. Segev, 2000a, Phys. Rev. E **62**, 2810.

Soljačić, M., and M. Segev, 2000b, Phys. Rev. A **62**, 043817(R).

Soljačić, M., S. Sears, and M. Segev, 1998, Phys. Rev. Lett. **81**, 4851.

Stenflo, L., 1976, Phys. Scr. **14**, 320.

Stenflo, L., G. Brodin, M. Marklund, and P. K. Shukla, 2005, J. Plasma Phys. **71**, 709.

Stenflo, L., and N. L. Tsintsadze, 1979, Astrophys. Space Sci. **64**, 513.

Sukenik, C. I., M. G. Boshier, D. Cho, V. Sandoghdar, and E. A. Hinds, 1993, Phys. Rev. Lett. **70**, 560.

Surko, C. M., and R. G. Greaves, 2004, Phys. Plasmas **11**, 2333.

Surko, C. M., M. Leventhal, and A. Passner, 1989, Phys. Rev. Lett. **62**, 901.

Tajima, T., 2003, Plasma Phys. Rep. **29**, 207.

Tajima, T., and J. Dawson, 1979, Phys. Rev. Lett. **43**, 267.

Tajima, T., and G. Mourou, 2002, Phys. Rev. ST Accel. Beams **5**, 031301.

Tajima, T., and T. Taniuti, 1990, Phys. Rev. A **42**, 3587.

Tamm, I. E., and I. M. Frank, 1937, Dokl. Akad. Nauk SSSR **14**, 107.

Thoma, M. H., 2000, Europhys. Lett. **52**, 498.

Thompson, C., and O. Blaes, 1998, Phys. Rev. D **57**, 3219.

Tomaras, T. N., N. C. Tsamis, and R. P. Woodard, 2000, Phys. Rev. D **62**, 125005.

Tsai, W.-Y., 1974a, Phys. Rev. D **10**, 1342.

Tsai, W.-Y., 1974b, Phys. Rev. D **10**, 2699.

Tsai, W., and T. Erber, 1975, Phys. Rev. D **12**, 1132.

Tsintsadze, N. L., and J. T. Mendonça, 1998, Phys. Plasmas **5**, 3609.

Tskhakaya, D. D., 1982, Phys. Rev. Lett. **48**, 484.

Unruh, W., 1976, Phys. Rev. D **14**, 870.

Valluri, S. R., U. D. Jentschura, and D. R. Lamm, 2003, in *High Energy Physics*, edited by A. H. Fariborz, AIP Conf. Proc. No. 687 (AIP, Melville), p. 203.

Ventura, J., 1979, Phys. Rev. D **19**, 1684.

Weiland, J. C., and H. Wilhelmsson, 1977, *Coherent Non-linear Interaction of Waves in Plasmas* (Pergamon, Oxford).

Weinberg, S., 1978, Phys. Rev. Lett. **40**, 223.

Weisskopf, V. S., 1936, K. Dan. Vidensk. Selsk. Mat. Fys. Medd. 14 (1).

Wilczek, F., 1978, Phys. Rev. Lett. **40**, 279.

Wilks, S. C., *et al.*, 1992, Phys. Rev. Lett. **69**, 1383.

Woolsey, N. C., C. Courtois, and R. O. Dendy, 2004, Plasma Phys. Controlled Fusion **46**, B397.

Yu, M. Y., P. K. Shukla, and N. L. Tsintsadze, 1982, Phys. Fluids **25**, 1049.

Zatsepin, G. T., and V. A. Kuzmin, 1966, JETP Lett. **4**, 78.

Zavattini, E., *et al.*, 2006, Phys. Rev. Lett. **96**, 110406.

Zepf, M., *et al.*, 2003, Phys. Rev. Lett. **90**, 064801.

Zharova, N. A., A. G. Litvak, and V. A. Mironov, 2003, JETP **96**, 643.